ANGULAR CORRELATION OF PHOTOPRODUCED PION PAIRS

Thesis by

David D. Elliott

In Partial Fulfillment of the Requirements

For the Degree of

Doctor of Philosophy

California Institute of Technology

Pasadena, California

1959

ACKNOWLEDGMENTS

The author wishes to express his sincere appreciation to Dr. Matthew Sands, his advisor in this work, for his counsel and active assistance in obtaining and analysing the experimental data and for his guidance during the author's graduate residence.

Many valuable discussions were held with Dr. Jon Mathews, Dr. Samuel Berman, and Dr. Arthur Clegg on the interpretation of experimental results. Dr. Michel Bloch and the members of the staff of the Synchrotron Laboratory have been helpful consultants on numerous occasions.

Mr. Bruce Rule, Mr. Daniel Sell, Mr. Lawrence Loucks and others of the engineering staff and crew of the Synchrotron Laboratory are to be thanked for their help during the execution of the experiment.

The interest and encouragement throughout the author's graduate residence of Dr. Robert F. Bacher is gratefully acknowledged. The partial support of the U. S. Atomic Energy Commission is appreciated.

ABSTRACT

The angular correlation between the two pions from the reaction $\gamma + P \rightarrow P + \pi^+ + \pi^-$ has been studied by observing coincidences between two pions produced simultaneously in a hydrogen target in the 1.1 Bev x-ray beam of the Cal Tech synchrotron. The negative pion was detected in a magnetic spectrometer set to accept 150 Mev pions at an angle, θ_-, of 35° with respect to the x-ray beam. The positive pion was detected in a counter telescope which was set at various angles, θ_+, with respect to the x-ray beam, and at azimuthal angles, ϕ_+, with respect to the azimuthal angle of the negative pion, of 0°, 90°, and 180°. For each set of angles the absorbers between the counters of the telescope were chosen such that the observed pairs could be separated into two groups: those produced by photons with energies between 650 and 825 Mev, and those produced by photons with energies from 825 to the bremsstrahlung cut-off energy of 1080 Mev. For pairs produced by photons in the lower energy group the cross-section shows no azimuthal dependence in the C. M. system within the statistical error of about 20 $^\circ/o$ at either of the two C. M. zenith angles $\theta'_+ = 70^\circ$ and 120°. For a C. M. azimuthal angle of 180° the cross-section appears to be independent of zenith angle, θ'_+, except at the most forward point ($\theta'_+ = 35^\circ$) where the cross-section is about 30 $^\circ/o$ larger than that observed at other angles. The value of the cross-section integrated over all π^+ directions is consistent with a direct measurement of the cross-section for the production of negative pions.

TABLE OF CONTENTS

I. INTRODUCTION

The photoproduction of pions from the interaction of high energy quanta with protons has been studied for quantum energies up to 1100 Mev. The most comprehensive work has been concerned with the two reactions:

$$\gamma + P \longrightarrow N + \pi^{+}$$

$$\gamma + P \longrightarrow P + \pi^{o}$$

in the quantum energy interval from threshold to 500 Mev (1, 2). The outstanding feature of the results is the appearance of a resonance in both production processes at 300 Mev. This resonance occurs in the pion-nucleon state with total angular momentum 3/2 and an isotopic spin 3/2 . More recent work has extended the experimental data to quantum energies of 900 Mev for the neutral pion production (3, 4, 5, 6) and to 1000 Mev for the positive pion production (7, 8). These results have shown a second resonance at 700 Mev which occurs in the pion-nucleon state with an isotopic spin 1/2 but, as yet, an unknown total angular momentum (9, 10).

At quantum energies above 400 Mev the photoproduction of pion pairs through the processes:

$$\gamma + P \longrightarrow P + \pi^{+} + \pi^{-}$$

$$\gamma + P \longrightarrow N + \pi^{+} + \pi^{o}$$

$$\gamma + P \longrightarrow P + \pi^{o} + \pi^{o}$$

becomes energetically possible. The photoproduction of pion pairs

was first observed in the 500 Mev bremsstrahlung beam of the Cal Tech synchrotron by observing the negative pions emitted from a hydrogen target (11, 12, 13, 14). The conservation of charge requires that at least one other positive light particle also be emitted, the negative pions are therefore presumed to arise from the pair reaction or from a reaction in which three or more pions are produced. Other workers (15, 16, 17) have extended the measurements of the yields of negative pions to higher bremsstrahlung energies. The most extensive work is that of Bloch and Sands (18, 19, 20, 21). They have measured the negative pion yields at 60° and at 120° for several pion energies and for several bremsstrahlung cut-off energies between 600 and 1100 Mev. The differences in the pion yields for successive cut-off energies were used to obtain the cross-section for photons of a particular energy. The cross-sections are given as a function of the negative pion energy for photon energies of 670, 830, and 1010 Mev. For all three photon energies the C. M. cross-section peaks at the lower pion energies, and there seems to be no strong dependence on the C. M. pion angle from 90° to 150°. The total cross-section from 670 to 1010 Mev is consistent with a constant value of about 5×10^{-29} cm^2.

Information about states which contain a nucleon and two pions has also been obtained from the study of inelastic nucleon-nucleon and pion-nucleon collisions. The results are said (22, 23, 24, 25) to indicate the formation and decay of a metastable pion-nucleon system which corresponds to the $T = 3/2$, $J = 3/2$ resonance in pion scattering. The cross-sections obtained by Bloch and Sands were compared to the predictions of such an "isobar model." The data agrees fairly well

with the negative pion spectrum predicted by a proton-negative pion isobar at 1010 Mev, the comparison is inconclusive at 830 Mev, and at 670 Mev the data agrees fairly well with the spectrum computed from a proton-positive pion isobar.

Cutkosky and Zachariasen (26) have attempted to describe theoretically the photoproduction of pion pairs using the Chew-Low theory (27). The predictions of the Cutkosky - Zachariasen calculation were compared with the results of Bloch and Sands at their lowest energy (670 Mev). Even though this energy is well above the energies for which the theory is expected to be valid, the agreement is quite satisfactory.

The work reported in this thesis is a study of the angular correlation between the two pions produced in the reaction $\gamma + P \longrightarrow P + \pi^+ + \pi^-$. The negative pion was detected in a magnetic spectrometer, and the positive pion was detected in a three-counter telescope. The coincidence rate between negative pions accepted by the spectrometer and the pions which traversed the telescope was measured for several angular positions of the telescope. In this experiment it was not necessary to make measurements with more than one bremsstrahlung cut-off energy because a knowledge of the direction and energy of both pions determined the energy of that photon in the bremsstrahlung beam responsible for the reaction. The counting rate was low, and in order to get reasonable statistics the measurements were restricted to one angle and one energy of the negative pion and to two photon energy intervals. The angle and energies used

were those at which a reasonable coincidence rate was expected. Negative pions were counted at 35° with the spectrometer set for an energy of 150 Mev. The observed pairs were divided into two groups: those produced by photons in the energy interval from 650 to 825 Mev, and those produced by photons in the energy interval from 825 to 1080 Mev. The production of negative pions without the requirement of a coincident positive pion was also studied at 35° for several pion energies and bremsstrahlung cut-off energies. These results were used to obtain an independent value for the pair cross-section integrated over all positive pion directions.

After the completion of this experiment, preliminary results were received from Sellen et al. (28, 29) on the measurements of photoproduced pion pairs observed in a hydrogen-filled diffusion cloud-chamber. In the C. M. system, for those events initiated by photons in the energy interval from 500 to 700 Mev, the measurements indicate that: (a) the energy spectrum of the π^+ peaks at higher π^+ energies; (b) the energy spectrum of the π^- peaks at lower π^- energies; (c) the π^+ is emitted isotropically; and (d) the π^- is emitted preferentially in the forward direction. The measurement of the total cross-section for multiplet production indicates that: (a) the total cross-section for pion pairs peaks about 600 Mev and falls slowly from 600 to 1000 Mev; and (b) the total number of triplets compared to the number of pairs produced by photons from threshold to 1000 Mev is roughly 4 $^{o}/_{o}$ (they reported no cases of more than three pion production).

II. EXPERIMENTAL APPARATUS AND TECHNIQUES

A. The Experiment

A diagram of the experimental arrangement is given in figure 1. Negative particles produced in the hydrogen target by the 1.1 Bev x-ray beam and emitted at an angle of 35^{o} with a momentum of 255 Mev/c were accepted by the magnetic spectrometer and were detected in a set of three scintillation counters and a Čerenkov counter. The Čerenkov counter permitted some discrimination against particles with a high velocity and hence allowed the separation of pions and electrons of the same momentum. A second particle emitted simultaneously with the negative meson was detected in the counter telescope. This particle and the coincident π^- traversing the spectrometer were assumed to be the π^+ and π^- from the reaction $\gamma + P \longrightarrow P + \pi^+ + \pi^-$ (see Section III. B. 3). The absorbers in the telescope were chosen such that if the observed pair had been initiated by a photon in the energy interval from 650 to 825 Mev, the π^+ would be able to penetrate the first two absorbers but not the third absorber, therefore, giving a pulse in C_5 and C_6 but not in C_7. A second photon energy interval from 825 to 1080 Mev was defined by those π^+ from the observed pairs which penetrated all three absorbers, therefore, giving a pulse in C_5, C_6, and C_7. The upper limit of this second interval was set by the bremsstrahlung cut-off energy which was 1080 Mev throughout the experiment. The number of coincidences between a count in the spectrometer and a count in the telescope was measured for each of several angular positions of the telescope.

Figure 1. Experimental Layout for Angular Correlation Measurement.

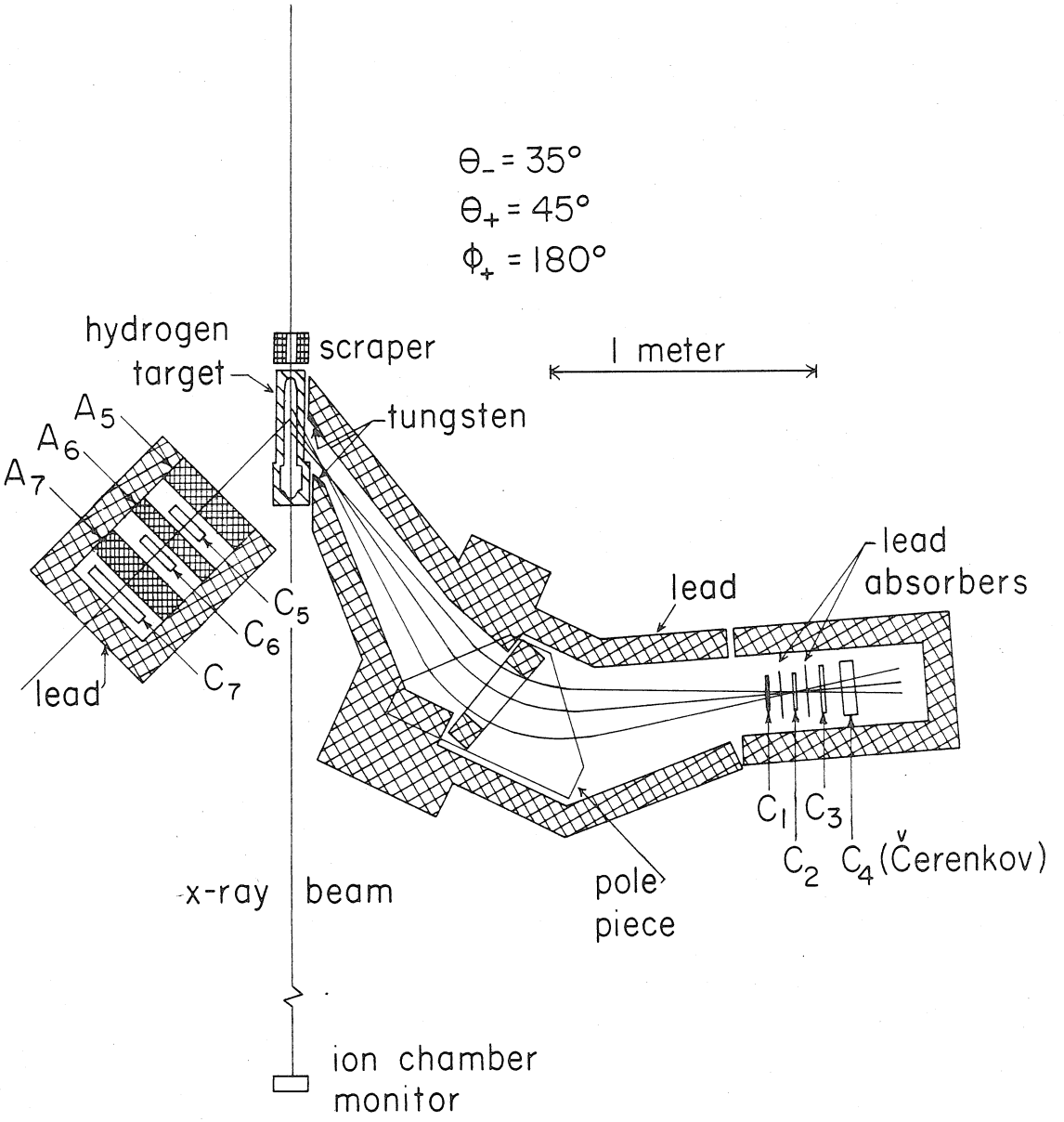
$\theta_- = 35°$
$\theta_+ = 45°$
$\phi_+ = 180°$
hydrogen target
scraper
1 meter
tungsten
A_5
A_6
A_7
C_5
C_6
C_7
lead
lead
lead absorbers
C_1
C_3
C_2
C_4 (v Cerenkov)
x-ray beam
pole piece
ion chamber monitor

Using the magnetic spectrometer alone, data was also taken of the π^- production at 35^o for several pion energies and several bremsstrahlung cut-off energies. The cross-section for π^- production was deduced from the measured rates by the method described in the work of Bloch and Sands (20, 21).

B. The X-Ray Beam

The x-ray beam was collimated at the synchrotron and was 3 cm. high and 2. 5 cm. wide at the target. The target was aligned so that the beam passed through without striking its side walls. A lead scraper immediately in front of the target prevented radiation scattered at the primary collimator from striking the target walls, but did not intercept any of the primary beam. After passing through the target, the beam traversed the scrapers and target of another experiment and entered a monitoring ionization chamber. The charge collected from the chamber was recorded by an integrating electrometer, and at each synchrotron energy was proportional to the energy flux in the beam. The proportionality constant varied slowly with the synchrotron energy and has been measured (30) with a quantameter constructed according to the design of Wilson (31). It is customary in this laboratory to normalize data to a standard beam monitor reading called BIP (beam integrator pulse). One BIP corresponds to 2.22×10^{-7} coulombs collected from the ionization chamber, the energy flux in the x-ray beam corresponding to this integrated charge is 0.99×10^{12} Mev at a bremsstrahlung cut-off energy of 497 Mev. The value of the BIP for other cut-off energies is shown in figure 2.

Figure 2. Energy Flux in the X-Ray Beam per BIP as a Function of the Synchrotron Energy.

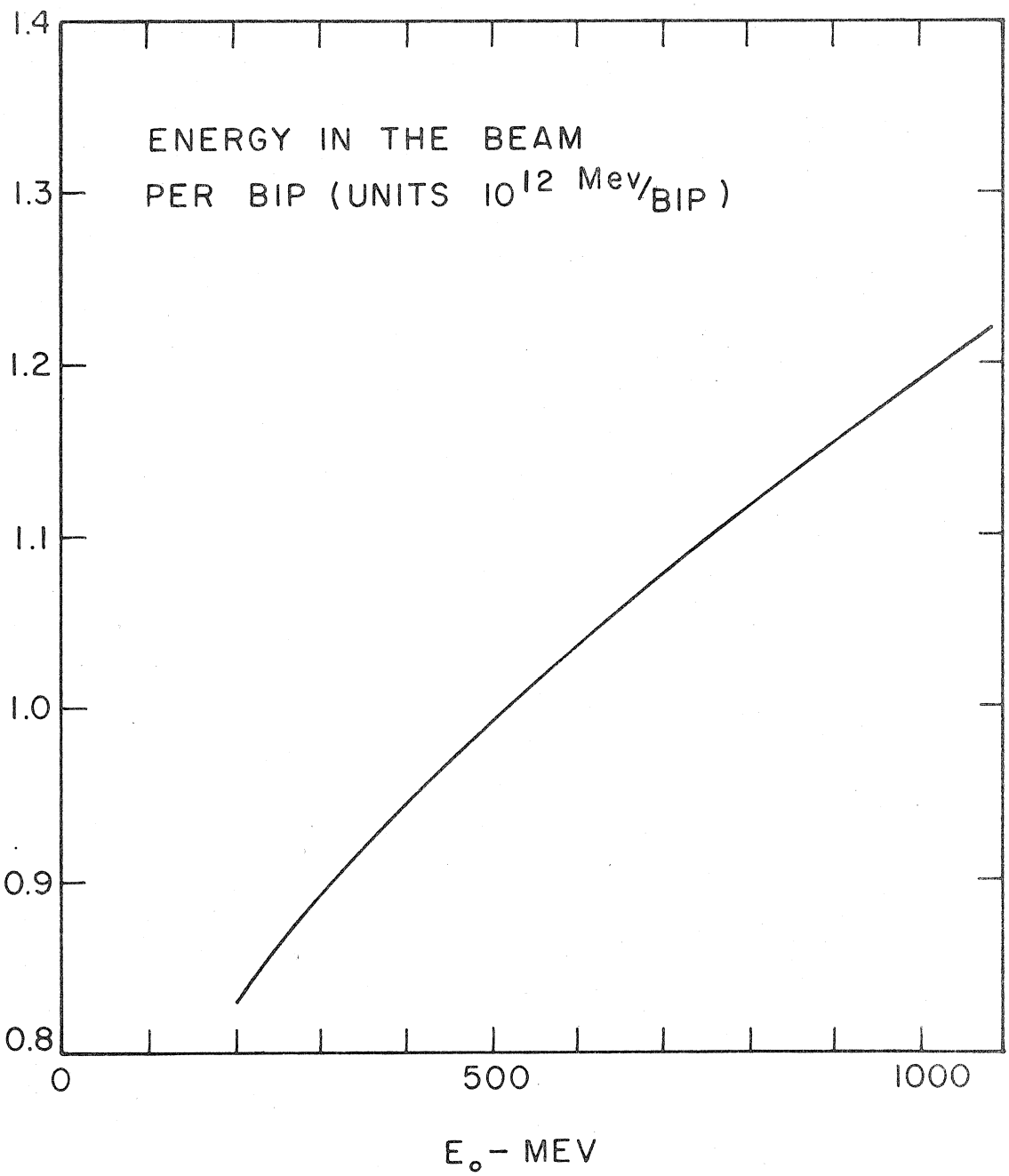
1.4
1.3
1.2
1.1
1.0
0.9
0.8
ENERGY IN THE BEAM
PER BIP (UNITS 10^{12} Mev/BIP)
0
500
1000
E_o - MEV

The synchrotron was operated so that the electrons struck the internal radiator at a more or less constant rate during a 20 millisecond "plateau" interval over which the magnetic field in the synchrotron was held constant to about 0.1 %. The energy of the electrons which struck the target in this interval was determined from a continual measurement of the magnetic field at the "plateau." The energy measurement has an uncertainty of perhaps a few per cent due to the unknown details of the orbit shape, but was reproducible to 0.1 % and had this accuracy for relative measurements at nearby energies.

The spectrum of the bremsstrahlung has been measured by Donoho, Emery, and Walker (32) using a pair spectrometer. The number of photons with energy in the range between k and k + dk per unit energy flux in the beam can be expressed as:

$$N(E_o, k)dk = \frac{1}{E_o} \frac{1}{k} B(E_o, k)dk . \qquad (1)$$

where E_o is the energy of the electrons at the target (bremsstrahlung cut-off). The function $B(E_o, k)$ was found to be the same function of k/E_o for E_o = 700 Mev and E_o = 1100 Mev. We have, therefore, taken $B(E_o, k)$ to be only a function of k/E_o for all synchrotron energies encountered in this experiment. $B(k/E_o)$ is shown in figure 3, and, as seen from its definition in equation 1, satisfies the condition $\int_0^1 B(k/E_o)d(k/E_o) = 1$. The solid curve in figure 3 was computed for a thin tantalum radiator with E_o = 750 Mev (using the Bethe - Heitler

Figure 3. Bremsstrahlung Energy Spectrum.

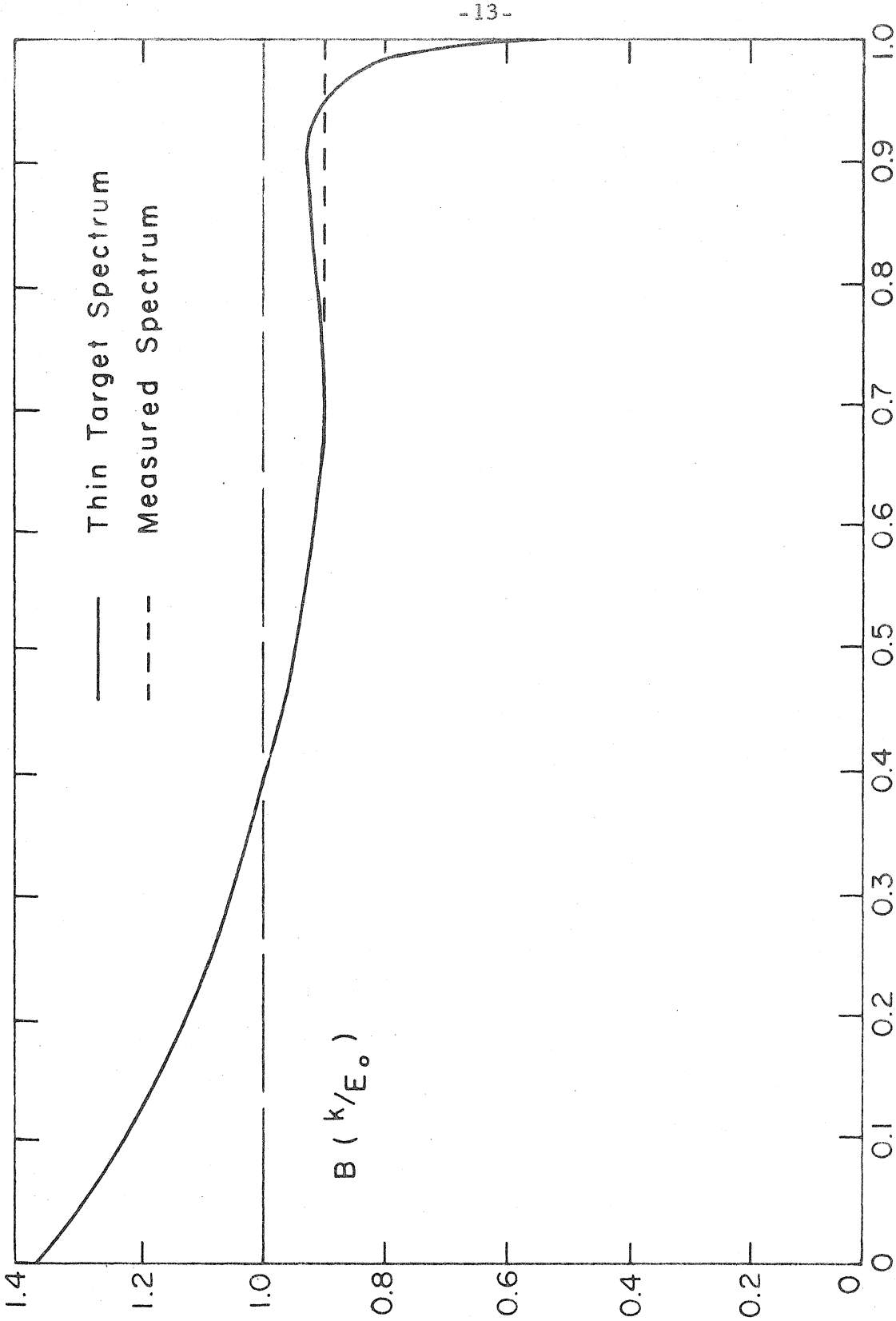
Thin Target Spectrum
Measured Spectrum
B (k/E₀)
k/E₀
0
0.1
0.2
0.3
0.4
0.5
0.6
0.7
0.8
0.9
1.0
0.2
0.4
0.6
0.8
1.0
1.2
1.4

formula (33)). The measured spectrum agrees with the "thin-target" spectrum for photon energies $k \leq 0.7E_0$, but at higher energies shows neither the gradual rise nor the smooth drop for k near E_0.

During this experiment the synchrotron was generally operated with a mean x-ray flux through the collimator of about 10^{11} Mev per pulse at one pulse per second.

C. The Gas Target

The hydrogen target consisted of a cylindrical vessel with hemispherical ends 43 cm. long and 5 cm. in diameter with a 0.075-cm. thick steel wall, surrounded by a 4-cm. layer of styrofoam insulation (see figure 4). The vessel was cooled, by thermal contact with a liquid nitrogen reservoir, to a mean temperature of about $100^{\circ}K$ as measured by thermocouples in contact with the walls at two points. Hydrogen gas held in the target at a pressure of 150 atmospheres (measured with a calibrated bourdon gauge) was assumed to be in thermal equilibrium with the target wall. The hydrogen density, determined from the measurements of pressure and temperature by Johnston et al. (34), was typically 0.03 gm/cm^3. The error in the determination of the gas density was about 3 %, but the relative error in the density measurement for different runs is estimated to be about 1 %.

D. The Magnetic Spectrometer

The origin of the negative particles accepted by the magnet was restricted to a region between the ends of the target (thus

Figure 4. The Hydrogen Gas Target

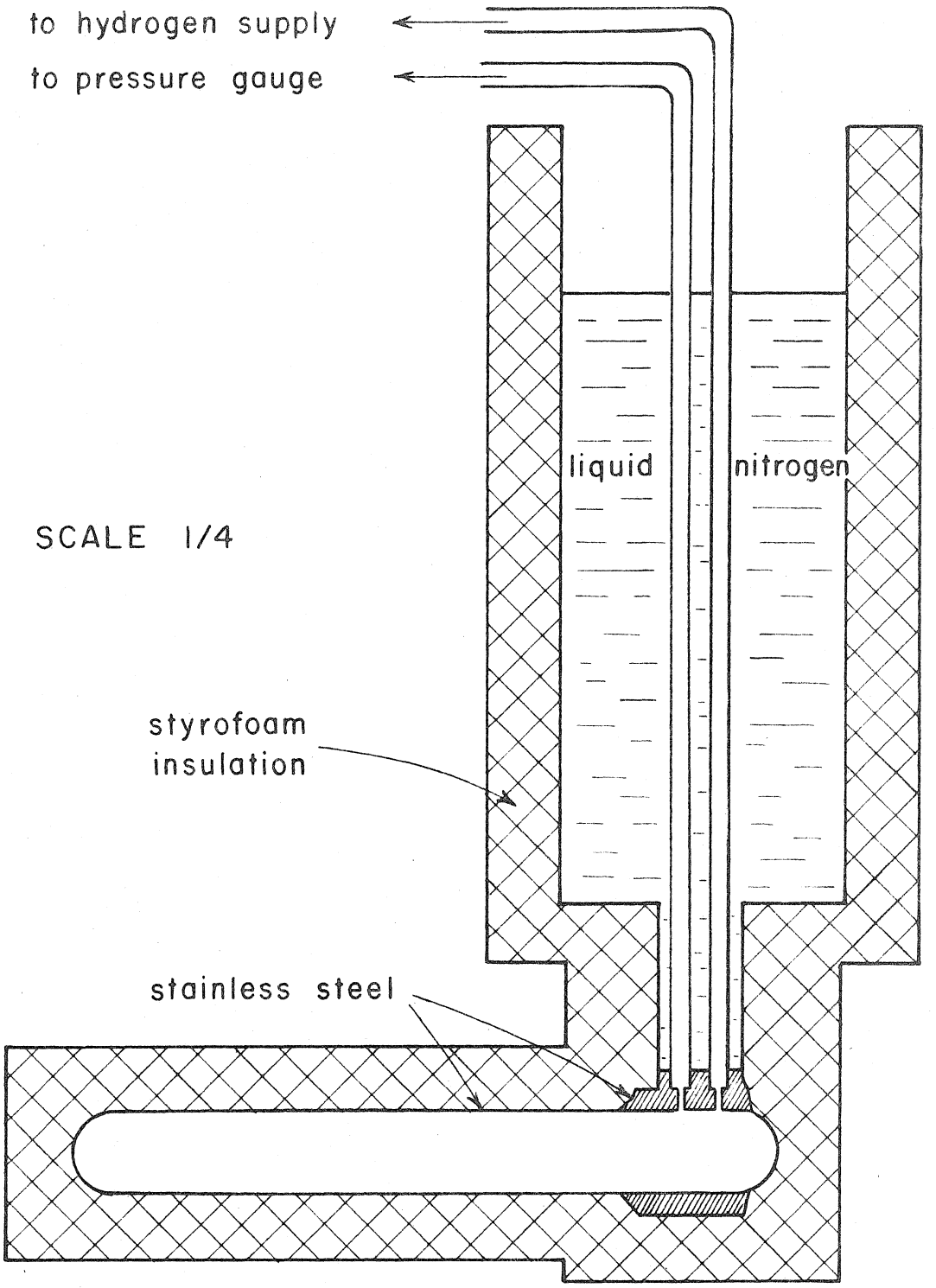
to hydrogen supply
to pressure gauge
liquid
nitrogen
SCALE 1/4
styrofoam
insulation
stainless steel

excluding the particles produced in the steel ends) by a tungsten and lead slit system placed near the target. The solid angle of acceptance of the spectrometer, 0.02 steradians, was determined by a lead aperture placed within the 10 cm. gap between the pole pieces 120. cm. from the target. This aperture was 25 cm. wide, about 6.5 cm. high, and was defined by lead which was about 10 cm. thick (in the direction along the trajectories) and was placed so that it intercepted particles from the target which were scattered from the pole surfaces. The dispersion of the spectrometer was such that particles accepted by the counters had momenta within $\pm$ 8 $^{o}/o$ of the central momentum. The central momentum was adjustable to a maximum of 255 Mev/c at a field of 1.4 w/m^2 (corresponding to a pion energy of 150 Mev). Lead "bridges" between the target and the magnet shielded the entrance of the spectrometer from charged particles produced in the air. Additional lead shielded the counters of the spectrometer so that only particles which traversed the spectrometer were detected. The design of the spectrometer and experimental tests of the magnet are described in a separate report (35).

E. The π^- Counter System

The π^- counter system consisted of three scintillation counters (C_1, C_2, C_3) and one Čerenkov counter (C_4). The first two counters were 15 cm. wide and determined the momentum acceptance interval. The last two counters were 18 cm. and 20 cm. wide, respectively, and they intercepted all particles which traversed the first two (see Table I for the dimensions of all counters). Minimum ionizing particles gave

TABLE I.

Counter	Material	Height	Width	Thickness	Phototube
C_1	Plastic Scin.	22.8 cm.	15.2 cm.	0.635 cm.	RCA 5819
C_2	"	22.8	15.2	1.27	"
C_3	"	25.4	17.8	1.27	Dumont 6292
C_4 ($\check{C}$)	Lucite	27.9	20.3	5.08	Dumont 6363
C_5	Liquid Scin.	22.8	15.2	2.54	RCA 6655
C_6	"	22.8	15.2	2.54	"
C_7	"	30.5	25.4	2.54	"

a pulse spectrum with a well-defined peak in all three scintillation counters. The Čerenkov counter response depended on the velocity of the particles, consequently, pions and electrons with the same momentum could be distinguished. Lead absorbers about 0. 3 cm. thick each were placed after the first and after the second scintillation counters. These had little influence on the pions traversing the counters, but served to remove a large background of spurious coincidences. This counter system was identical to the one used by Bloch who described the design of the system in detail (20).

F. The π^+ Telescope

The π^+ telescope consisted of three scintillation counters (C_5, C_6, C_7) and three lead absorbers (A_5, A_6, A_7) (see figure 1). The dimensions of the counters are given in Table I, and the absorber thicknesses are given in Table IV. The largest counter (C_7) was placed in the last position and intercepted all particles which traversed the first two counters and penetrated all three absorbers. For those particles which traversed the first two counters or which traversed all three counters, the solid angle subtended by the telescope was defined by the second counter. The solid angle was typically 0. 1 steradians. Minimum ionizing particles gave a pulse spectrum with a well-defined peak in all three counters. The energy interval of the particles traversing the telescope was determined from their range in the lead absorbers. By a suitable selection of lead bricks and lead sheets any desired absorber thickness could be obtained to within 0. 6 cm.

G. Electronics

Figure 5 is a block diagram of the electronics used in this experiment. The outputs of all seven counters were first amplified and shaped in preamplifiers located near the counters. The Model 25 Preamp. has a rise time of less than 0.05 microseconds and delay line clipping. The Čerenkov Preamp. has a rise time of 0.15 microseconds and delay line clipping. The pulse width for each counter is shown in figure 6. The signals were brought from the experimental area on 25 meters of RG-114 U coaxial cables. The outputs from counters 1, 3, 4, and 5 were amplified (the Model 522A Amplifier has a rise time of 0.07 microseconds), and the amplified signals from counters 1, 3, and 5 were fed to a coincidence circuit which was biased to operate on pulse amplitudes well below the peaks of the pulse distribution from each of the three counters. The coincidence circuit registered those events which gave pulses in all three counters within the resolving time of 0.25 μ sec. The signals from counters 2, 6, 7, and the unamplified signal from counter 1 were passed through different lengths of delay cable and mixed in a linear adding circuit. The amplified signals from counters 3, 4, and 5 were delayed by different amounts and combined in another adding circuit. Finally the pulse train (3, 4, 5) was attenuated and mixed with the pulse train (1, 2, 6, 7). The single pulse train which contained the outputs of all seven counters went to the vertical input of a Model 531 Tektronix oscilloscope. The output signal from the coincidence circuit was used to trigger the sweep circuit of the oscilloscope, and the trace was photographically

Figure 4. Electronics Block - Diagram.

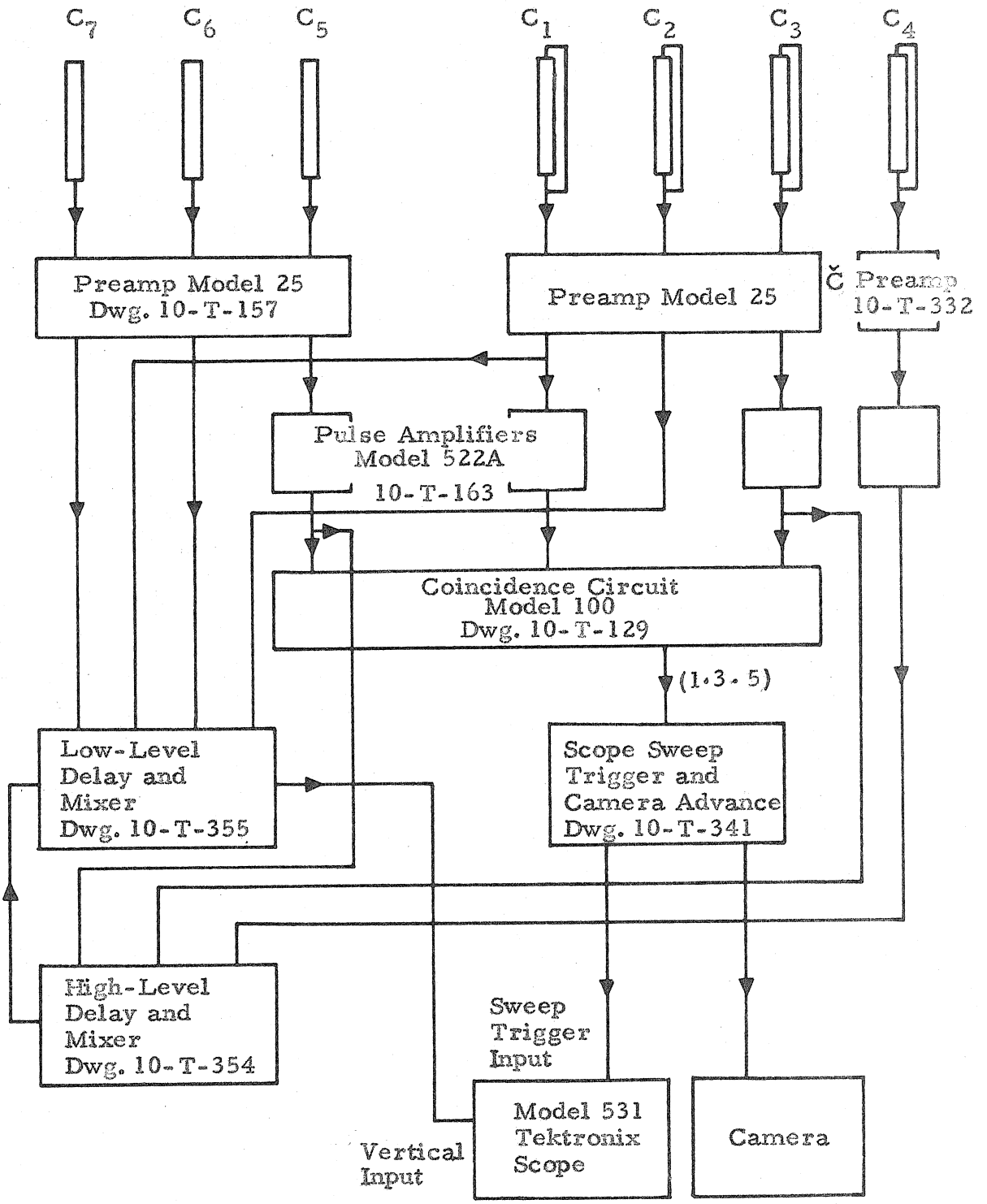
C7
C6
C5
C1
C2
C3
C4
Preamp Model 25
Dwg. 10-T-157
Preamp Model 25
Č Preamp
10-T-332
Pulse Amplifiers
Model 522A
10-T-163
Coincidence Circuit
Model 100
Dwg. 10-T-129
(1·3·5)
Low-Level
Delay and
Mixer
Dwg. 10-T-355
Scope Sweep
Trigger and
Camera Advance
Dwg. 10-T-341
High-Level
Delay and
Mixer
Dwg. 10-T-354
Sweep
Trigger
Input
Vertical
Input
Model 531
Tektronix
Scope
Camera

recorded. (The details of the data presentation and recording are given in the following section.) Because of the faster rise time of those pulses which were not amplified in the Model 522A, they were assigned the shortest pulse widths (with the exception of counter 1). The high frequency response of the delay line was such that these short pulse had to have the shortest delays in order to preserve this fast rise time, therefore, the pulses from counters 2, 6, and 7 are first in the sequence shown in the pulse train in figure 6.

The number of single pulses from either counter 1, 3, or 5 was monitored during each run by a binary scaler followed by a decimal scaler. The (1·3) and (1·3·5) coincidence rates were registered in decimal scalers. All scalers and the oscilloscope sweep trigger were turned on only during the x-ray spill-out time by a "beam-gate" pulse (about 40 m.sec. long). The total on-time of each run was determined by counting in one of the gated scalers pulses from a source which provided pulses at a uniform rate of 120 pulses per second.

H. Data Recording

A drawing of the pulse train for a true coincidence in all counters is shown in figure 6. The shape, width, and sign of any pulse was distinctive so that a pulse from a particular counter was easily identified. The oscilloscope trace was photographed by a Model 200-P Bell and Howell 16 mm. movie camera which was modified by the Traid Corporation so that it would advance the film one frame when supplied with a 28 v. pulse for 1/4 second. The camera shutter had been

Figure 6. Pulse Train Showing True Coincidence in all Seven Counters. (1 • 2 • 3 • 4 • 5 • 6 • 7)

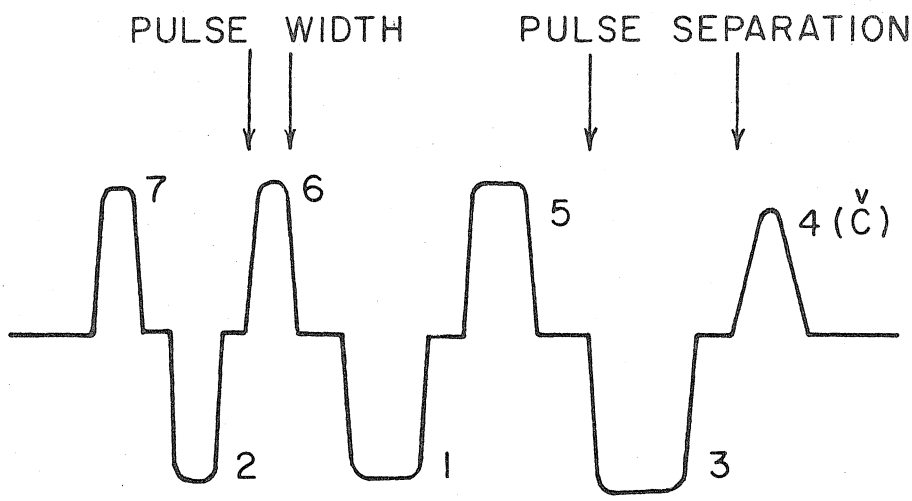

COUTER	PULSE WIDTH	SIGN	SEPARATION
7	0.15 μsec.	+	
			0.5 μsec.
2	0.225	−	
			0.5
6	0.15	+	
			0.65
1	0.45	−	
			0.65
5	0.3	+	
			0.8
3	0.4	−	
			0.8
4	0.25	+	

removed so that the camera was always open and recorded all oscilloscope traces. The film advanced one frame after each x-ray spill-out time interval during which the coincidence circuit registered a (1 • 3 • 5) event. The trigger to the sweep circuit of the oscilloscope and the pulse to advance the film were both supplied by the Sweep Trigger and Camera Advance circuit which was itself triggered by the output of the coincidence circuit. The camera lens was a Bell and Howell Augenieux with a focal length of 2.4 cm, f/0.95, and a minimum object distance of 18 inches. A 1/16 inch spacer was placed between the lens and the camera so that the image of the oscilloscope trace was 9 mm. long on the film, and the object distance was 12 inches. The magnification was 0.09. The camera was operated at f/0.95 and with the distance setting at 10 feet. The film used was Cine-Kodak Tri-X Negative.

The π^- production data was recorded electronically as described in the work of Bloch and Sands (20, 21).

1. Data Reading

The data film was examined frame by frame in a projector which magnified about 3x and presented the image on a ground glass with a graticule. The graticule allowed a measurement of pulse heights and relative positions of the pulses in the train. In fact, millimeters on the graticule were used as the time scale for measuring the relative time between pulses. One millimeter corresponded to about 0.1 μ sec. A picture of the pulse train for a true coincidence in all counters was obtained by introducing a signal from a pulser in parallel with each

counter. From this picture an overlay was made and all frames were checked against this standard. The resolving time of the coincidence measurement was determined by the ability to resolve visually the displacements of the pulses from their expected positions as shown on the overlay. The "resolving time" was estimated to be $\pm$ 0.2 mm on the graticule, and hereafter will be called the resolving displacement.

For those events listed below the pulse amplitude from each counter was recorded. The following biases were set on the pulses (in units of mm. on the graticule). Counters 2, 6, and 7 had biases set at 1 mm, pulses smaller than this could not be definitely identified in the visual scanning; counters 1, 3, and 5 had biases set at about 3mm. by the electronic biases of the coincidence circuit (see figures 11 and 12); and counter 4 had a bias set at 2 mm. (see Section III.B.1.). In the case of all counters except counter 4 the biases were well below the peaks in the pulse spectra. The information which was recorded from the film was the number of each of the events listed below for each telescope setting (in units of the number of events per unit energy flux in the x-ray beam).

$$N_{56} = (1 \cdot 2 \cdot 3 \cdot \overline{4} \cdot 5 \cdot 6 \cdot \overline{7})$$

$$N_{567} = (1 \cdot 2 \cdot 3 \cdot \overline{4} \cdot 5 \cdot 6 \cdot 7)$$

$$N_{456} = (1 \cdot 2 \cdot 3 \cdot 4 \cdot 5 \cdot 6 \cdot \overline{7})$$

$$N_{4567} = (1 \cdot 2 \cdot 3 \cdot 4 \cdot 5 \cdot 6 \cdot 7)$$

N^{a}_{56} = $(1 \cdot 2 \cdot 3 \cdot \overline{4})$ event and a $(5 \cdot 6 \cdot \overline{7})$ event within the resolving displacement of $\pm$ 2.0 mm.

N^{a}_{567} = $(1 \cdot 2 \cdot 3 \cdot \overline{4})$ event and a $(5 \cdot 6 \cdot 7)$ event within the resolving displacement of $\pm$ 2.0 mm.

The conventional is used of a bar over a number to indicate no pulse from that particular counter. Figure 7 shows an enlargement of the data film with some typical events.

Figure 7. Oscilloscope Traces Showing Typical Events.

TRUE COINCIDENCE
FROM PULSER

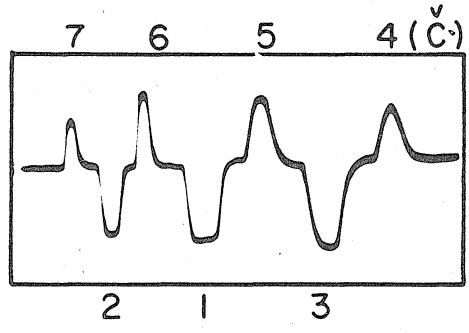

(a.)

π PAIR FROM PHOTON
IN RANGE 825 – 1080 MEV

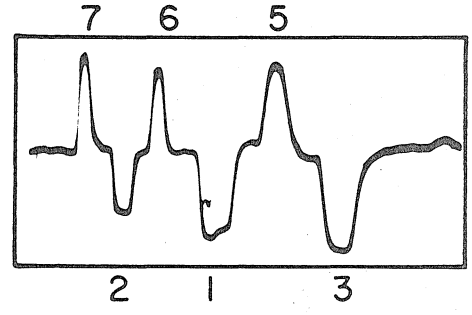

(b.)

(c.)

π PAIR FROM PHOTON
IN RANGE 650 – 825 MEV.

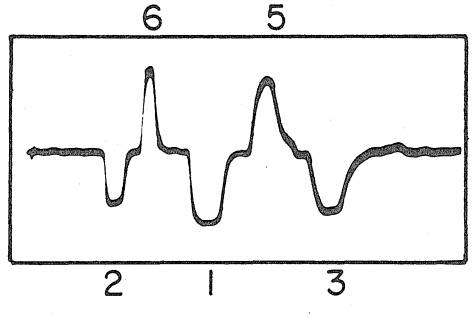

(d.)

ELECTRON PLUS 5 ACCIDENTAL

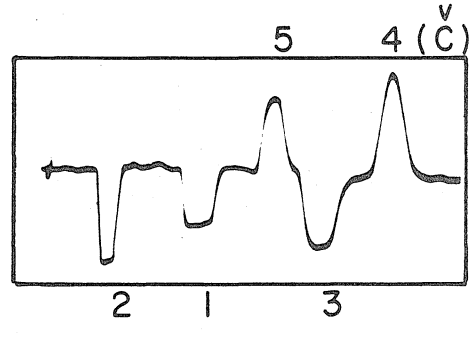

III. EXPERIMENTAL PROCEDURE

A. Kinematics

There are a total of ten kinematical parameters which describe the pair reaction. Of these ten, one is arbitrary (the plane from which azimuthal angles are measured), and four can be expressed in terms of the others from energy and momentum conservation. This leaves five independent variables and the one arbitrary choice. The angular coordinates of all the particles in the reaction are defined in figure 8, and we have defined the five independent parameters to be the zenith angle (θ_-) and the total energy (E_-) of the π^-, the zenith angle (θ_+) and the azimuthal angle (ϕ_+) of the π^+, and the photon energy. The expression for the momentum of the π^+ in terms of these quantities is:

$$p_+ = \frac{AB + C\left[A^2 - \mu^2 (C^2 - B^2)\right]^{\frac{1}{2}}}{C^2 - B^2} \qquad (2)$$

where:

$$A = kM + kp_- \cos\theta_- + \mu^2 - kE_- - ME_-$$

$$B = k\cos\theta_+ - p_- (\sin\theta_+ \sin\theta_- \cos\phi_+ + \cos\theta_+ \cos\theta_-)$$

$$C = k + M - E_-$$

$$k = \text{photon energy}$$

$$M = \text{proton mass}$$

Figure 8. Definition of the Angular Coordinates for Each Particle in the Pair Process.

$$\gamma + p \rightarrow \pi_- + \pi_+ + p$$

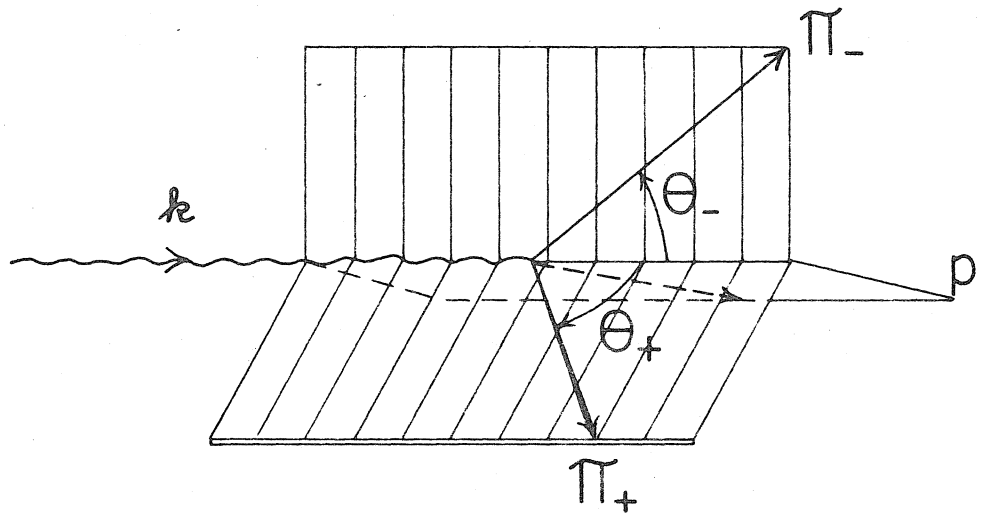

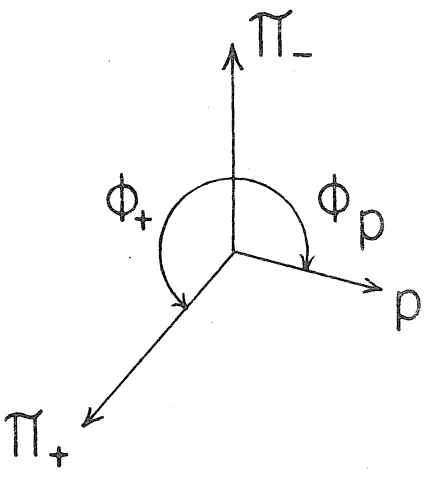

PARAMETERS

k

T_-, θ_-

T_+, θ_+, ϕ_+

T_p, θ_p, ϕ_p

INDEPENDENT PARAMETERS

$k, T_-, \theta_-, \theta_+ \phi_+$

$k = F(T_-, \theta_-, \theta_+ \phi_+, T_+)$

μ = pion mass

p_- = π^- momentum

E_- = π^- total energy

Setting $\theta_- = 35^\circ$ and $E_- = 290$ Mev, the kinetic energy of the π^+ was computed as a function of θ_+ for several photon energies and is shown in figures 9 and 10 for $\phi_+ = 180^\circ$ and 90°, respectively.

From the kinematics of the reaction and the range-energy curves for lead, it was possible to choose the telescope absorbers so that those π^+ (in coincidence with a π^- event in the spectrometer) which penetrated A_5 and A_6 but not A_7 were produced in pairs initiated by photons in the energy interval from 650 to 825 Mev. Those π^+ (in coincidence with a π^- event in the spectrometer) which penetrated A_5, A_6, and A_7 were produced in pairs initiated by photons with energies greater than 825 Mev but less than 1080 Mev (the bremsstrahlung cut-off energy throughout the experiment). The windows set by the telescope are shown in figure 9 in the case $\theta_+ = 45^\circ$ and $\phi_+ = 180^\circ$. Due to multiple scattering the effective path length of π^+ in the absorbers was greater than the absorber thickness (this problem has been studied by Worlock (36)). When the absorbers were chosen for each π^+ direction, it was this effective length which was used to determine the correct thicknesses from the range - energy curves. In Table IV both the geometric and effective thicknesses are given.

Figure 9. Kinetic Energy of the π^+ as a Function of θ_+ for $\phi_+ = 180^\circ$. The window set by the telescope is shown for $\theta_+ = 45^\circ$.

Figure 10. Kinetic Energy of the π^+ as a Function of θ_+ for $\phi_+ = 90^\circ$.

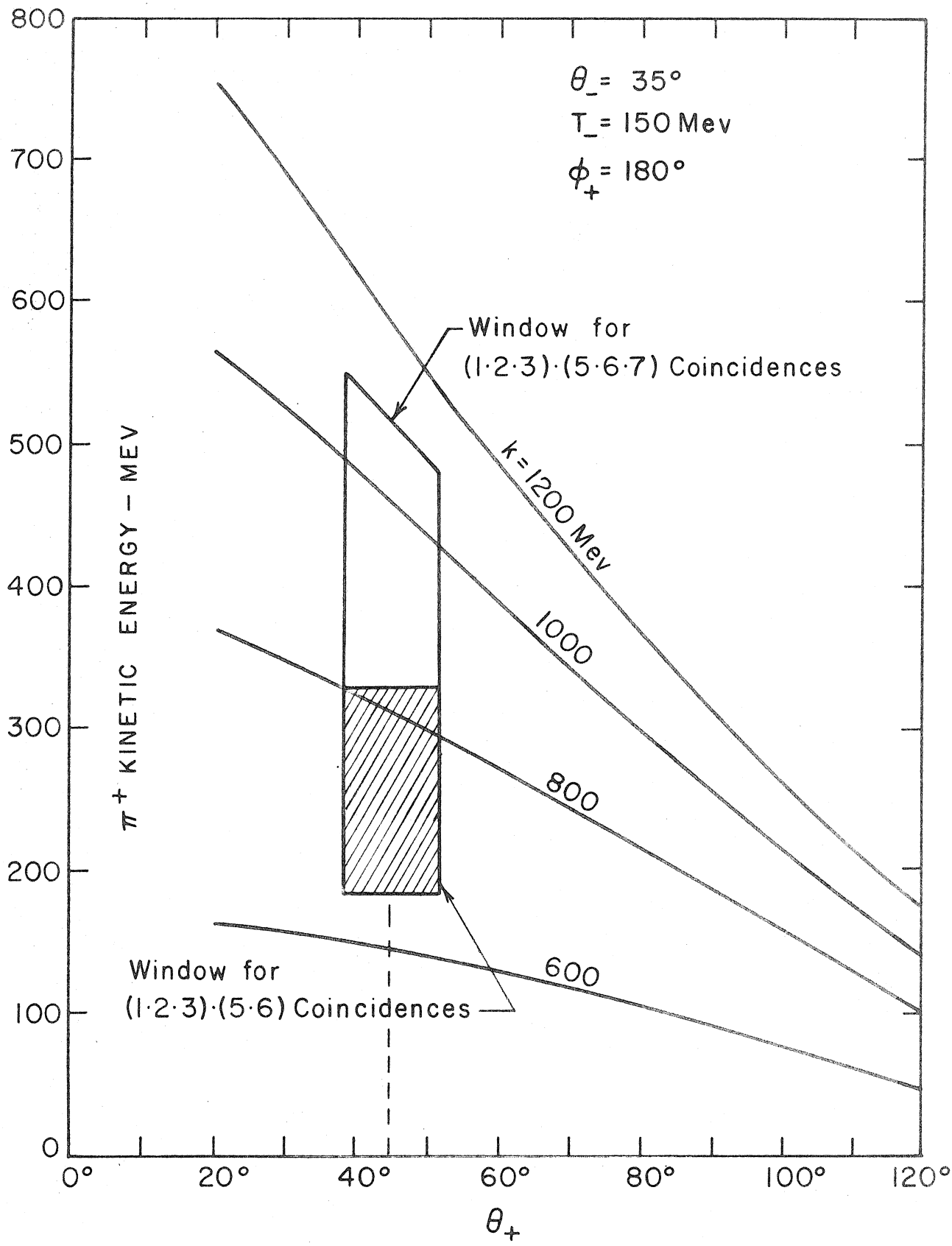
800
700
600
500
400
300
200
100
0
0°
20°
40°
60°
80°
100°
120°
θ_+
π^+ KINETIC ENERGY – MEV
θ_- = 35°
T_- = 150 Mev
ϕ_+ = 180°
Window for
(1·2·3)·(5·6·7) Coincidences
k = 1200 Mev
1000
800
600
Window for
(1·2·3)·(5·6) Coincidences

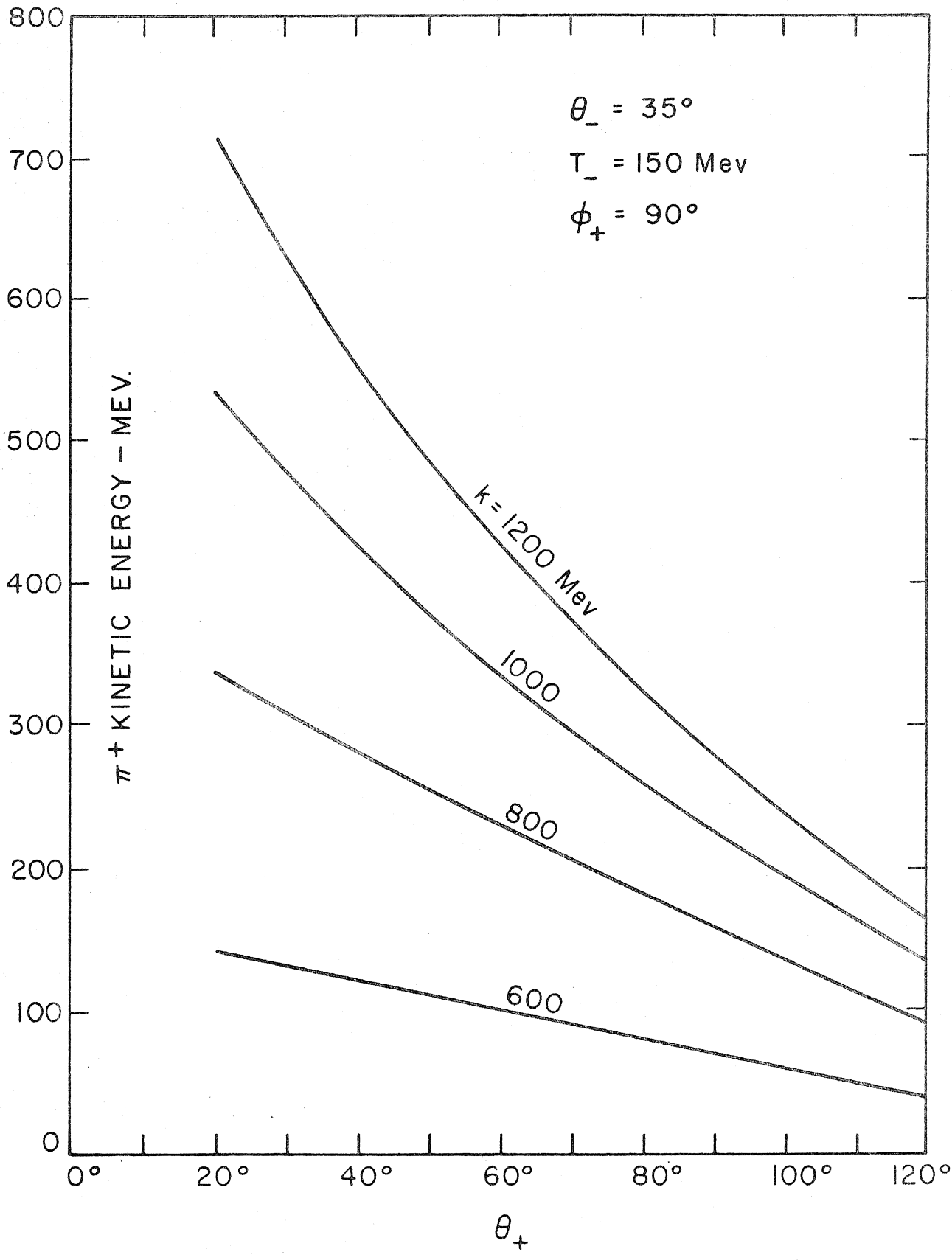
800
700
600
500
400
300
200
100
0
θ_- = 35°
T_- = 150 Mev
ϕ_+ = 90°
K = 1200 Mev
1000
800
600
π+ KINETIC ENERGY – MEV.
0°
20°
40°
60°
80°
100°
120°
θ_+

B. Preliminary Measurements

Measurements were made of the response of the π^- counters to pions and to electrons, and the response of the π^+ counters to minimum ionizing particles. The results of these measurements were used to check the identity of the particles being counted in the coincidence between the spectrometer and the telescope. Other measurements were made to check that the observed reaction was pair formation. These measurements are described below.

1. π^- Identification

The requirements which had to be satisfied in order that the negative particles traversing the magnet could be identified as pions were: (a) a 3-fold coincidence in the scintillation counters, (b) a pulse height spectrum similar to one obtained with only pions traversing the counters, and (c) a pion-like response in the Čerenkov counter. To obtain an intense, essentially pure pion beam traversing the counters a low Z, high hydrogen density material (CH_2) was used as a target, and the magnet was set to accept high energy positive particles (150 Mev). Under these conditions the number of electrons counted was negligible within the counting statistics and knowledge of the Čerenkov efficiency for pions and electrons. The pulse height spectrum of these pions in all three counters was measured with an 8-channel pulse-height analyser, and it was assumed that these distributions would be the same for both positive and negative mesons. In order to check these distributions against the pulse-height distributions in the three counters taken from the data, the analyzer and the amplitudes

of the pulses on the data film were calibrated with a pulser. In figure 11 the comparison of the two distributions is shown for counter 1. The smooth curve is the distribution measured in the analyzer and the histogram is taken from the data film for $\pi^+ - \pi^-$ coincidence events. The agreement is satisfactory.

The pion beam was also used to measure the pion response of the Čerenkov counter. A coincidence in counters 1, 2, and 3 was used to trigger the oscilloscope sweep, and the trace containing the normal pulse train was photographed. The film was examined and the height of the pulses from counter 4 was recorded for each (1·2·3) event. The result of the measurement was that 5 °/o of the pions gave a pulse in counter 4 greater than 2 mm. The Čerenkov response was assumed to be the same for both positive and negative pions.

The Čerenkov response to electrons was measured with a pure electron beam traversing the counter system. This electron beam was obtained by using a lead target, and setting the magnet for a low enough momentum (90 Mev/c) so that pions of this momentum were not able to penetrate the two absorbers in the counter system. The result of this measurement was that 75 °/o of the electrons gave a Čerenkov pulse greater than 2 mm. At the momentum 90 Mev/c the electrons are extremely relativistic ($\beta = 1 - 1.5 \times 10^{-5}$). Neither the intensity nor the angle of Čerenkov emission is sensitive to small changes in β for velocities above the threshold (the threshold for Čerenkov light was $\beta = 0.67$, however, the counter was designed by Bloch (20) so that little of the Čerenkov light reached the phototubes

Figure 11. Comparison of the Pulse - Height Distributions for Pions and those Particles Assumed to be π^- from the Pair Reaction. (Counter 1)

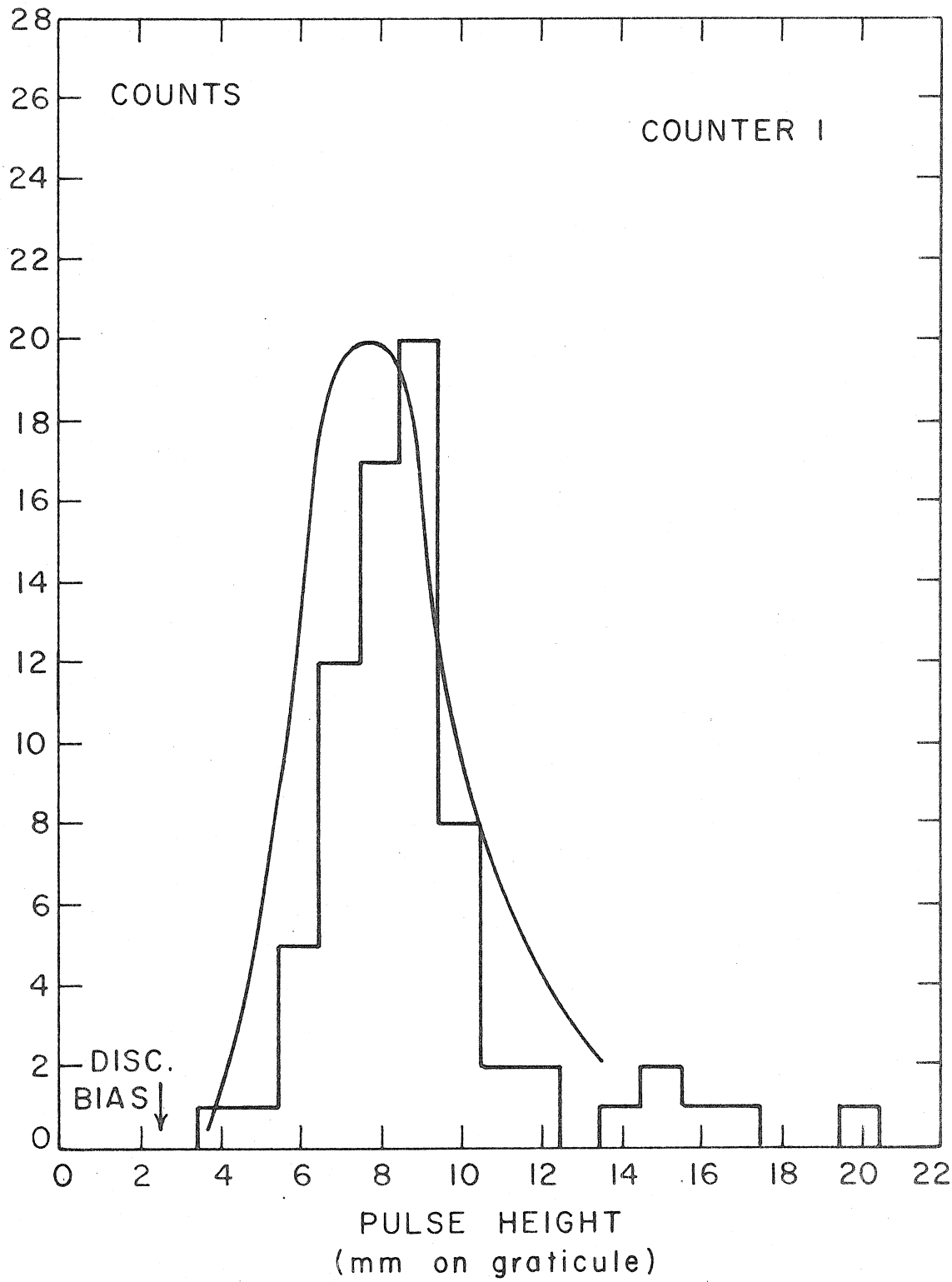
COUNTS
COUNTER I
28
26
24
22
20
18
16
14
12
10
8
6
4
2
0
DISC.
BIAS
0
2
4
6
8
10
12
14
16
18
20
22
PULSE HEIGHT
(mm on graticule)

until the β for internal reflection was exceeded ($\beta = 0.9$). The Čerenkov response to 90 Mev/c electrons was, therefore, assumed to be the same as for 255 Mev/c electrons ($\beta = 1 - 2 \times 10^{-6}$) which corresponded to the magnet setting at which the experiment was done.

As stated in Section II. I., the bias set on pulses from counter 4 was 2 mm. From the measurements described above, the Čerenkov efficiencies for pulses greater than 2 mm are:

$$\epsilon_{\pi} = 0.05$$

$$\epsilon_{e} = 0.75$$

These efficiencies are used in Section IV. B. 2 to determine the number of events in which an electron was detected in the spectrometer in coincidence with a π^+ in the telescope.

2. π^+ Identification

No restriction was placed on the charge of the particles traversing the telescope, and the only requirement which had to be satisfied in order to accept the particles as pions was their ability to penetrate at least the first two absorbers. The identification of these particles in the case of a coincidence between the telescope and the spectrometer is discussed in the following section. It was possible, however, to estimate the contribution to all the particles traversing the telescope due to nucleons, electrons, or mesons.

(a) Nucleon Component

No proton produced in a photo-reaction would have enough energy to penetrate the first two absorbers, and a neutron would not be

detected by the scintillation counters (neglecting the effect of the neutron producing a charged knock-on in each counter). Nucleons could produce penetrating charged secondaries by inelastic collisions in the absorbers, however, and these secondaries could be counted. Several workers have examined the problem of meson production from nucleon-nucleus collisions (37, 38, 39), and using their results it was possible to compute the counting rate due to nucleon-produced secondaries. This counting rate was less than 1 $^{o}/_{o}$ of the observed (5 · 6) rate from hydrogen.

(b) Electron Component

Electrons or γ-rays striking the front absorber would initiate showers which would dissipate themselves in the absorbers. It was possible to compute the number of electrons emitted from the steel ends of the hydrogen target in the direction of the telescope, and using Wilson's shower curves (40), it was seen that electron initiated showers contributed much less than 1 $^{o}/_{o}$ of the observed (5 · 6) counting rate.

(c) Meson Component

Using the cross-section for the photoproduction of π^{+} from hydrogen measured at Cal Tech (8), and assuming that the cross-section increases as $A^{2/3}$ for more complex nuclei, it was possible to estimate the number of mesons emitted from the hydrogen target (including the steel ends) in the direction of the telescope. Assuming, further, that the absorption cross-section for mesons in the telescope absorbers was geometric, the (5 · 6 · 7) counting rate was computed to

be 130 ± 10 °/o counts/BIP at 90°. The measured rate was 120 ± 11 which is satisfactory agreement and indicates that essentially all the telescope counting rate was due to mesons. (The number of mesons of both charge from the steel ends of the target was computed to be 20 °/o of those from the hydrogen, consequently, roughly 90 °/o of the telescope counting rate was due to π^+.)

The pulse-height spectrum in all three counters was measured for minimum ionizing pions. For counters 5 and 6 the spectrum was measured with an 8-channel pulse-height analyzer which was gated so that it accepted pulses when there was a coincidence in counters 5, 6, and 7. Absorber A_7 was chosen so that pions which gave (5 · 6 · 7) events were energetic enough to be minimum ionizing in counters 5 and 6. In order to measure the spectrum in counter 7 for minimum ionizing pions, a fourth counter (called counter 8) was placed behind the telescope with 4 inches of lead between it and counter 7. The gate to the analyzer was opened by (5 · 6 · 8) events. Counter 8 was 3" x 3" and so only the response of a part of the area of counter 7 could be measured at one time. By moving counter 8 to various positions a map of the response of counter 7 to minimum ionizing particles over its total area was measured, and at all points there was a well-defined peak in the pulse spectrum. The distribution measured in each counter was compared to the pulse-height distribution taken from the data film for $\pi^+ - \pi^-$ coincidences. This comparison is shown in figure 12 for counter 5, and indicates that the particles accepted as π^+ did have the pulse spectrum of minimum ionizing particles.

Figure 12. Comparison of the Pulse-Height Distributions for Pions and those Particles Assumed to be π^+ from the Pair Reaction. (Counter 5)

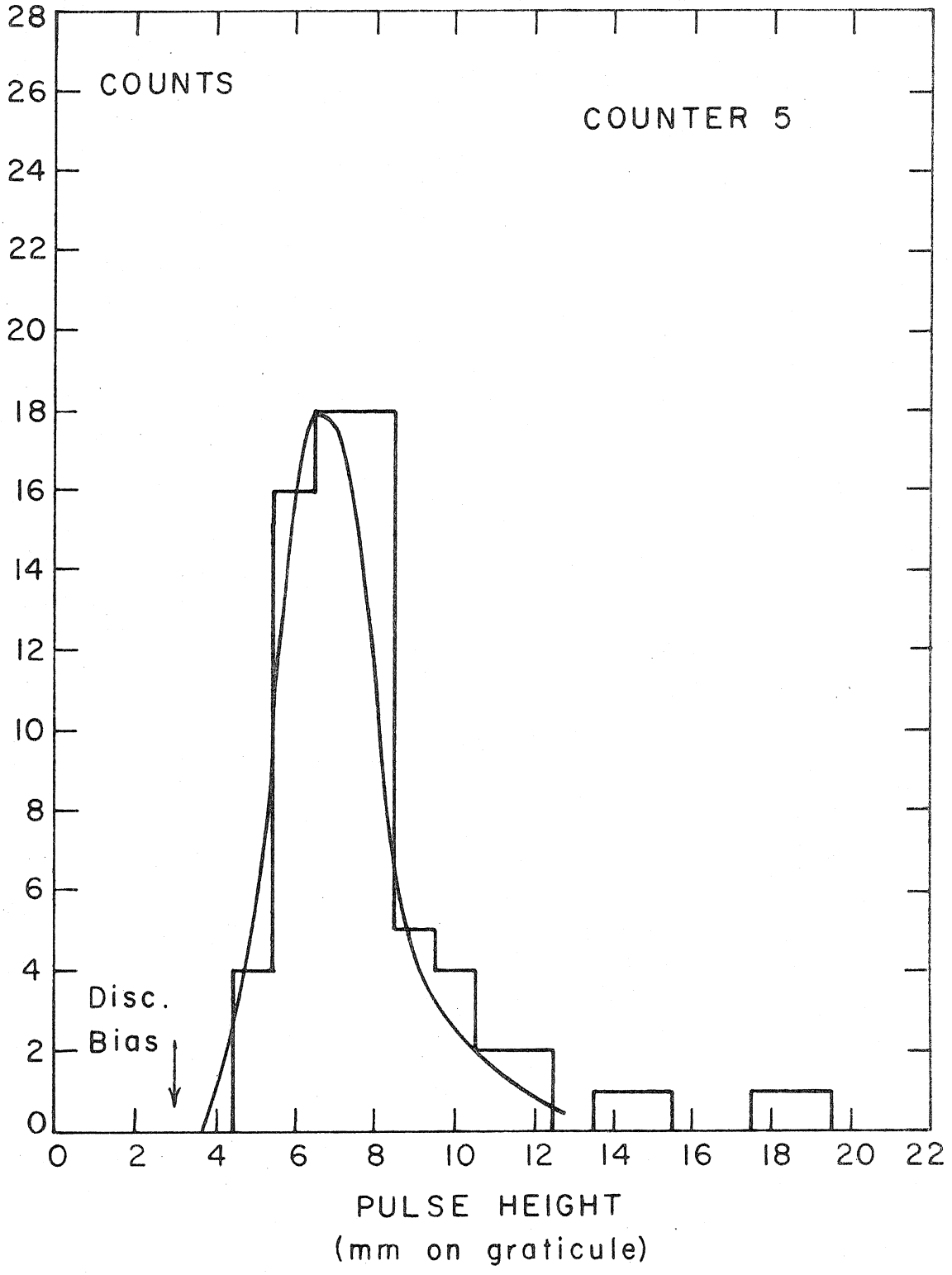
COUNTS
COUNTER 5
28
26
24
22
20
18
16
14
12
10
8
6
4
2
0
Disc.
Bias
0
2
4
6
8
10
12
14
16
18
20
22
PULSE HEIGHT
(mm on graticule)

3. Reaction Identification

Several different measurements were made in order to demonstrate that the observed events (a coincidence between a count in the telescope and a count in the spectrometer) were due to the two pions from the reaction $\gamma + P \rightarrow P + \pi^+ + \pi^-$.

a. The reaction was produced in hydrogen. Empty target runs gave no coincidences in an accumulated running time which would normally have given 100 coincidences from the hydrogen - filled target. These runs were interspersed with the runs with the target filled.

b. The π^+ and π^- were in coincidence within the resolving time of the coincidence measurements. If the count in the spectrometer and the count in the telescope came from unrelated events, then the time separation of the two events should be random (within the 0.25 μsec. resolving time of the coincidence circuit which was triggered by a (1·3·5) event). Such a random distribution was found, but was always 10 °/o or less of those $\pi^+ - \pi^-$ events which had a time separation of less than ± 20 mμ sec. (the "resolving time" of the measurements made on the projection of the photographs). Figure 13 shows the number of $\pi^+ - \pi^-$ events as a function of the time separation of the two events. The data shown is the sum of all events taken at the angles $\theta_+ = 45^\circ$, 90°, and 120° for $\phi_+ = 180^\circ$.

c. Two points on an excitation curve were measured. With the telescope set a $\theta_+ = 45^\circ$ and $\phi_+ = 90^\circ$, data was taken in the usual case for photons in the energy interval from 650 to 825 Mev. The absorbers were then changed ($A_5 = 0.64$ cm., $A_6 = 0.64$ cm., and

Figure 13. Number of (1 · 2 · 3) and (5 · 6) Events as a Function of Their Relative Displacement in Time. (Unit of time is 0.1 μ sec per mm.)

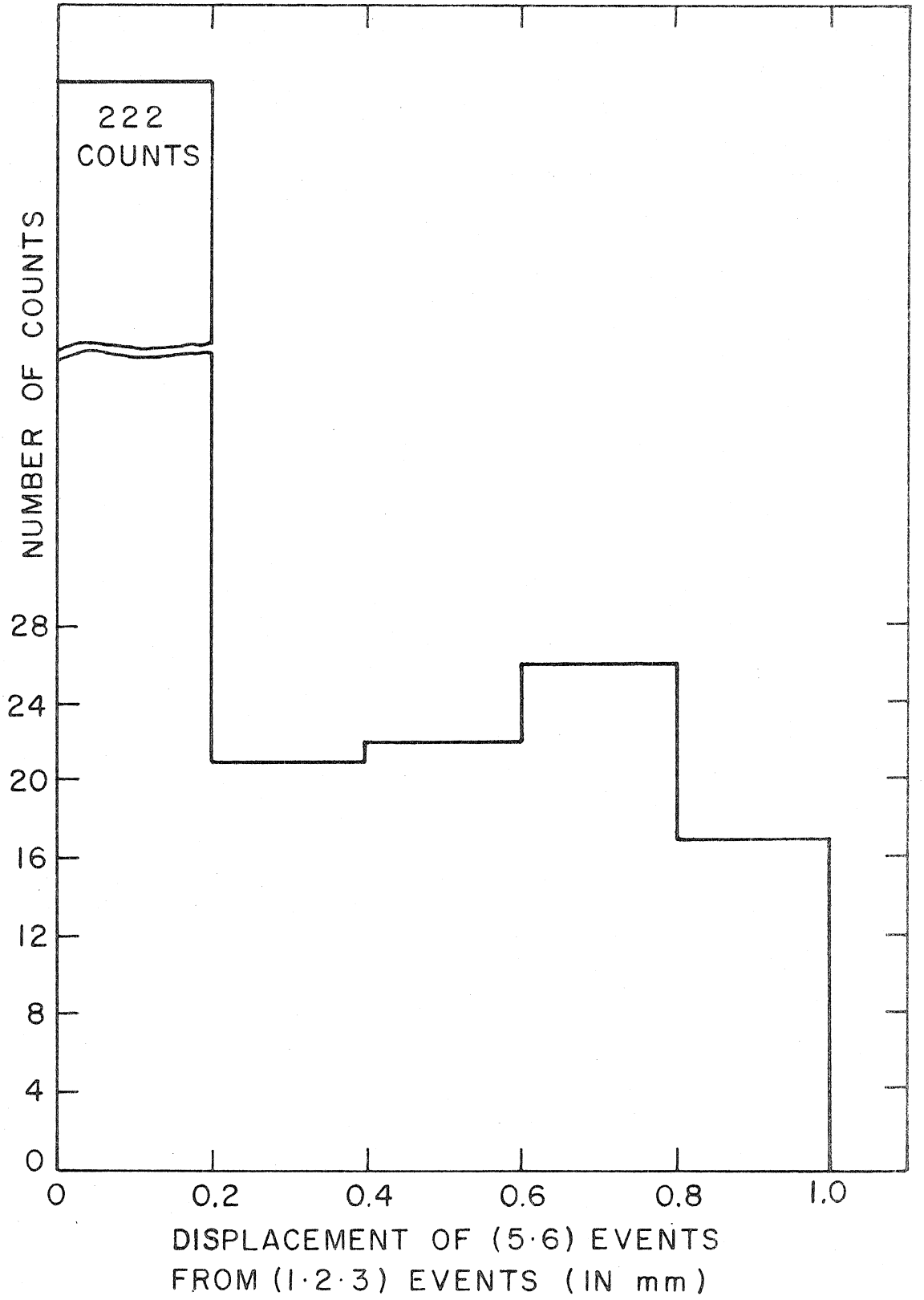
222
COUNTS
NUMBER OF COUNTS
28
24
20
16
12
8
4
0
0
0.2
0.4
0.6
0.8
1.0
DISPLACEMENT OF (5·6) EVENTS
FROM (1·2·3) EVENTS (IN mm)

A_7 = 5.0 cm.) so that all $\pi^+ - \pi^-$ coincidences which gave a $(1 \cdot 2 \cdot 3 \cdot \overline{4} \cdot 5 \cdot 6 \cdot \overline{7})$ were initiated by photons in the energy interval from 520 to 610 Mev (holding E_o = 1080 Mev). The results of the two measurements are shown in figure 14 and appear to be consistent with an excitation function falling to zero at threshold, but due to the large error are not conclusive.

d. The $\pi^+ - \pi^-$ coincidence rate was measured at $\theta_+ = 45^o$ and $\phi_+ = 180^o$ for the three negative pion kinetic energies 50, 100, and 150 Mev, choosing the telescope absorbers in each case so that the initiating photons were in the energy interval from 650 to 825 Mev (holding E_o = 1080 Mev). (See Table II for the absorber thicknesses in each case.) By the method described in Section IV. B., the cross-section for the reaction was deduced from the counting rates and transformed to the center-of-mass system of the reaction. The results are given in Table II. The π^- production rate was also measured for the two kinetic energies 100 and 150 Mev at both E_o = 825 Mev and E_o = 650 Mev. By the method described in Section IV. A., the cross-section for π^- production was deduced for photons in the energy interval from 650 to 825 Mev and transformed to the C. M. system. The results are given in Table II along with the cross-section at T_- = 50 Mev measured by Woodward et al. (17). If the π^+ from the pair is assumed to be emitted isotropically in the C. M. system, then the π^- C. M. cross-sections should be equal to 4π times the C. M. cross-sections deduced from the $\pi^+ - \pi^-$ coincidence rate for each of the three T_-. The comparisons are given in Table II and indicate

Figure 14. Excitation Function at $\theta_+ = 45^\circ$ and $\phi_+ = 90^\circ$.

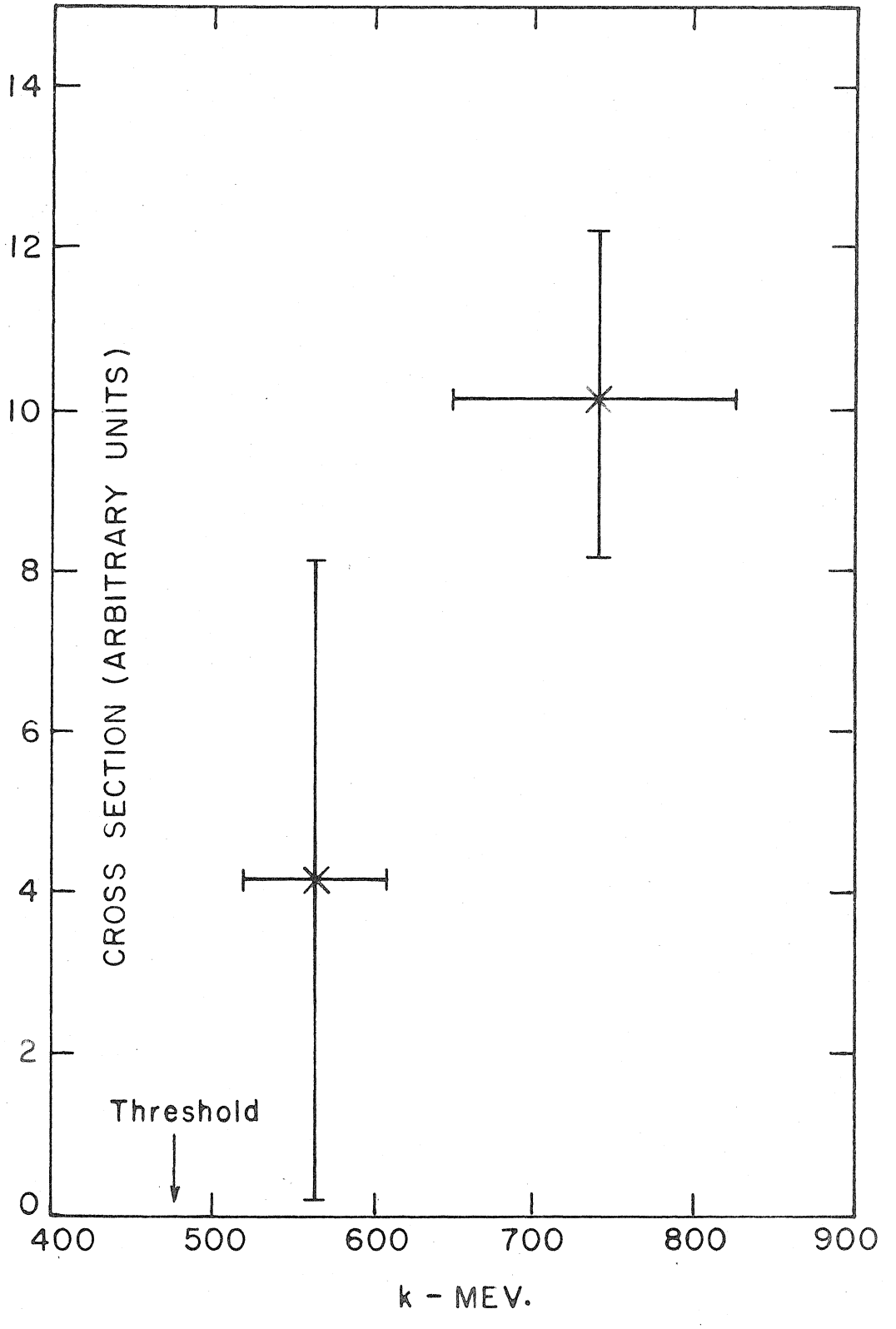
14
12
10
8
6
4
2
0
CROSS SECTION (ARBITRARY UNITS)
Threshold
400
500
600
700
800
900
k - MEV.

TABLE II.

T_-	T_+	A_5	A_6	A_7	σ_{+-} (C. M.)	σ_- (C. M.)	$\frac{\sigma_-(\text{C. M.})}{4\pi}$
50 Mev	325 Mev	11.4 cm	6.35 cm.	10.2 cm.	$1.1 \pm 1.5 \times 10^{-33}$	$3.4 \pm 1.1 \times 10^{-32}$ (from Cornell data)	$2.7 \pm 0.9 \times 10^{-33}$
100	300	10.2	5.08	10.2	3.6 ± 0.9	3.8 ± 0.68	3.07 ± 0.54
150	270	6.35	5.08	11.4	3.2 ± 0.6	4.14 ± 0.56	3.30 ± 0.45

σ_{+-} in units cm^2/Mev-(Ster.)^2

σ_- in units cm^2/Mev-Ster.

that within the errors the $\pi^+ - \pi^-$ cross-section has the same T - dependence as the π^- cross-section.

e. The $\pi^+ - \pi^-$ cross-section when integrated over the π^+ directions gave the same result as was obtained by measuring the π^- cross-section directly (see Sections IV. A. and IV. B.). By extrapolating the line through the experimental points at $\phi_+ = 180^o$, and assuming azimuthal independence, the $\pi^+ - \pi^-$ cross-section was numerically integrated over the π^+ directions. The result agrees within the errors with the π^- cross-section measured for photons in the energy interval from 650 to 825 Mev.

It has been assumed that photoproduced π^- from hydrogen come mainly from the pair reaction. The fact that the cross-section deduced from the measured $\pi^+ - \pi^-$ coincidence rate has the same T_- dependence as the π^- cross-section, and the fact that the coincidence cross-section integrated over the π^+ direction equals the π^- cross-section give strong evidence that the coincidences are indeed due to the two pions from the pair reaction.

None of the above measurements would separate the contribution of triple meson production from the observed coincidences, but the results from Cornell (29) indicate that this contribution is small and would be negligible within the statistics of this experiment.

C. Operation

The π^- production data was taken at the values of pion kinetic energies and bremsstrahlung cut-off energies given in Table III. Empty target runs were made for the 1080 and 900 Mev data, but the back-

grounds for the 825 and 650 Mev data were not measured (due to conflicts in scheduling) and were instead inferred from the 1080 Mev backgrounds by the method described in Appendix I.

The $\pi^+ - \pi^-$ coincidence data was taken at the π^+ angles given in Table IV. (Table IV also gives the telescope solid angle and absorber thicknesses for each case.) Each run for a particular π^+ direction was long enough to accumulate 50 to 60 coincidence events and was typically about 5000 BIPS. Empty target runs were made from time to time but never gave any coincident events.

TABLE III.

π^- Production

E_o (Mev)	T_- (Mev)
1080	150
	100
	50
900	150
	100
	50
825	150
	100
650	150
	100

TABLE IV.

$\pi^+ - \pi^-$ Coincidence Measurement

ϕ_+	θ_+	$\Delta\Omega_+$(Ster.)	$\Delta\theta_+$	$\Delta\phi_+$	A_5	A_6	A_7	A_5(eff.)	A_6(eff.)	A_7(eff.)
180°	22°	0.0416	4.8°	7.2°	6.35 cm.	6.35 cm.	12.7 cm.	6.9 cm.	7.2 cm.	14.1 cm.
	45°	0.080	6.6°	10°	6.35	5.07	11.4	6.6	5.9	12.5
	67°	0.125	8.3°	12.5°	5.07	3.81	7.61	5.6	4.4	8.6
	90°	0.17	9.7°	14.5°	5.07	1.27	6.35	5.6	1.57	7.2
	120°	0.04	4.7°	7.0°	2.54	1.27	3.81	2.8	1.57	4.4
90°	45°	0.077	6.5°	9.8°	5.07	3.81	10.2	5.6	4.4	11.4
	90°	0.445	15.7°	23.5°	2.54	1.27	5.07	2.8	1.57	5.9
0°	90°	0.102	7.5°	11.2°	2.04	1.27	4.57	2.3	1.57	5.6

IV. RESULTS OF THE MEASUREMENTS

A. Results of π^- Measurement

The methods used in analyzing the π^- data have been discussed in detail in Bloch's thesis (20) and in the paper of Bloch and Sands (21). Only the briefest outline of the reduction and analysis of the data is given below.

1. Pion Counting Rate

The spectrometer counting rates for 3-fold coincidences with and without a coincidence pulse in the Čerenkov counter were measured. The cosmic-ray background, the accidental coincidences, and the empty target background were measured and subtracted from these counting rates. Defining n_3 and n_4 to be the corrected 3-fold and 4-fold counting rates (in counts per unit energy flux in the x-ray beam), the π^- rate is given by:

$$n_{\pi^-} = \frac{\epsilon_e}{\epsilon_e - \epsilon_\pi} \left[n_3 \quad \frac{(1 - \epsilon_e)}{\epsilon_e} \quad n_4 \right] \tag{3}$$

where ϵ_e and ϵ_π are the Čerenkov counter efficiencies for electrons and pions. Bloch measured ϵ_e and ϵ_π. He found ϵ_e was constant for electron energies from 100 to 250 Mev and equal to 0.70 ± 0.02. His measured values of ϵ_π as a function of pion energy are shown in figure 15. Table V gives the 3-fold and 4-fold coincidence counting rates (corrected for accidentals and cosmic-rays) with and without hydrogen in the target. The last column of the table gives the values of

Figure 15. Čerenkov Counter Efficiency for Pions as a Function of Pion Energy.

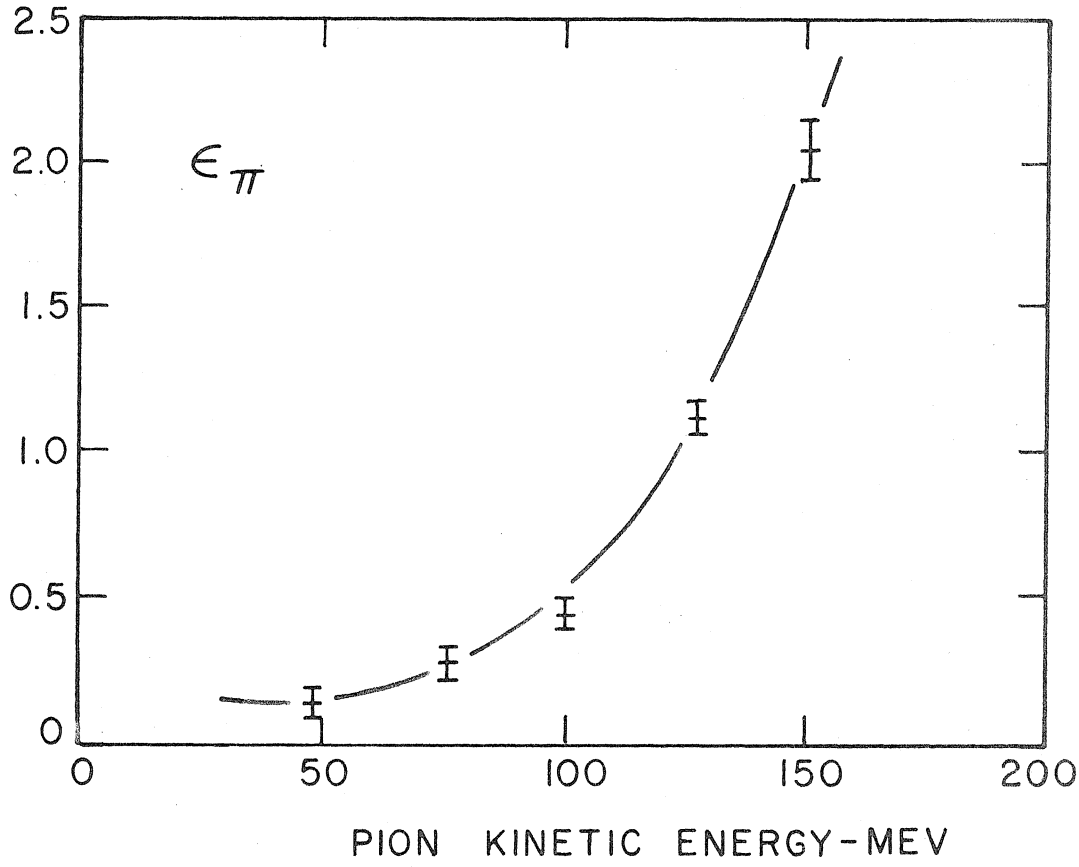
2.5
2.0
1.5
1.0
0.5
0
ϵ_π
0
50
100
150
200
PION KINETIC ENERGY-MEV

TABLE V.

Counting Rates per 10^{12} Mev in X-Ray Beam

E_o(Mev)	T(Mev)	$n_3(H_2)$	$n_4(H)$	n_3(B. G.)	n_4(B. G.)	n_π
1080	50	1.86 ± 0.05	0.56 ± 0.03	0.41 ± 0.04	0.20 ± 0.02	1.32 ± 0.07
1080	100	2.74 ± 0.07	0.27 ± 0.02	0.29 ± 0.03	0.07 ± 0.02	2.51 ± 0.08
1080	150	2.88 ± 0.07	0.36 ± 0.03	0.19 ± 0.03	0.18 ± 0.02	3.60 ± 0.11
900	50	1.90 ± 0.06	0.57 ± 0.03	0.34 ± 0.04	0.45 ± 0.04	1.52 ± 0.07
900	100	2.65 ± 0.10	0.48 ± 0.05	0.25 ± 0.03	0.03 ± 0.02	2.34 ± 0.10
900	150	2.76 ± 0.09	0.54 ± 0.04	0.23 ± 0.04	0.05 ± 0.03	3.19 ± 0.12
825	100	2.74 ± 0.15	0.37 ± 0.06	Not measured.		2.18 ± 0.18
825	150	2.69 ± 0.11	0.39 ± 0.04	Inferred from back-		2.67 ± 0.21
650	100	1.85 ± 0.14	0.36 ± 0.07	grounds at 1080 Mev		1.13 ± 0.17
650	150	1.49 ± 0.11	0.30 ± 0.06	and 900 Mev. See Appendix I.		0.90 ± 0.21

n_{π^-} which were computed. All errors listed are due to the counting statistics except in the case of n_{π^-} where the uncertainties in ϵ_e and ϵ_π are included.

2. Pion Yields

The relation between the measured counting rate and the cross-section for π^- production is:

$$n_{\pi^-} = \eta_- \, C \Delta\Omega \, \Delta T \int_0^{E_o} \sigma_-(T, \theta, k) \, N(E_o, k) \, dk \qquad (4)$$

where:

$\sigma_-(T, \theta, k)$ = cross-section for the production in hydrogen, by a photon of energy k, of a π^- of kinetic energy T at the angle θ, per unit energy interval (in T) and per unit solid angle.

$N(E_o, k)dk$ = number of photons in the energy interval between k and k + dk which traverse the target per unit energy flux in the beam, for a bremsstrahlung cut-off energy E_o.

$\Delta\Omega$ = solid angle of acceptance of the magnet.

ΔT = interval of pion energies accepted by the magnet.

C = number of hydrogen atoms per unit area in the effective length of the target.

η_- = correction factor for those pions which are not counted due to decay in flight or absorption in the counter system.

For reactions in which it is not possible to infer the relevant photon energy from the kinematics of the observed particle, it is usual to express the observations in terms of a "yield per equivalent quantum" which has the dimensions of a cross-section and is defined as:

$$\sigma_-^* (T, \theta, E_o) = E_o \int_0^{E_o} \sigma_-(T, \theta, k)\, N(E_o, k)\, dk \qquad (5)$$

The yield per equivalent quantum is then given in terms of the pion rate by:

$$\sigma_-^* (T, \theta, E_o) = \frac{E_o}{\eta_- C \Delta\Omega \Delta T} \; n_{\pi^-} \qquad (6)$$

The instrumental coefficient $\left[\eta_- C\Delta\Omega \Delta T\right]$ was determined in terms of the known cross-section for the single production of positive pions by reversing the magnetic field and counting positive pions at a synchrotron energy of 510 Mev. This measurement was made for 150 Mev pions which are emitted at the resonance in the single production cross-section. The observed positive pion counting rate is related to the known cross-section by:

$$n_{\pi^+} = \left[\eta_+ C\Delta\Omega \Delta T\right] N(E_o, k_o)\, \sigma_+ (\theta, k_o) \frac{\partial k_o}{\partial T} \qquad (7)$$

where:

k_o = photon energy responsible for the photoproduction of a single meson emitted with kinetic energy T and in direction θ.

$\frac{\partial k_o}{\partial T}$ = rate of change of k_o with T holding θ constant.

For $\theta = 35^o$ and T = 150 Mev, k_o = 300 Mev. $\sigma_+ (\theta, k_o)$ = $19.0 + 0.9 \times 10^{-30}$ cm^2/Ster. from the data of Walker et al. (41). The photon spectrum is known and $\frac{\partial k_o}{\partial T}$ was calculated, so the quantity in brackets in equation 7 was determined from the measurement of η_{π^+}. The instrumental coefficient was assumed to be the same for positive and negative pions of the same energy. The part of η_- that corresponds to the correction for decay in flight and ΔT are both functions of T, therefore it was necessary to deduce the value of the instrumental coefficient for the two other kinetic energies at which the π^- production was measured from the one measured at 150 Mev. The energy dependence of the correction for decay in flight is discussed in detail in an appendix in Bloch's thesis (20), and ΔT is assumed to be proportional to βp. The instrumental coefficients have the values:

T = 50 Mev	$0.41 \pm .03 \times 10^{23}$ Ster-Mev/cm^2
100 Mev	$0.84 \pm .07$
150 Mev	1.24 ± 0.1

The errors in the instrumental coefficient apply to all results given below, where, however, only the statistical errors of the experiment are given.

The yields per equivalent quantum obtained in this experiment are given in Table VI and are shown in figure 16. The broken line parts of the curves are smooth extrapolations to the kinematic thresholds for the two pion process which are indicated by the arrows along the abscissas. The Cornell results of Woodward et al. (17) for measurements of 40 Mev pions at 35° are also shown in figure 16 and appear to be consistent with our results. The yields have the same general behavior as those measured by Bloch and Sands. The three curves are higher than the corresponding curves at 60° which are in turn higher than those at 120°, and the yields increase with decreasing pion energy. For the 50 Mev pions the yield is apparently constant for E_o greater than 900 Mev which corresponds to the cross-section being zero for k greater than 900 Mev.

3. Pion Cross-Sections

The cross-section can be obtained in terms of the yields and the photon spectrum of the x-ray beam.

$$\sigma_-(E_o) = \frac{E_o}{B_o}\left[\frac{d\sigma_-^*(E_o)}{dE_o} + \frac{1}{B_o}\int_0^{E_o}\frac{\partial^2 B(E_o, E_o')}{\partial E_o\,\partial E_o'}\,\sigma_-^*(E_o')dE_o'\right] \qquad (8)$$

where the T and θ variables in the arguments of σ_- and σ_-^* have been suppressed. The quantity B was defined in equation 1, and $B_o = \lim_{k\to E_o} B(E_o, k) = 0.9$. Making the approximations:

$$\frac{d\sigma_-^*(E_o)}{dE_o} = \frac{\sigma_-^*(E_2) - \sigma_-^*(E_1)}{E_2 - E_1} \qquad (9)$$

TABLE VI.

Yields Per Equivalent Quantum

(in units of 10^{-32} cm^2/Mev-Ster.)

E_o(Mev)	T(Mev)	$\sigma^*_-(T, \theta, E_o)$
1080	50	3.48 ± 0.17
1080	100	3.22 ± 0.11
1080	150	3.13 ± 0.10
900	50	3.34 ± 0.15
900	100	2.51 ± 0.11
900	150	2.32 ± 0.09
825	100	2.14 ± 0.18
825	150	1.79 ± 0.14
650	100	0.87 ± 0.13
650	150	0.47 ± 0.11

Figure 16. Yields of Negative Pions at 35° with Kinetic Energies 50, 100, and 150 Mev (per Equivalent Quantum) as a Function of the Bremsstrahlung Cut-Off Energy.

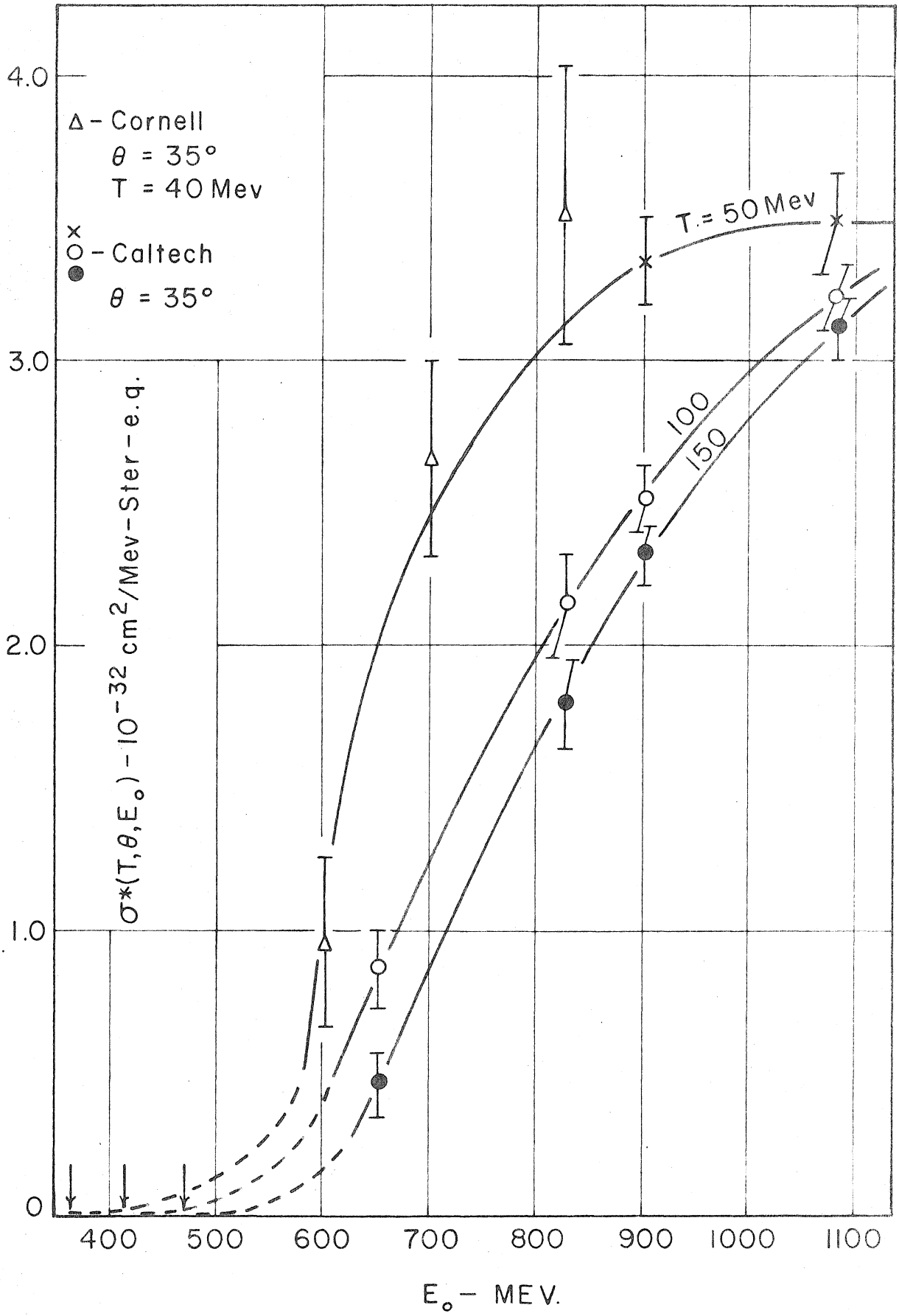
Δ - Cornell
θ = 35°
T = 40 Mev
× ○ - Caltech
θ = 35°
T = 50 Mev
100
150
σ*(T, θ, E₀) - 10⁻³² cm²/Mev-Ster-e.q.
E₀ - MEV.
0
1.0
2.0
3.0
4.0
400
500
600
700
800
900
1000
1100

and

$$E_o = \frac{E_1 + E_2}{2} \tag{10}$$

one can compute an average cross-section for photon energies between E_1 and E_2 from the measured yields at these successive bremsstrahlung cut-off energies. The average σ_- between threshold and the first bremsstrahlung cut-off energy above threshold at which data was taken (650 Mev) was obtained by setting E_1 equal to the threshold energy and $\sigma_-^*(E_1) = 0$. The cross-sections deduced from the yields are given in Table VII. The errors are due exclusively to counting statistics, all other random errors being negligible compared with these. Of course the systematic uncertainty of about 10 $^o/o$ in the absolute value of the yields applies also to the cross-sections.

The cross-section can be referred to the center-of-mass system of the incoming photon and the proton.

$$\sigma_-'(T', \theta', k) = p'/p\,\sigma_-(T, \theta, k) \tag{11}$$

where p and p' are the momenta of the pion in the laboratory and C. M. system, respectively. (Note that as is customary the photon energy is given in the LAB. system even in the case of the C. M. cross-section.) For each entry in Table VII the corresponding energy and angle in the C. M. system and the C. M. cross-section have been computed. The C. M. cross-sections are given in Table VIII and are plotted along with the data of Bloch and Sands in figures 17, 18, and 19. The angle of emission of the pion in the C. M. system is given above or

TABLE VII.

Lab. Cross-Section for Negative Pion Photoproduction
(in units of 10^{-32} cm^2/Mev-Ster.)

$\bar{k}$(Mev)	Δk(Mev)	T(Mev)	$\sigma_-(T, \theta, k)$
990	180	50	0.5 ± 1.4
990	180	100	4.18 ± 0.97
990	180	150	4.85 ± 0.82
860	75	100	4.8 ± 2.7
860	75	150	6.8 ± 2.1
740	175	100	5.9 ± 1.0
740	175	150	6.13 ± 0.83
560	180	150	1.62 ± 0.38
530	235	100	2.15 ± 0.32

TABLE VIII.

C. M. Cross-Section for Negative Pion Photoproduction
(in units of 10^{-32} cm^2/Mev-Ster.)

$\bar{k}$(Mev)	θ'	T'(Mev)	$\sigma_-'(T', \theta', k)$
990	84°	20	0.3 ± 0.8
990	69°	46	2.59 ± 0.60
990	65°	75	3.10 ± 0.53
860	66°	47	3.0 ± 1.7
860	62°	78	4.4 ± 1.4
740	62°	50	3.85 ± 0.68
740	59°	82	4.14 ± 0.56
560	54°	90	1.17 ± 0.28
530	56°	56	1.50 ± 0.23

Figure 17. C. M. Cross - Section for Negative Pion Production at $\bar{k}$ = 740 Mev as a Function of C. M. Pion Energy and C. M. Pion Angle.

Figure 18. C. M. Cross-Section at $\bar{k}$ = 860 Mev.

Figure 19. C. M. Cross-Section at $\bar{k}$ = 990 Mev.

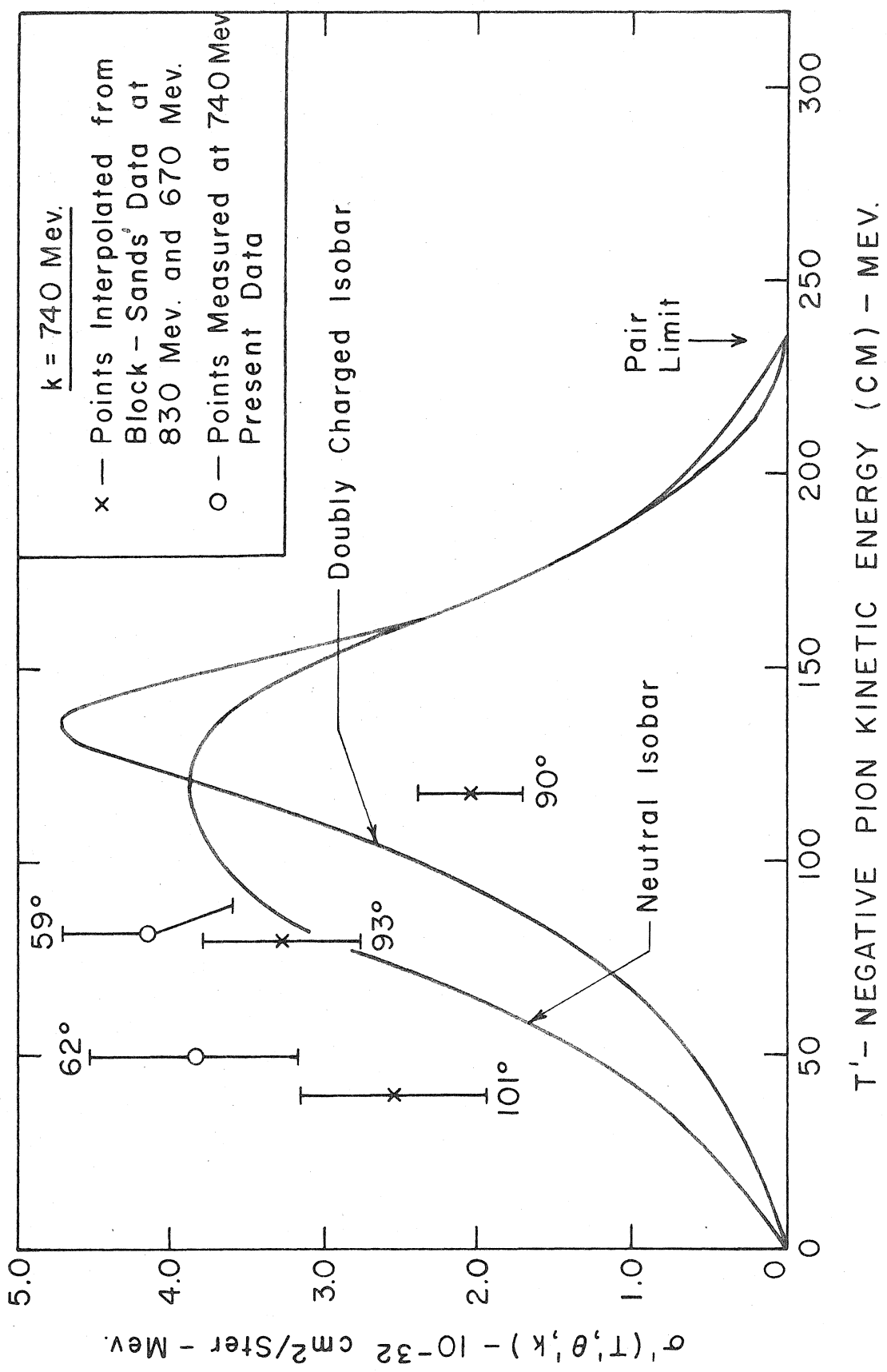
k = 740 Mev.
x — Points Interpolated from Block – Sands' Data at 830 Mev. and 670 Mev.
o — Points Measured at 740 Mev Present Data
Doubly Charged Isobar
Neutral Isobar
Pair Limit
59°
62°
93°
101°
90°
5.0
4.0
3.0
2.0
1.0
0
50
100
150
200
250
300
σ'(T',θ',k) – 10⁻³² cm²/Ster – Mev.
T'– NEGATIVE PION KINETIC ENERGY (CM) – MEV.

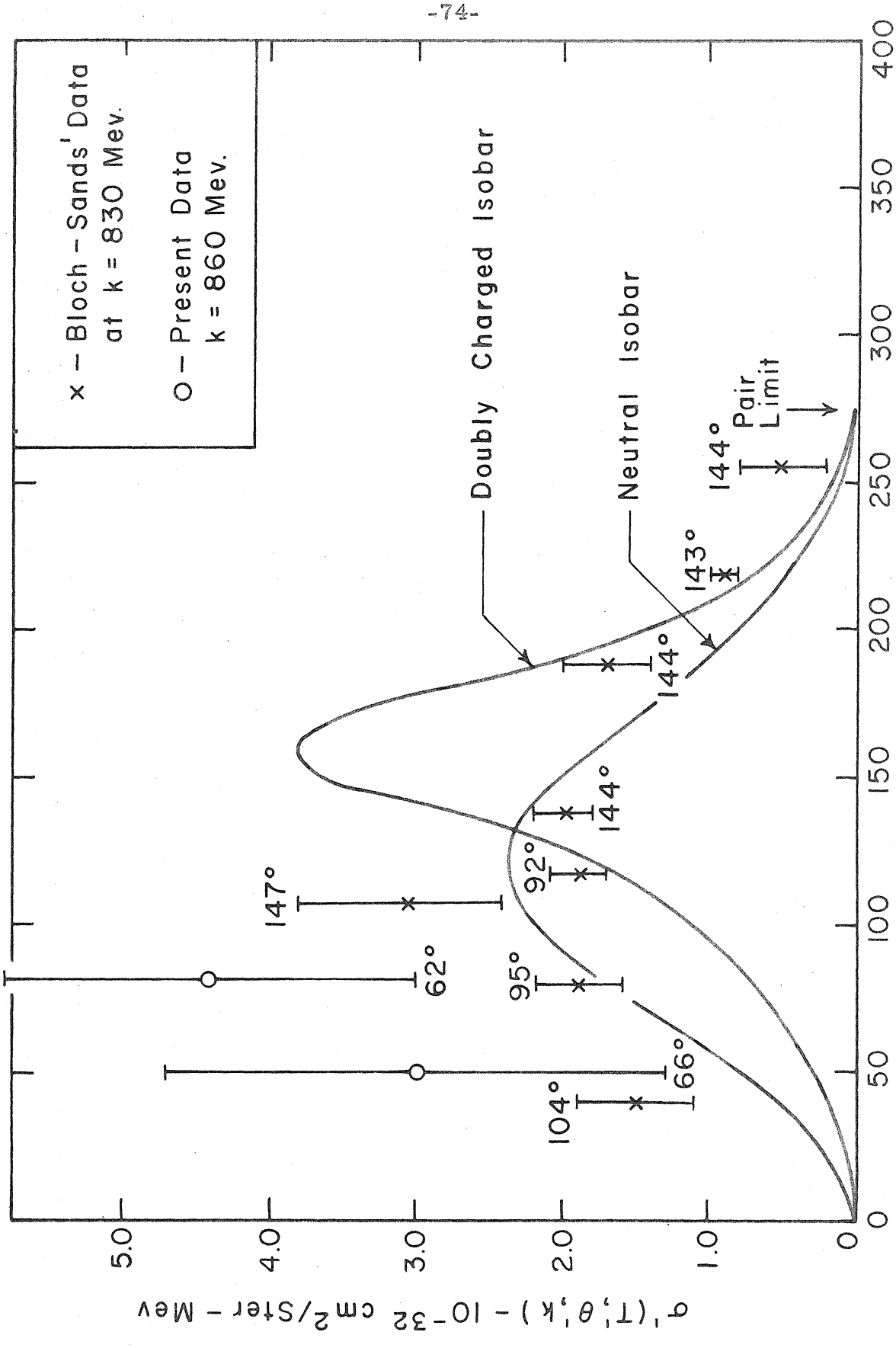
x – Bloch – Sands' Data at k = 830 Mev.
O – Present Data k = 860 Mev.
Doubly Charged Isobar
Neutral Isobar
Pair Limit
147°
62°
95°
92°
144°
144°
104°
66°
143°
144°
σ'(T', θ', k) – 10⁻³² cm²/Ster – Mev
T' – NEGATIVE PION KINETIC ENERGY (CM) – MEV.
0
1.0
2.0
3.0
4.0
5.0
0
50
100
150
200
250
300
350
400

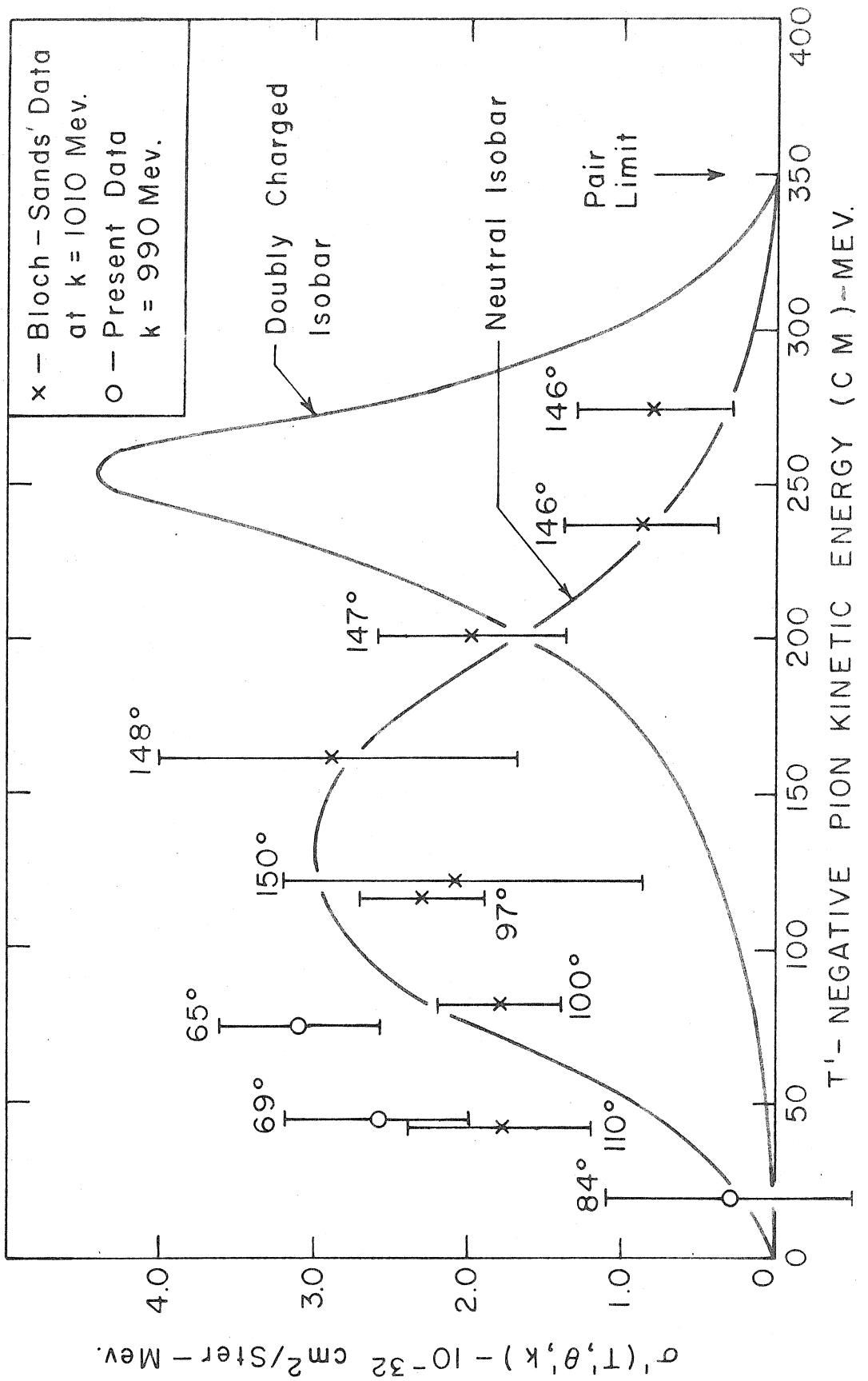
x — Bloch–Sands' Data at k = 1010 Mev.
o — Present Data k = 990 Mev.
Doubly Charged Isobar
Neutral Isobar
Pair Limit
146°
146°
147°
148°
150°
97°
100°
65°
69°
110°
84°
0
50
100
150
200
250
300
350
400
T'– NEGATIVE PION KINETIC ENERGY (C M)–MEV.
0
1.0
2.0
3.0
4.0
σ'(T',θ',k) – 10⁻³² cm²/Ster – Mev.

below each point. The energetic upper limit for π^- from a pair is indicated by an arrow along the abscissas. In order to compare our data with that of Bloch and Sands at the photon energy of 740 Mev, a linear interpolation was made between their data at 830 and 670 Mev. The curves in the figures are the energy spectra predicted by the isobar model which is discussed in Section V. C.

Our points appear to be consistently higher than the points of Bloch and Sands at those T_-' where they can be compared. Roughly, the ratio of the value of our data to theirs is 3 to 2, and this agrees qualitatively with the results of Sellen et al. (29).

B. Results of the Angular Correlation Measurements

1. $\pi^+ - \pi^-$ Coincidence Rate

The information recorded from the data film is described in Section II. I. The number of each of the types of events listed in that Section are given in Table IX for each telescope setting. The errors are due to the counting statistics.

2. Corrected Coincidence Rates

The rate at which pion pairs were produced with the correct kinematical parameters to be detected differs from the observed coincidence rate due to several effects. The following corrections were made to the observed rates to obtain the corrected coincidence rates.

a. Some of the events registered as coincidence events would be due to unrelated $(1 \cdot 2 \cdot 3)$ and $(5 \cdot 6)$ or $(5 \cdot 6 \cdot 7)$ events having a

TABLE IX.

Counting Rates per 10^{15} Mev in X-Ray Beam

ϕ_+	θ_+	N_{56}	N_{567}	N_{456}	N_{4567}	N_{56}^a	N_{567}^a
180°	22°	9.7 ± 1.1	2.0 ± 0.6	0	0	12.2 ± 1.2	3.1 ± 0.6
	45°	9.6 ± 1.4	2.2 ± 0.8	0.6 ± 0.3	0	6.5 ± 1.1	0.6 ± 0.3
	67°	8.1 ± 1.2	2.1 ± 0.7	0.2 ± 0.2	0	6.0 ± 1.1	0.4 ± 0.3
	90°	9.2 ± 1.4	2.5 ± 0.8	0.8 ± 0.4	0	7.3 ± 1.2	1.6 ± 0.6
	120°	1.3 ± 0.6	0.3 ± 0.3	0	0	0.9 ± 0.5	0.2 ± 0.2
90°	45°	9.8 ± 1.6	2.6 ± 0.9	0.8 ± 0.4	0	9.8 ± 1.6	1.6 ± 0.7
	90°	26.0 ± 3.5	4.3 ± 1.5	0.5 ± 0.5	0	31.6 ± 3.9	1.4 ± 0.8
0°	90°	9.0 ± 1.8	2.1 ± 0.8	1.1 ± 0.4	0	13.0 ± 1.5	0.9 ± 0.4

time separation less than the resolving time of the coincidence measurement ($\pm$ 0. 2 mm). This accidental coincidence rate can be computed from the numbers N^a_{56} and N^a_{567} which gave all such unrelated events having a time separation less than $\pm$ 2. 0 mm. Figure 13 shows that the time separation of these unrelated events was randomly distributed, consequently, those events with a time separation less than $\pm$ 0. 2 mm would be 11 $^o/o$ of N^a_{56} and N^a_{567}. The accidental rates $N^{Acc.}_{56}$ and $N^{Acc.}_{567}$ are given in Table X and Table XI, respectively.

b. The rates of coincidence events which were due to an electron being counted in the spectrometer and a (5·6) or (5·6·7) event being counted in coincidence in the telescope are given by:

$$N^e_{56} = \alpha N_{456} + \beta N_{56} \tag{13}$$

$$N^e_{567} = \alpha N_{4567} + \beta N_{567} \tag{14}$$

where:

$$\alpha = \frac{1 - \epsilon_\pi}{\epsilon_e - \epsilon_\pi} \tag{15}$$

$$\beta = - \frac{\epsilon_\pi}{\epsilon_e - \epsilon_\pi} \tag{16}$$

(The measurement of ϵ_π and ϵ_e is described in Section III. B. 1.). The value of N_{4567} was zero at each of the telescope settings (see

Table IX) and so N^{e}_{567} is taken to be zero also. The values of N^{e}_{56} are given in Table X.

c. Due to the nuclear absorption of the π^{+} as they traversed the absorbers of the telescope, there would be a reduction in the number of coincidence events detected. The question of the correct absorption cross-section to be used is discussed in Appendix II, and the summary of the available information indicates that the cross-section is geometric. The mean free path in lead is then $\lambda = 15.0 + 15\ ^{o}/_{o}$ cm. To correct the coincidence rate for the effect of the absorption, the $(1 \cdot 2 \cdot 3 \cdot 5 \cdot 6)$ rate is multiplied by:

$$C^{Abs.}_{56} = e^{\frac{A_5 + A_6}{\lambda}} \tag{17}$$

and the $(1 \cdot 2 \cdot 3 \cdot 5 \cdot 6 \cdot 7)$ rate is multiplied by:

$$C^{Abs.}_{567} = e^{\frac{A_5 + A_6 + A_7}{\lambda}} \tag{18}$$

These corrections are given in Table X and Table XI.

Some of the π^{+} from $(1 \cdot 2 \cdot 3 \cdot 5 \cdot 6 \cdot 7)$ events would be absorbed in the absorber between counters 6 and 7, and would therefore be registered as $(1 \cdot 2 \cdot 3 \cdot 5 \cdot 6)$ events. The rate of such false $(1 \cdot 2 \cdot 3 \cdot 5 \cdot 6)$ events is given by:

$$N^{F}_{56} = \left(e^{A_7/\lambda} - 1\right)\left(N_{567} - N^{e}_{567} - N^{Acc.}_{567}\right) \tag{19}$$

The values of N^{F}_{56} are given in Table X.

d. It is convenient to consider the correction arising from the π^+ decay in flight as consisting of three parts, and examine these parts one at a time. (Because of the large statistical errors associated with the data at $\bar{k}$ = 950 Mev, the relatively small corrections due to the decay in flight and multiple scattering in the telescope absorbers are not made to this data.) The case in which the effect of the π^+ decay would be most significant was for $\theta_+ = 120^\circ$ and $\phi_+ = 180^\circ$ where 9 °/o of the pions would decay over the total length of their path from the target to counter 7. The estimate of the size of each correction listed below was computed for this largest case, and in computing the estimates all pion decays were assumed to take place before the pions entered the telescope (in the case at $\theta_+ = 120^\circ$ and $\phi_+ = 180^\circ$, 75 °/o of the decays would occur before the pions reached the telescope).

(i) The decay muons would be emitted in a cone defined by an angle of 10° with respect to the direction of motion of the pions. Some of these muons would therefore miss the telescope counting solid angle although their parent pions would have been counted. This would give a loss of less than 2 °/o of the $\pi^+ - \pi^-$ coincidence counting rate. Some π^+ which were emitted from the target at the wrong angle to be detected would, however, decay and their muons could enter the counting solid angle. This effect should essentially cancel any loss in counting rate arising from the first process.

(ii) The decay muons would have an energy spread of about $\pm$ 20 °/o of the energy of the parent pions. Because of this energy spread, and the slight difference in range of pions and muons of the

same energy, the effective energy interval of those photons which initiated (1 · 2 · 3 · 5 · 6) events would be from 620 to 795 Mev for those events where the π^+ decayed. The Δk in this case happens to be the same as it was for the usual photon energy interval, and so if the cross-section for pion pairs does not change rapidly as a function of photon energy in the region around 740 Mev, this small shift of the photon energy interval should have a negligible effect.

(iii) The experimental arrangement allowed no differentiation between those (1 · 2 · 3 · 5 · 6) events from π^- - π^+ coincidences and those in which the π^+ decayed and the decay muons traversed the telescope giving π^- - μ^+ coincidences. In computing the corrected coincidence rate the absorption correction was made to both types of events. Fast muons are not absorbed in nuclear collisions, however, and so the corrected coincidence would be systematically too high. The correction for this effect (C_μ) amounts to about 5 °/o in the largest case at $\theta_+ = 22^\circ$ and $\phi_+ = 180^\circ$ (because of the thick absorbers), and its value is given for each telescope setting in Table X.

e. Due to the multiple scattering of the π^+ as they traversed the telescope absorbers, some pions would be scattered out of the counting solid angle, but also some π^+ which were emitted from the target at the wrong angle to be detected in the telescope would be scattered by absorber A_5 into the counting solid angle. (Only those π^+ scattered into the counting solid angle by the front absorber would give the required coincidence in C_5 and C_6, otherwise, the scattering in and scattering out should essentially cancel.) Using the scattering

theory given by Rossi (42), the effect of the scattering in and scattering out was computed and gave a net loss in counting rate of about 10 °/o in the largest case when the telescope was set at $\theta_+ = 22^\circ$ and $\phi_+ = 180^\circ$. The r. m. s. scattering angle in this largest case is about 10° for the π^+ traversing the first two absorber A_5 and A_6. This corresponds to a mean lateral displacement from the original direction of motion of about 1/2 inch at counter C_6. The correction for the effect of multiple scattering (C_s) is given in Table X for each telescope setting.

The corrected coincidence rates are given in terms of the above corrections by:

$$R_{56} = C_s C_\mu C_{56}^{Abs.} (N_{56} - N_{56}^{e} - N_{56}^{Acc.} - N_{56}^{F}) \qquad (20)$$

$$R_{567} = C_{567}^{Abs.} (N_{567} - N_{567}^{e} - N_{567}^{Acc.}) \qquad (21)$$

The statistical error in the corrected coincidence rates would be made up of a great number of terms, each representing the uncertainty in the value of one of the corrections or the uncertainty in the value of the uncorrected coincidence rate. An examination of each of these uncertainties shows that some terms may be neglected because they are always small compared to the dominate terms. If only the significant terms are kept, the errors are given to a good approximation by:

$$(\Delta R_{56})^2 = (C_s C_\mu C_{56}^{Abs.})^2 \left\{ \left[(\Delta N_{56})^2 + (e^{A_7/\lambda} - 1)^2 (\Delta N_{567})^2 \right] + \left[(N_{56} - N_{56}^e - N_{56}^{Acc.} - N_{56}^F)^2 \left(\frac{A_5 + A_6}{\lambda} \frac{\Delta\lambda}{\lambda} \right)^2 \right] \right\} \quad (22)$$

$$(\Delta R_{567})^2 = (C_{567}^{Abs.})^2 \left[(\Delta N_{567})^2 + (N_{567})^2 \left(\frac{A_5 + A_6 + A_7}{\lambda} \frac{\Delta\lambda}{\lambda} \right)^2 \right] \quad (23)$$

ΔN_{56} and ΔN_{567} are due to the counting statistics, and $\frac{\Delta\lambda}{\lambda} = 15\ ^o/o$. The values of the corrected coincidence rates and their errors are given in Table X and Table XI.

3. Cross-Section and Angular Correlation Function

Let $\sigma_{+-}(k, E_-, \theta_-, \theta_+, \phi_+)$ be the cross-section for the production in hydrogen, by a photon of energy k, of a negative pion with total energy E_- and at the zenith angle θ_-, and the production of a positive pion at the zenith angle θ_+ and azimuthal angle ϕ_+, per unit energy interval (in E_-), per unit solid angle for the positive pion, and per unit solid angle for the negative pion. The cross-section is related to the corrected coincidence rates by:

$$R_{56} = (\eta_- C \Delta E_- \Delta\Omega_-)\, \Delta\Omega_+ \int_{650}^{825} dk N(E_o, k)\, \sigma_{+-}(k, E_-, \theta_-, \theta_+, \phi_+) \quad (24)$$

$$R_{567} = (\eta_- C \Delta E_- \Delta\Omega_-)\, \Delta\Omega_+ \int_{825}^{1080} dk N(E_o, k)\, \sigma_{+-}(k, E_-, \theta_-, \theta_+, \phi_+) \quad (25)$$

TABLE X.

Corrections to (1 • 2 • 3 • 5 • 6) Rates

Counting Rates Per 10^{15} Mev in X-Ray Beam

ϕ_+	θ_+	N_{56}	$N_{56}^{Acc.}$	N_{56}^{e}	N_{56}^{F}	$C_{56}^{Abs.}$	C_{ω}	C_s	R_{56}
180°	22°	9.7 ± 1.1	1.2 ± 0.1	0 ± 0.2	2.5 ± 0.9	2.61	0.94	1.12	16.4 ± 3.0
	45°	9.6 ± 1.4	0.7 ± 0.1	0.2 ± 0.4	2.5 ± 1.0	2.34	0.96	1.09	15.3 ± 3.1
	67°	8.1 ± 1.2	0.6 ± 0.1	0 ± 0.3	1.4 ± 0.5	1.97	0.98	1.07	13.0 ± 2.4
	90°	9.2 ± 1.4	0.7 ± 0.1	0.4 ± 0.5	1.3 ± 0.5	1.72	0.98	1.03	11.8 ± 2.1
	120°	1.3 ± 0.6	0.1 ± 0.1	0 ± 0.3	0.1 ± 0.1	1.35	0.98	1.03	1.5 ± 0.8
90°	45°	9.8 ± 1.6	1.0 ± 0.2	0.3 ± 0.5	2.4 ± 1.0	1.97	0.97	1.07	13.0 ± 2.7
	90°	26.0 ± 3.5	3.2 ± 0.4	0 ± 0.7	1.8 ± 0.7	1.35	1.0	1.03	29.3 ± 4.5
0°	90°	9.0 ± 1.8	1.3 ± 0.2	1.0 ± 0.5	0.8 ± 0.4	1.3	0.99	1.03	7.8 ± 1.7

TABLE XI.

Corrections to (1 · 2 · 3 · 5 · 6 · 7) Rates

Counting Rates Per 10^{15} Mev in X-Ray Beam

ϕ_+	θ_+	N_{567}	$N_{567}^{Acc.}$	$C_{567}^{Abs.}$	R_{567}
180°	22°	2.0 ± 0.6	0.31 ± 0.06	6.82	11.7 ± 7.0
	45°	2.2 ± 0.8	0.06 ± 0.03	5.47	11.7 ± 6.0
	67°	2.1 ± 0.7	0.04 ± 0.03	3.56	7.4 ± 3.0
	90°	2.5 ± 0.8	0.16 ± 0.06	2.72	6.4 ± 2.5
	120°	0.3 ± 0.3	0.02 ± 0.02	1.82	0.6 ± 0.7
90°	45°	2.6 ± 0.9	0.16 ± 0.07	4.31	10.6 ± 5.0
	90°	4.3 ± 1.5	0.14 ± 0.08	2.01	8.4 ± 3.5
0°	90°	2.1 ± 0.8	0.09 ± 0.04	1.95	4.1 ± 1.6

where $(\eta_- C \Delta E_- \Delta \Omega_-)$ is the instrumental coefficient which was measured (see Section IV. A. 2.), and its value is $1.24 \pm 0.1 \times 10^{23}$ Ster-Mev/cm^2; $N(E_o, k)\,dk$ is the number of photons in the energy interval from k to k + dk per unit energy flux in the x-ray beam for a bremsstrahlung cut-off energy E_o = 1080 Mev; and $\Delta\Omega_+$ is the solid angle of the telescope. In calculating the value of $\Delta\Omega_+$, a correction was made to take account of the fact that the hydrogen target was not a point source, and that the counter C_6 which defined the telescope solid angle had a plane surface rather than being part of a spherical surface centered at the target. The effective solid angle, $\Delta\Omega_+$ (eff.), is given in Table XII for each π^+ direction.)

If it is assumed that the cross-section is only a slowly varying function of the photon energy, then equations 24 and 25 can be solved for the cross-section.

$$\sigma_{+-}(\bar{k}) = \frac{R(\bar{k})}{(\eta_- C \Delta E_- \Delta \Omega_-)\Delta\Omega_+ N(E_o, \bar{k})\Delta k} \qquad (26)$$

$\bar{k}$ is the central value of the photon energy in each of the two intervals, that is, $\bar{k}$ = 740 Mev for the 650 - 825 Mev interval and $\bar{k}$ = 950 Mev for the 825 - 1080 Mev interval. $N(E_o, \bar{k})\Delta k$ is the number of photons in each of the two intervals per unit energy flux in the x-ray beam.

It is convenient to express the data in terms of an angular correlation function which is defined as:

$$P(\bar{k}, \theta_+, \phi_+)d\Omega_+ = 4\pi \frac{\sigma_{+-}(\bar{k}, E_-, \theta_-, \theta_+, \phi_+)d\Omega_+}{\sigma_-(\bar{k}, E_-, \theta_-)} \quad (27)$$

where $\sigma_-(k, E_-, \theta_-)$ is the cross-section for the production of a π^- at 35° with a kinetic energy of 150 Mev, initiated by a photon of energy $\bar{k}$. σ_- is related to σ_{+-} by:

$$\sigma_- = \oint d\Omega_+ \; \sigma_{+-} \quad (28)$$

The angular correlations function equals 4π times the probability of the π^+ being emitted with direction angles θ_+ and ϕ_+, per unit solid angle, given that the π^- was emitted with the correct angle and energy to be accepted by the spectrometer. The correlation function is given in terms of the measured counting rates by:

$$P(\bar{k}, \theta_+, \phi_+) = 4\pi \frac{R(\bar{k})}{\Delta\Omega_+ N(E_o, \bar{k}) \frac{\bar{k}}{B_o}\left[E_2 n_{\pi^-}(E_2) - E_1 n_{\pi^-}(E_1)\right]} \quad (29)$$

where $n_{\pi^-}(E)$ is the π^- counting rate for a bremsstrahlung cut-off energy E, the values of n_{π^-} are given in Table V; the numbers E_1 and E_2 are the lower and upper photon energy limits, respectively, of the energy interval in which the $\pi^+ - \pi^-$ coincidence rate was measured (E_1 = 650 Mev and E_2 = 825 Mev for $\bar{k}$ = 740 Mev, and E_1 = 825 Mev and E_2 = 1080 Mev for $\bar{k}$ = 950 Mev); and B_o is defined in Section IV. A. 3. and is equal to 0. 9.

The error in the correlation is due both to the uncertainty in the coincidence rate and to the uncertainties in the π^- rates, however, only the statistical errors arising from the uncertainties in the coincidence rates are given with the values of the correlation function in Table XII. The error in the value of the denominator of equation 29 is equal to about 20 ^{o}/o for both the energy intervals corresponding to $\bar{k}$ = 740 Mev and $\bar{k}$ = 950 Mev. The fact that these errors are not included in the errors in the correlation function has the effect of making the absolute value of the correlation function uncertain to about 20 ^{o}/o.

The correlation function can be transformed to the C. M. system of the incoming photon and proton.

$$P'(\bar{k}, \theta_+', \phi_+') = P(\bar{k}, \theta_+, \phi_+) \quad \frac{p_-}{p_-'} \quad \frac{d\Omega_+}{d\Omega_+'} \quad \frac{dE_-}{dE_-'} \quad \frac{d\Omega_-}{d\Omega_-'} \tag{30}$$

where the primes indicate quantities in the C. M. system. The values of the π^+ angles and energies in the C. M. system are shown in three curves for $\bar{k}$ = 740 Mev. Figure 20 shows θ_+' as a function of θ_+ for $\phi_+ = 180^{o}$, figure 21 shows θ_{+-}' (the angle between the two pions) as a function of θ_+' for $\phi_+' = 180^{o}$ and 90^{o}, and figure 22 shows E_+' as a function of θ_{+-}'. The product of the three derivatives in equation 30 is given by:

$$\frac{d\Omega_+}{d\Omega_+'} \quad \frac{dE_-}{dE_-'} \quad \frac{d\Omega_-}{d\Omega_-'} = \frac{p_-'}{p_-} \quad \frac{p_+'}{p_+} \left[\frac{(\bar{k}+M-E_-)-\frac{1}{\beta_+}(\bar{k}\cos\theta_+-p_-\cos\theta_{+-})}{\sqrt{M^2+2\bar{k}M} - E_-' + \frac{p_-'}{\beta_+'}\cos\theta_+' -} \right] \tag{31}$$

TABLE XII.

Lab. Correlation Function

ϕ_+	θ_+	$\Delta\Omega_+$(eff.)	P(740, θ_+, ϕ_+)(per ster.)	P(950, θ_+, ϕ_+)(per ster.)
180°	22°	0.041 ster.	3.24 ± 0.57	4.1 ± 2.3
	45°	0.079	1.66 ± 0.34	2.1 ± 1.1
	67°	0.12	0.90 ± 0.16	0.87 ± 0.35
	90°	0.16	0.64 ± 0.11	0.56 ± 0.22
	120°	0.04	0.32 ± 0.16	0.2 ± 0.25
90°	45°	0.076	1.54 ± 0.32	2.0 ± 0.9
	90°	0.40	0.62 ± 0.09	0.30 ± 0.12
0°	90°	0.10	0.64 ± 0.14	0.58 ± 0.23

Figure 20. π^+ Angle Transformation. (LAB. to C. M.)

Figure 21. C. M. Angle Between the Two Pions in the Pair as a Function of π^+ C. M. Angle for $\phi_+' = 180^\circ$ and 90°.

Figure 22. π^+ C. M. Total Energy as a Function of the C. M. Angle Between the Two Pions.

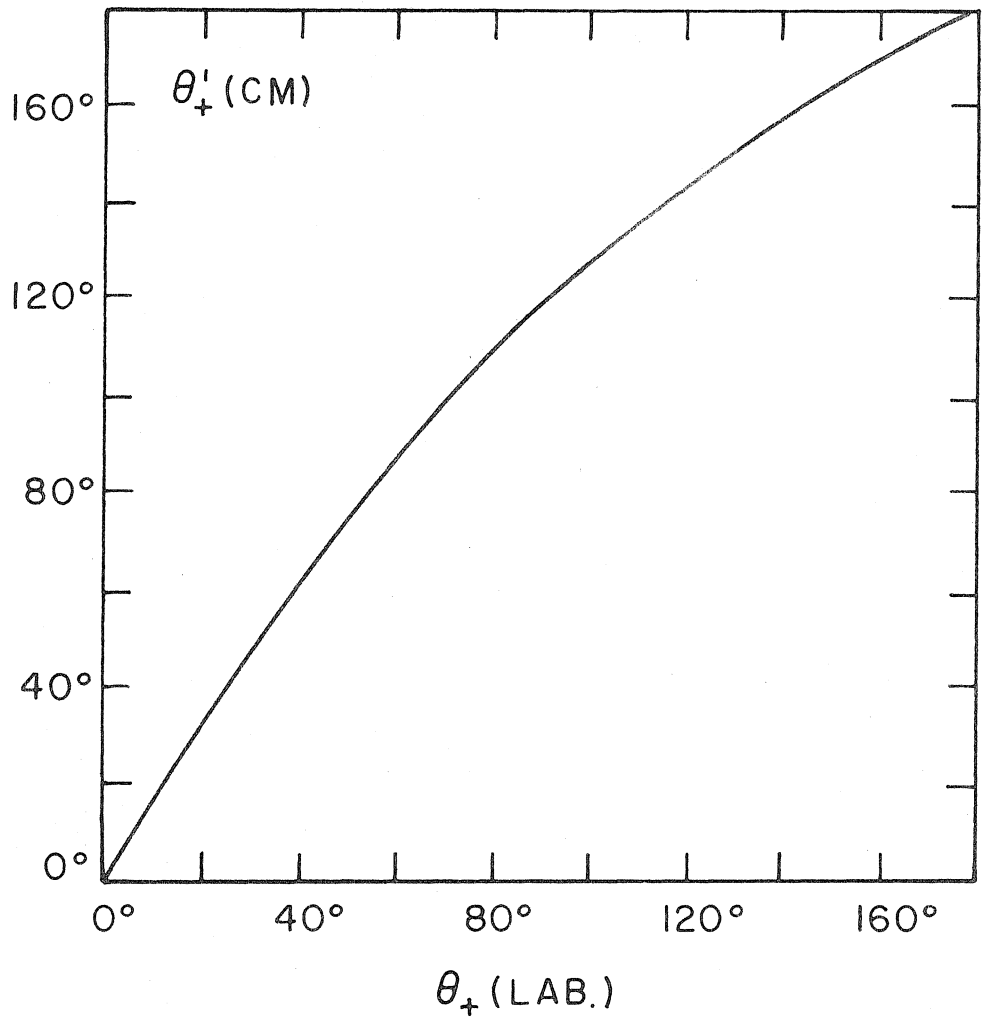
θ'_+ (CM)
160°
120°
80°
40°
0°
0°
40°
80°
120°
160°
θ_+ (LAB.)

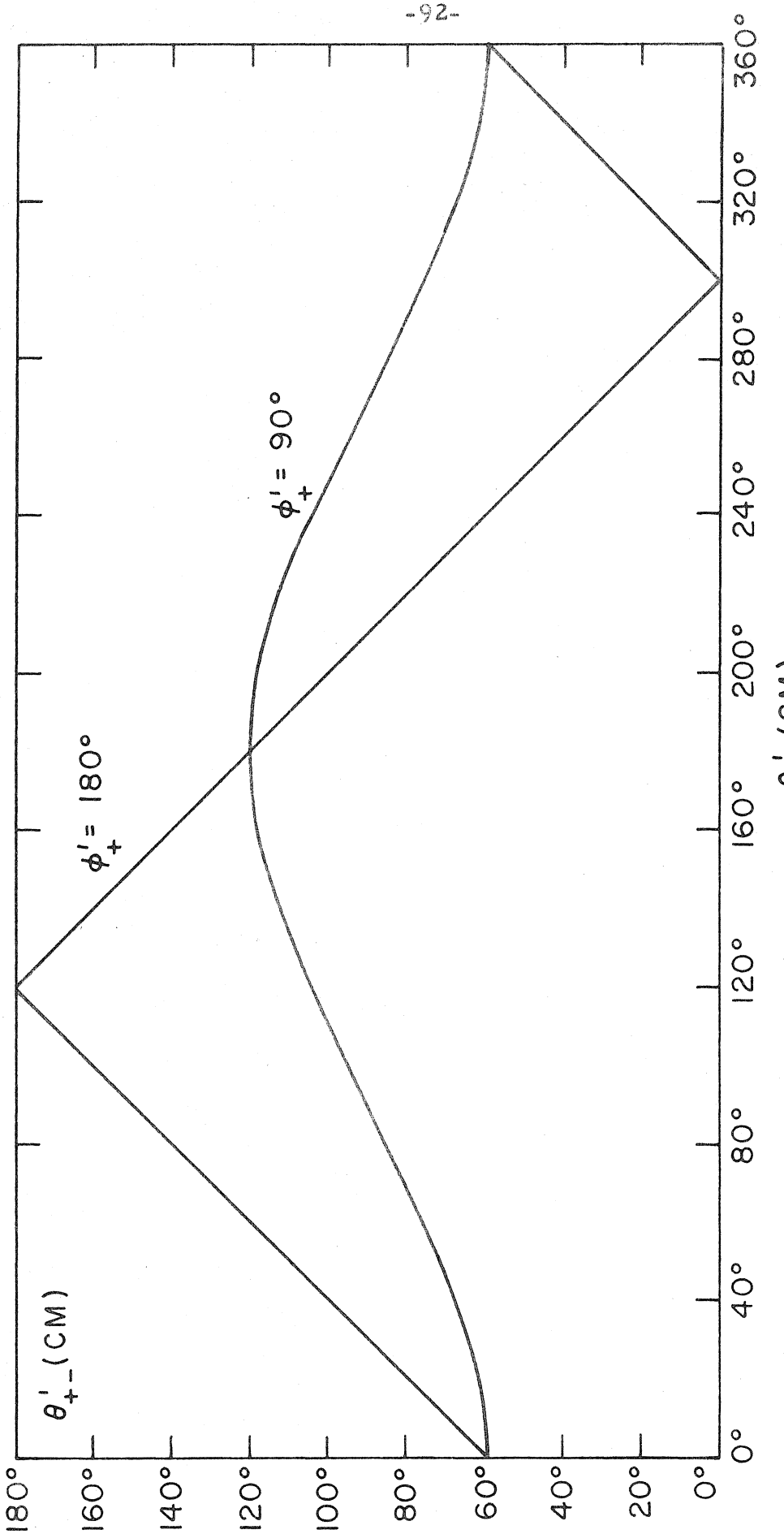
θ'_{+-} (CM)
$\phi'_{+} = 180°$
$\phi'_{+} = 90°$
θ'_{+} (CM)
0°
20°
40°
60°
80°
100°
120°
140°
160°
180°
0°
40°
80°
120°
160°
200°
240°
280°
320°
360°

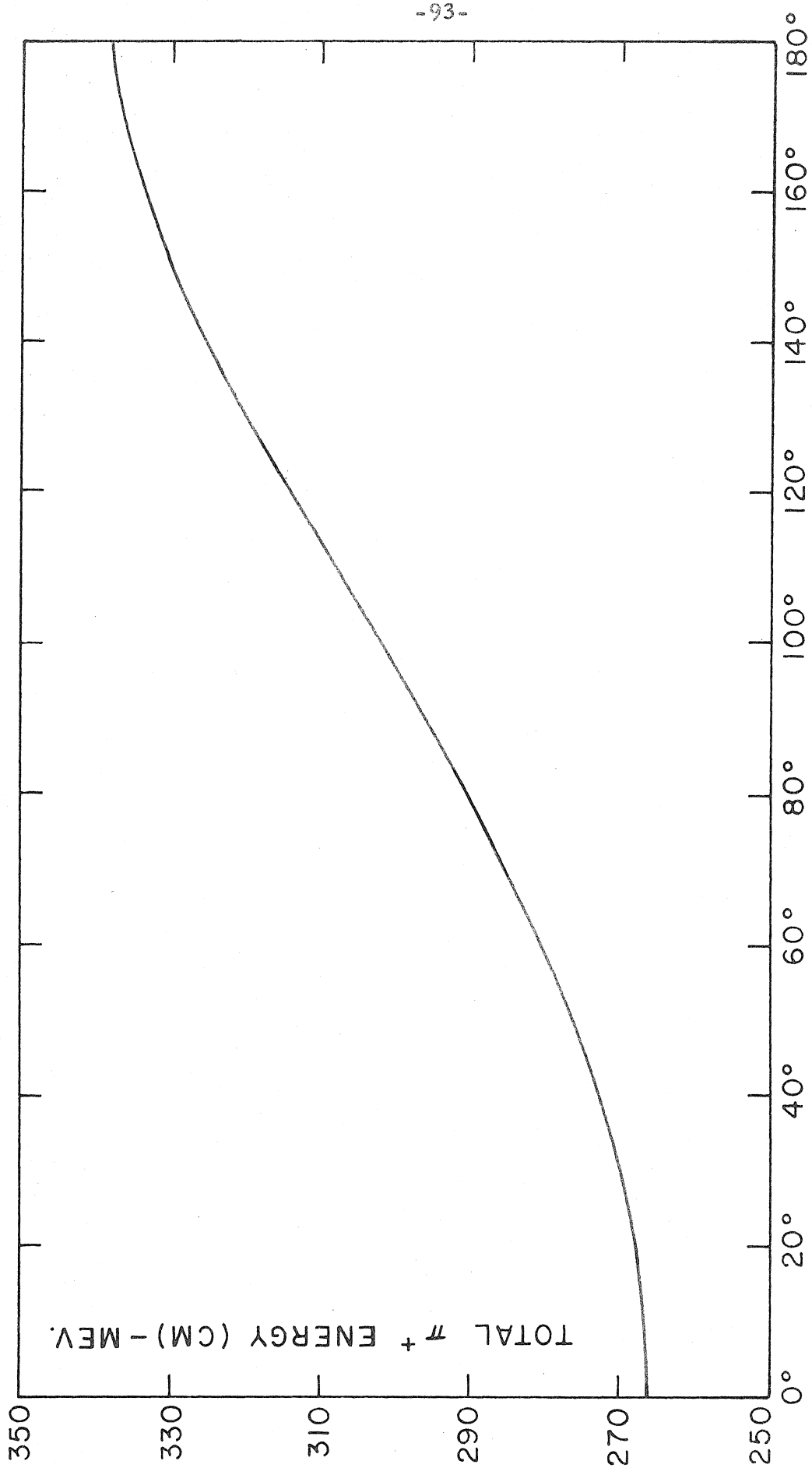
TOTAL π^+ ENERGY (CM) - MEV.
350
330
310
290
270
250
0°
20°
40°
60°
80°
100°
120°
140°
160°
180°
θ'_{+-} (CM)

(The method used to derive equation 31 is due to Dr. Jon Mathews who reduced a usually laborious computation to a relatively easy one. The method is described in Appendix III.) Figure 23 shows the values of the transformation given by equation 31 as a function of θ_+ for $\phi_+ = 180^o$ and for $\bar{k} = 740$ Mev. This transformation and the angle transformation shown in figure 20 are both quite insensitive to variations in ϕ_+, changing by only a few per cent over the complete range of the azimuth angle.

Table XIII and figures 24, 25 and 26 give the values of $P'(\bar{k}, \theta_+', \phi_+')$ for $\bar{k} = 740$ Mev. The uncertainties in the angles of the experimental points shown in the figures were due to the finite size of the counter in the telescope which defined the solid angle. The straight line at $P' = 1.0$ corresponds to an isotropic distribution. The data seems to indicate that the angular correlation function is nearly constant in the backward direction and increases in the forward direction, however, except for the point at 35^o the correlation function could be interpreted to be constant at all angles. The correlation function appears to have no strong azimuthal variation. An isotropic angular distribution of the π^+ would agree with the recent Cornell results (29), however, their statistics are not good enough to observe the correlation between the two pions and so it is not possible to check the forward peaking of the correlation function.

The values of $P'(\bar{k}, \theta_+', \phi_+')$ for $\bar{k} = 950$ Mev are given in Table XIV and are shown in figures 27, 28, and 29. The errors in P' are so large that no statement can be made about the shape of the

Figure 23. Laboratory Cross-Section to Center-of-Mass Cross-Section Transformation

$$\frac{d\Omega_+}{d\Omega'_+} \quad \frac{dE_-}{dE'_-} \quad \frac{d\Omega_-}{d\Omega'_-} \quad .$$

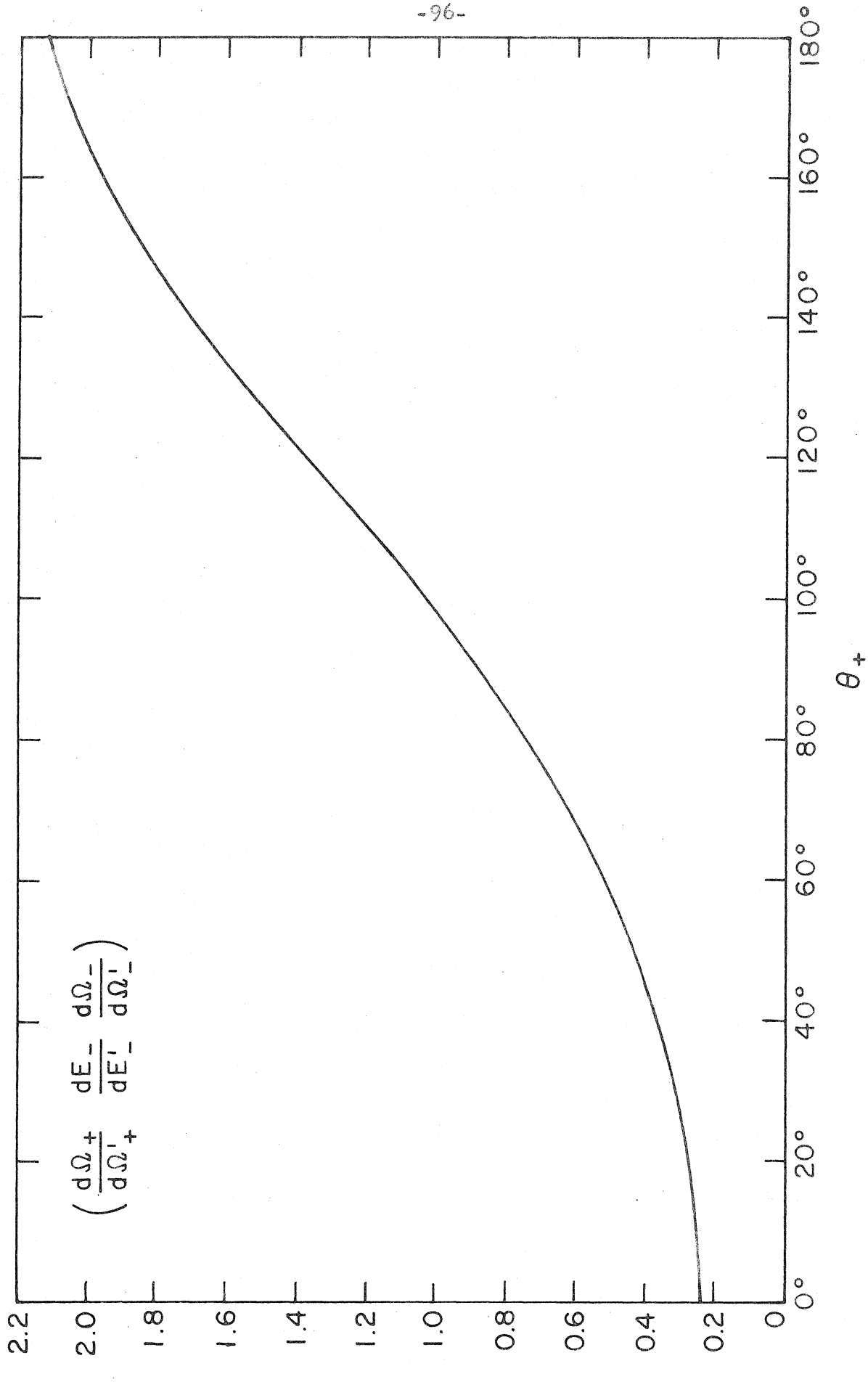
$\left(\frac{d\Omega_+}{d\Omega'_+}\frac{dE_-}{dE'_-}\frac{d\Omega_-}{d\Omega'_-}\right)$
2.2
2.0
1.8
1.6
1.4
1.2
1.0
0.8
0.6
0.4
0.2
0
0°
20°
40°
60°
80°
100°
120°
140°
160°
180°
θ_+

TABLE XIII.

C. M. Correlation Function

$\bar{k}$ = 740 Mev

ϕ_+	θ_+	θ_+'	T_+' (Mev)	$P'(\theta_+', \phi_+')$(per ster.)
180°	22°	35°	161	1.30 ± 0.23
	45°	70°	183	0.97 ± 0.19
	67°	95°	193	0.77 ± 0.14
	90°	120°	197	0.81 ± 0.15
	120°	143°	200	0.64 ± 0.33
90°	45°	71°	150	0.85 ± 0.18
	90°	120°	167	0.78 ± 0.12
0°	90°	121°	140	0.83 ± 0.18

Figure 24. π^+ C. M. Correlation Function as a Function of θ_+' for $\phi_+' = 180^\circ$. $\bar{k}$ = 740 Mev.

Figure 25. π^+ C. M. Correlation Function as a Function of ϕ_+' for $\theta_+' = 70^\circ$. $\bar{k}$ = 740 Mev.

Figure 26. π^+ C. M. Correlation Function as a Function of ϕ_+' for $\theta_+' = 120^\circ$. $\bar{k}$ = 740 Mev.

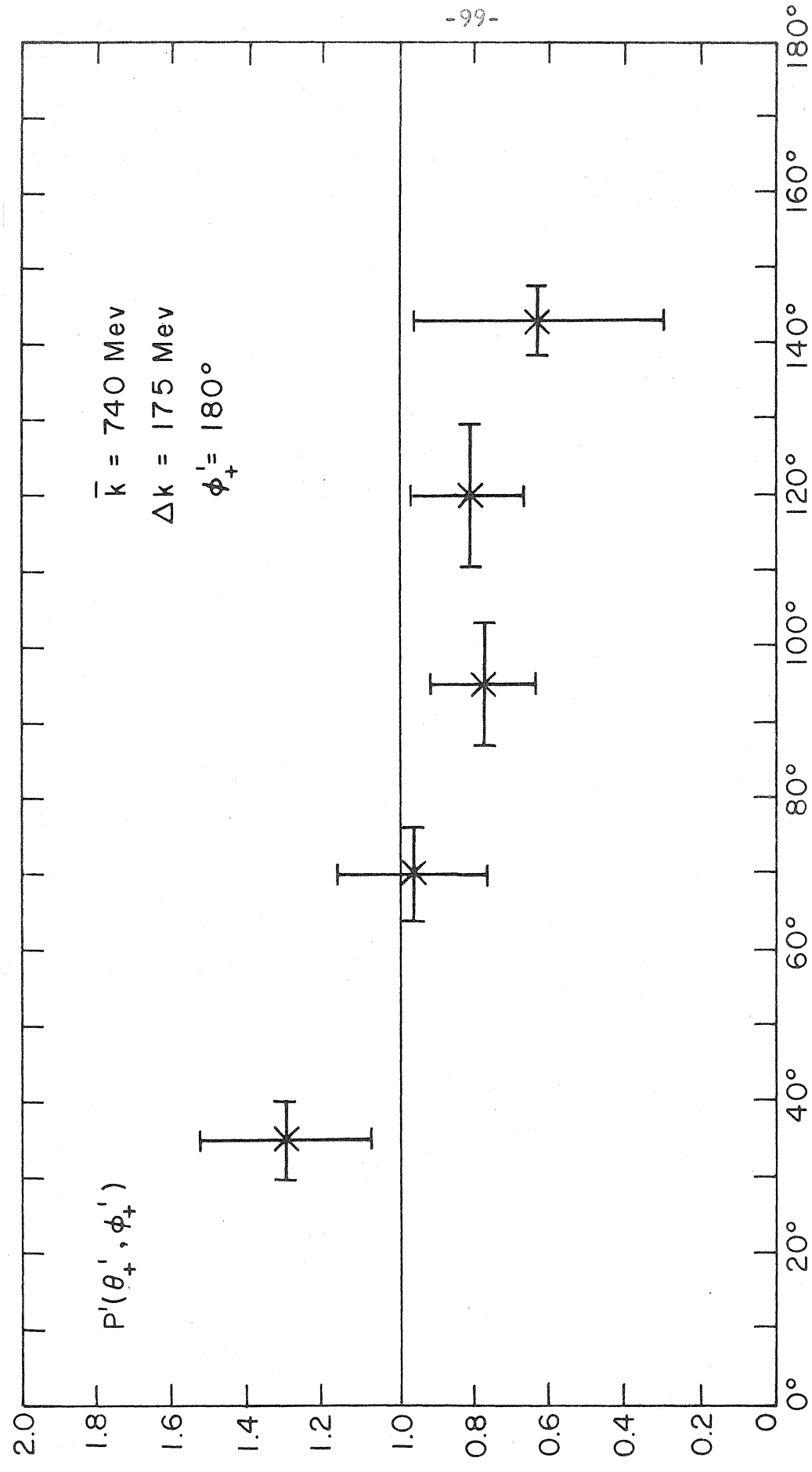
$\bar{k}$ = 740 Mev
Δk = 175 Mev
ϕ_+' = 180°
$P'(\theta_+', \phi_+')$
θ_+' (CM)
0°
20°
40°
60°
80°
100°
120°
140°
160°
180°
0
0.2
0.4
0.6
0.8
1.0
1.2
1.4
1.6
1.8
2.0

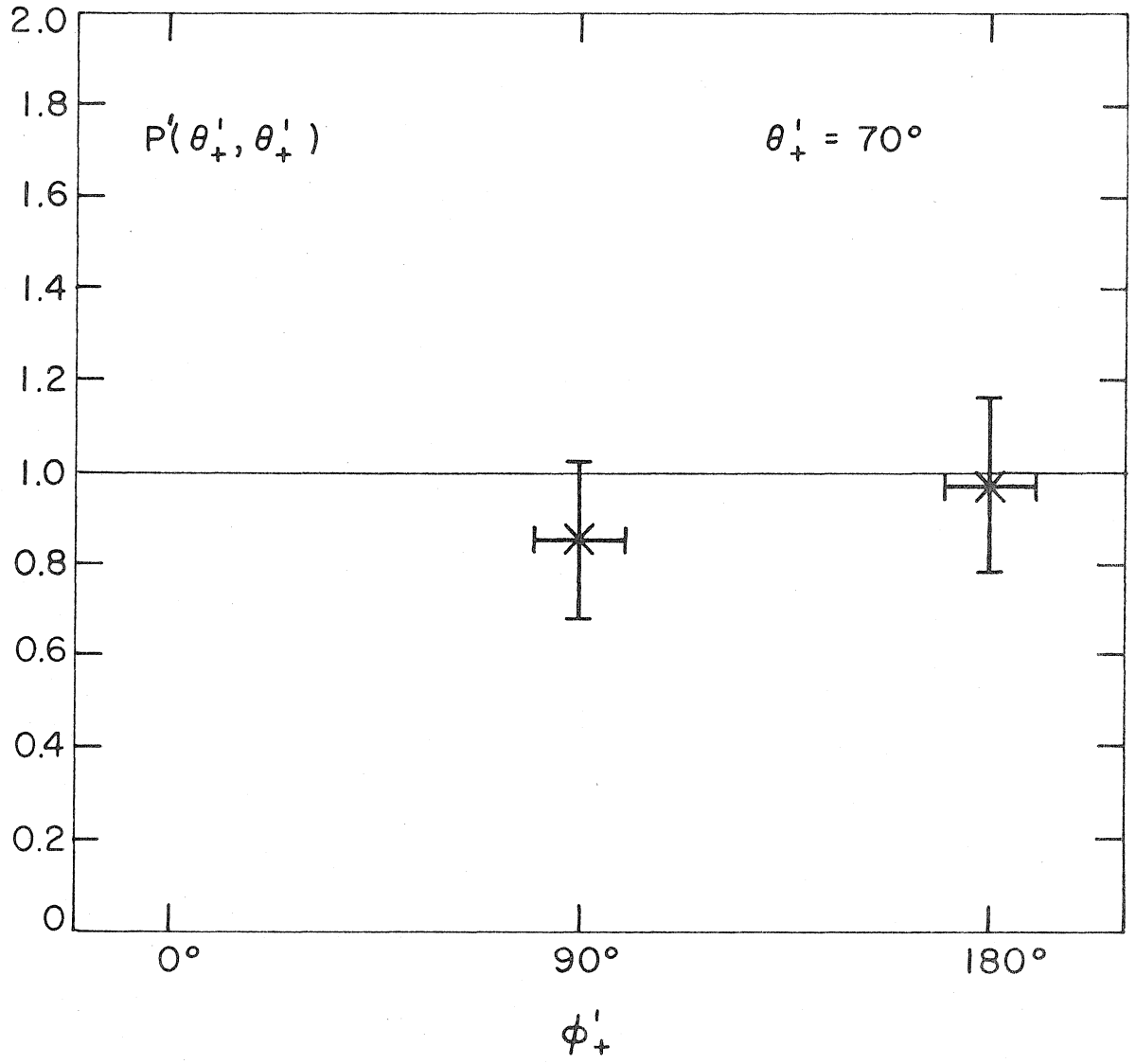
2.0
1.8
1.6
1.4
1.2
1.0
0.8
0.6
0.4
0.2
0
P'(θ'+, θ'+)
θ'+ = 70°
0°
90°
180°
φ'+

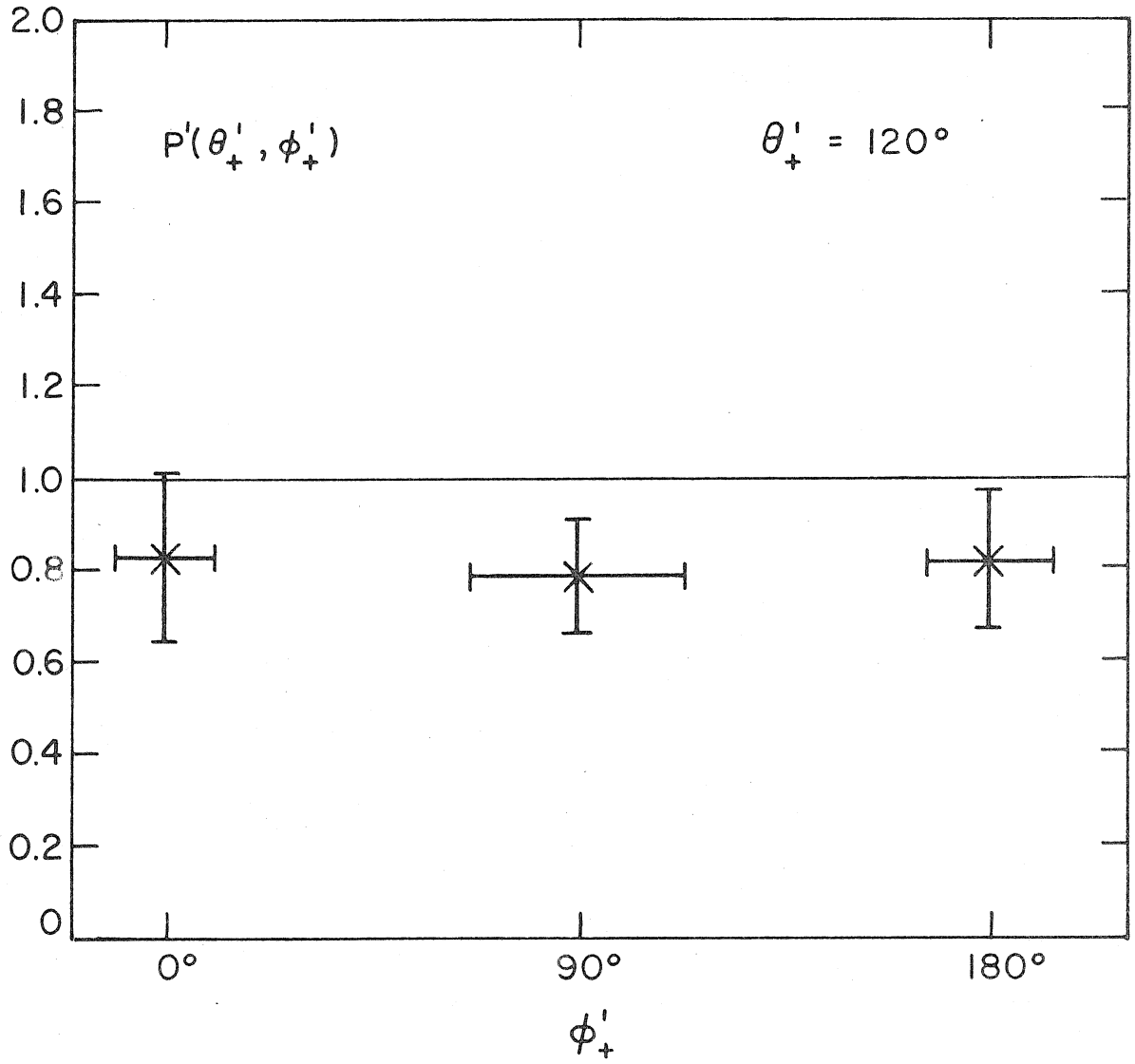
2.0
1.8
1.6
1.4
1.2
1.0
0.8
0.6
0.4
0.2
0
P'(θ'+ , φ'+)
θ'+ = 120°
0°
90°
180°
φ'+

TABLE XIV.

C. M. Correlation Function

$\bar{k}$ = 950 Mev

ϕ_+	θ_+	θ_+'	T_+' (Mev)	$P'(\theta_+', \phi_+)$ (per ster.)
180°	22°	38°	261	1.4 ± 0.8
	45°	73°	285	1.1 ± 0.6
	67°	100°	303	0.7 ± 0.3
	90°	123°	306	0.8 ± 0.3
	120°	145°	307	0.4 ± 0.5
90°	45°	73°	250	1.0 ± 0.5
	90°	123°	268	0.4 ± 0.2
0°	90°	123°	231	0.8 ± 0.3

Figure 27. π^+ C. M. Correlation Function as a Function of θ_+' for $\phi_+' = 180^\circ$. $\bar{k} = 950$ Mev.

Figure 28. π^+ C. M. Correlation Function as a Function of ϕ_+' for $\theta_+' = 73^\circ$. $\bar{k} = 950$ Mev.

Figure 29. π^+ C. M. Correlation Function as a Function of ϕ_+' for $\theta_+' = 123^\circ$. $\bar{k} = 950$ Mev.

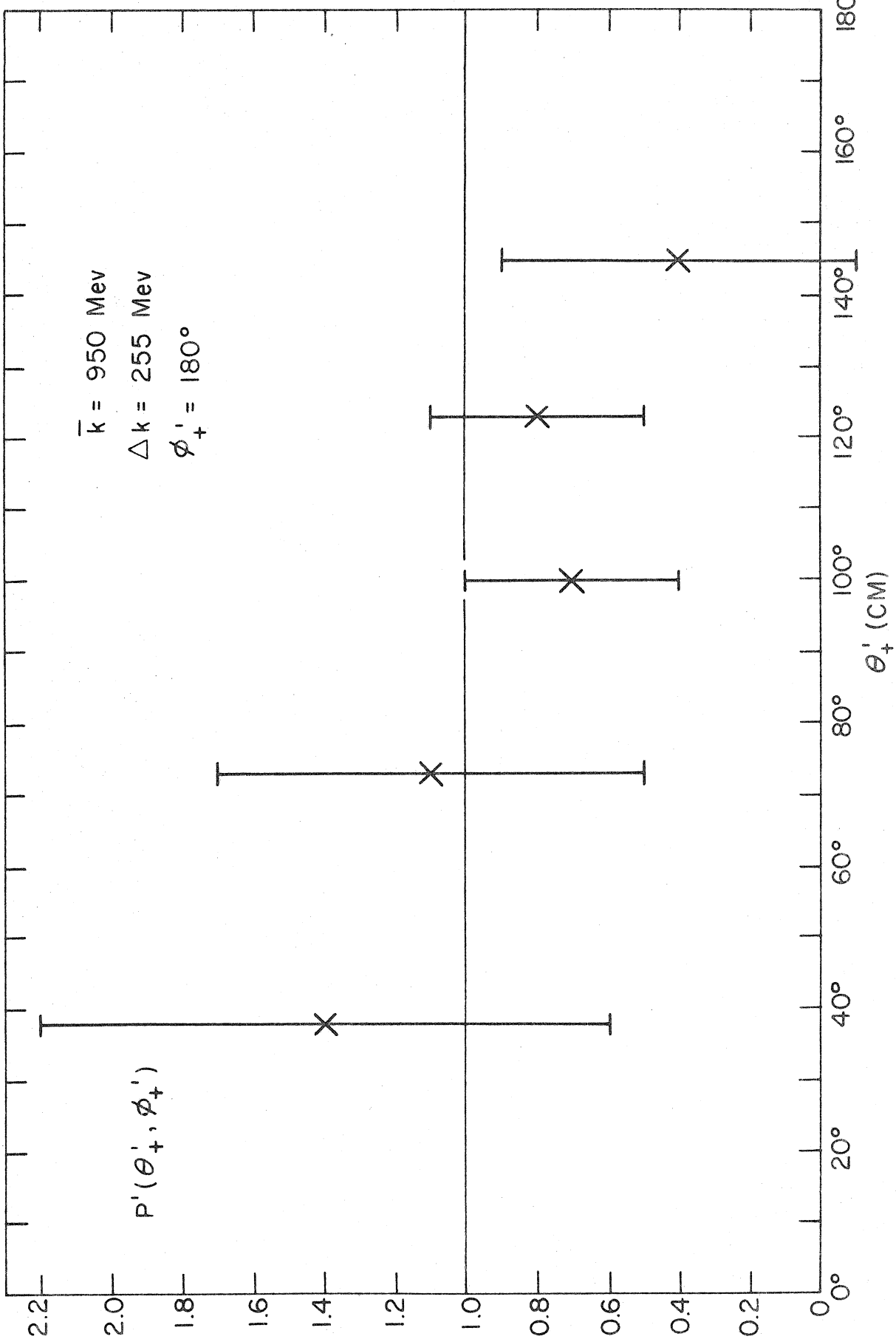
$\bar{k}$ = 950 Mev
Δk = 255 Mev
ϕ_+' = 180°
$P'(\theta_+', \phi_+')$
θ_+' (CM)
0
0.2
0.4
0.6
0.8
1.0
1.2
1.4
1.6
1.8
2.0
2.2
0°
20°
40°
60°
80°
100°
120°
140°
160°
180°

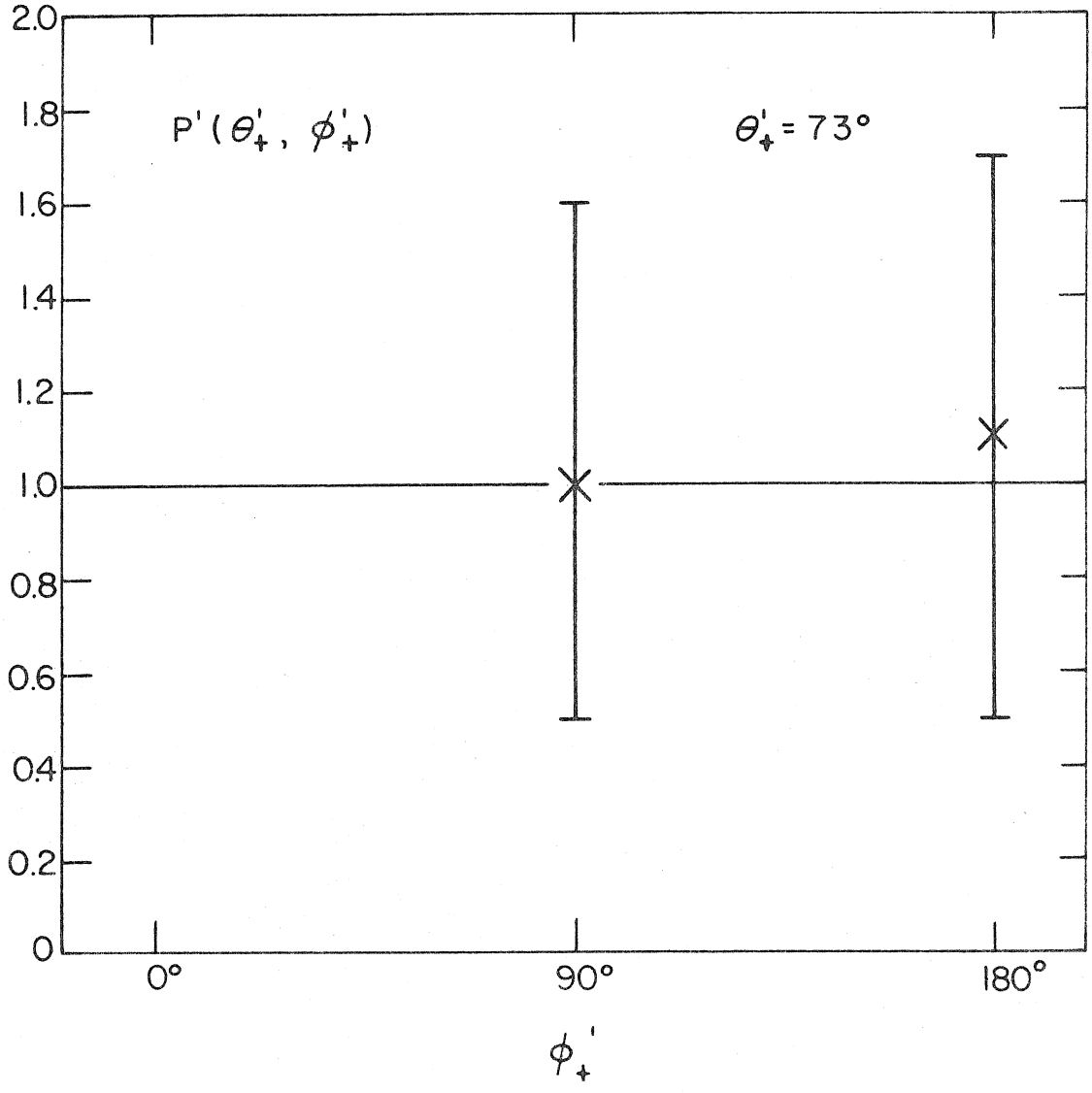
2.0
1.8
1.6
1.4
1.2
1.0
0.8
0.6
0.4
0.2
0
P'(θ'+, φ'+)
θ'+ = 73°
0°
90°
180°
φ'+

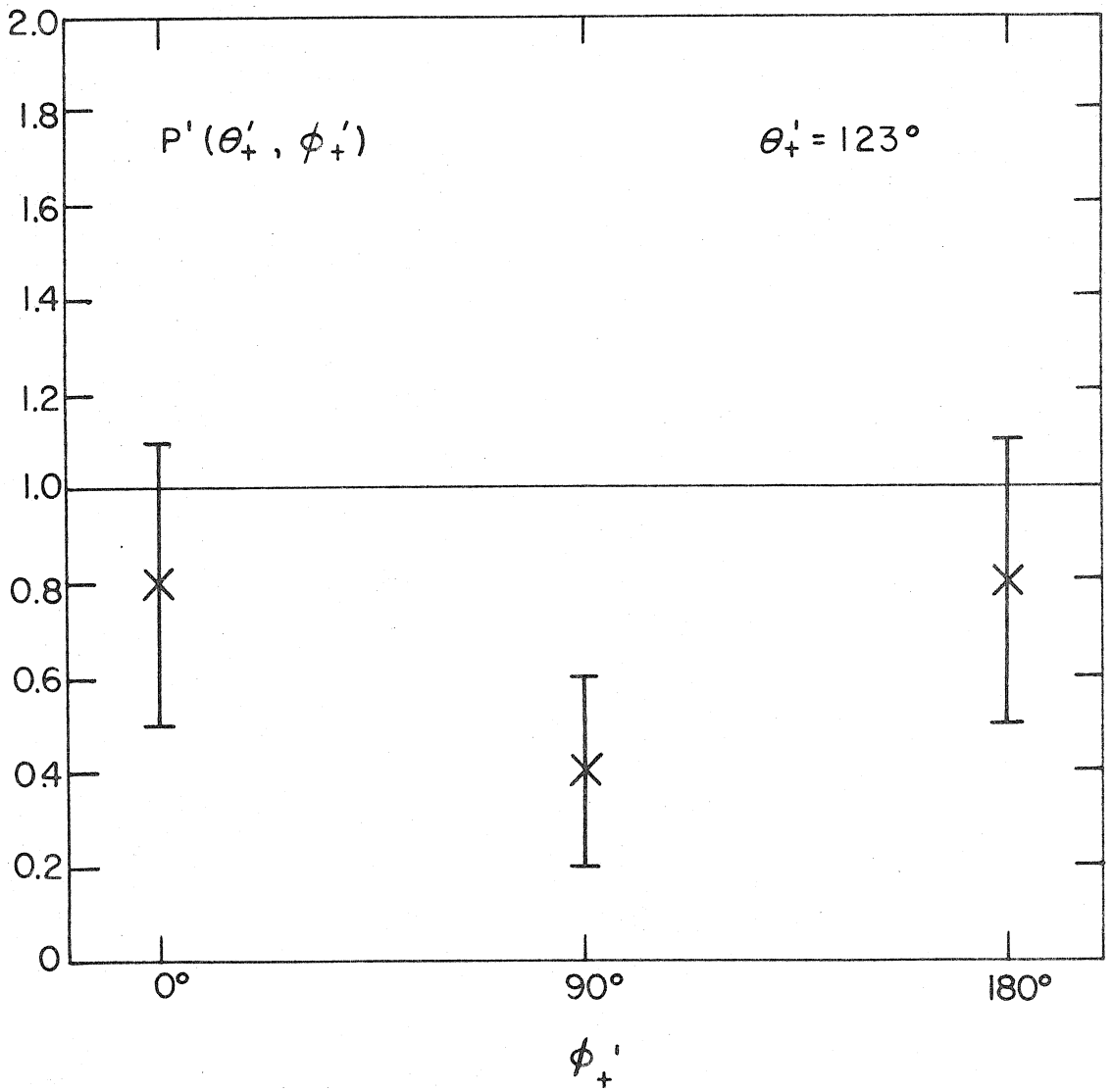
2.0
1.8
1.6
1.4
1.2
1.0
0.8
0.6
0.4
0.2
0
P'(θ+', φ+')
θ+' = 123°
0°
90°
180°
φ+'

correlation function except for noting a possible forward peaking in the zenith angle dependence for $\phi_+' = 180^\circ$, and a possible azimuthal dependence at $\theta_+' = 123^\circ$.

V. INTERPRETATION ATTEMPTS

There is, as yet, no theoretical description of the photoproduction of pion pairs at high energies. Near threshold the theory of Cutkosky and Zachariasen agrees with the experimental results, and the predictions of this theory and the predictions of several heuristic models have been compared with our data. These comparisons have only been made with the angular correlation function at $\bar{k} = 740$ Mev, the correlation function at $\bar{k} = 950$ Mev has such large errors as to make the comparisions inconclusive.

A. Cutkosky - Zachariasen Calculation

The Chew - Low theory has been applied by Cutkosky and Zachariasen (26) to calculate the photoproduction of pion pairs near threshold neglecting the effects of the nucleon recoil and considering only the case in which one pion is produced in an S state and the other pion in a P state. They give the following expression for the cross-section:

$$\sigma_{+-} = \frac{12\alpha}{(4\pi)^2}\left(\frac{\hbar}{\mu c}\right)^2 \frac{\mu^3 p_+ p_-}{k}\left[p_+^2 \Sigma_+^2 F_-^2 \left(\tfrac{1}{2}\sin^2\theta_+ + \tfrac{1}{3}\right) + \frac{1}{9} p_-^2 \Sigma_-^2 F_+^2 \left(\tfrac{1}{2}\sin^2\theta_- + \tfrac{1}{3}\right) - \frac{1}{3} p_+ p_- \Sigma_+ \Sigma_- F_+ F_- \cos(\delta_+ - \delta_-) \times \left(\frac{5}{3}\cos\theta_{+-} - \cos\theta_+ \cos\theta_-\right)\right] \qquad (32)$$

where:

$$\Sigma_{\pm} = (p_{\pm})^{-3} \sin \delta_{\pm}$$

$$F_{\pm} = 1 - \frac{2}{3k} (E_{\pm} - \mu)$$

μ = pion mass

$\delta_{\pm} = \frac{3}{2}, \frac{3}{2}$ scattering phase shift

θ_{+-} = angle between two pions

The values of δ_{33} were computed from the expression given by the Chew - Low theory (27).

$$\cot \delta_{\pm} = \frac{3}{4} \frac{E_{\pm}}{f^2 p_{\pm}^2} \left(1 - \frac{E_{\pm}}{\omega_o} \right) \qquad (33)$$

where:

$f^2 = 0.08$

ω_o = 290 Mev.

μ = pion mass

The correlation function is proportional to the cross-section, and the proportionality constant is equal to 4π divided by the integral of the cross-section over all π^+ directions holding k, p_-, and θ_- fixed. Figures 30 and 31 show the comparison between the data and the computed correlation function. The predicted curve does not agree with the observed distribution. It must be noted that the coordinate

Figure 30. Comparison of the Cutkosky - Zachariasen Theory with the Data as a Function of θ_+' for $\phi_+ = 180^\circ$. $\bar{k} = 740$ Mev.

Figure 31. Comparison of the Cutkosky - Zachariasen Theory with the Data as a Function of ϕ_+' for $\theta_+' = 120^\circ$.

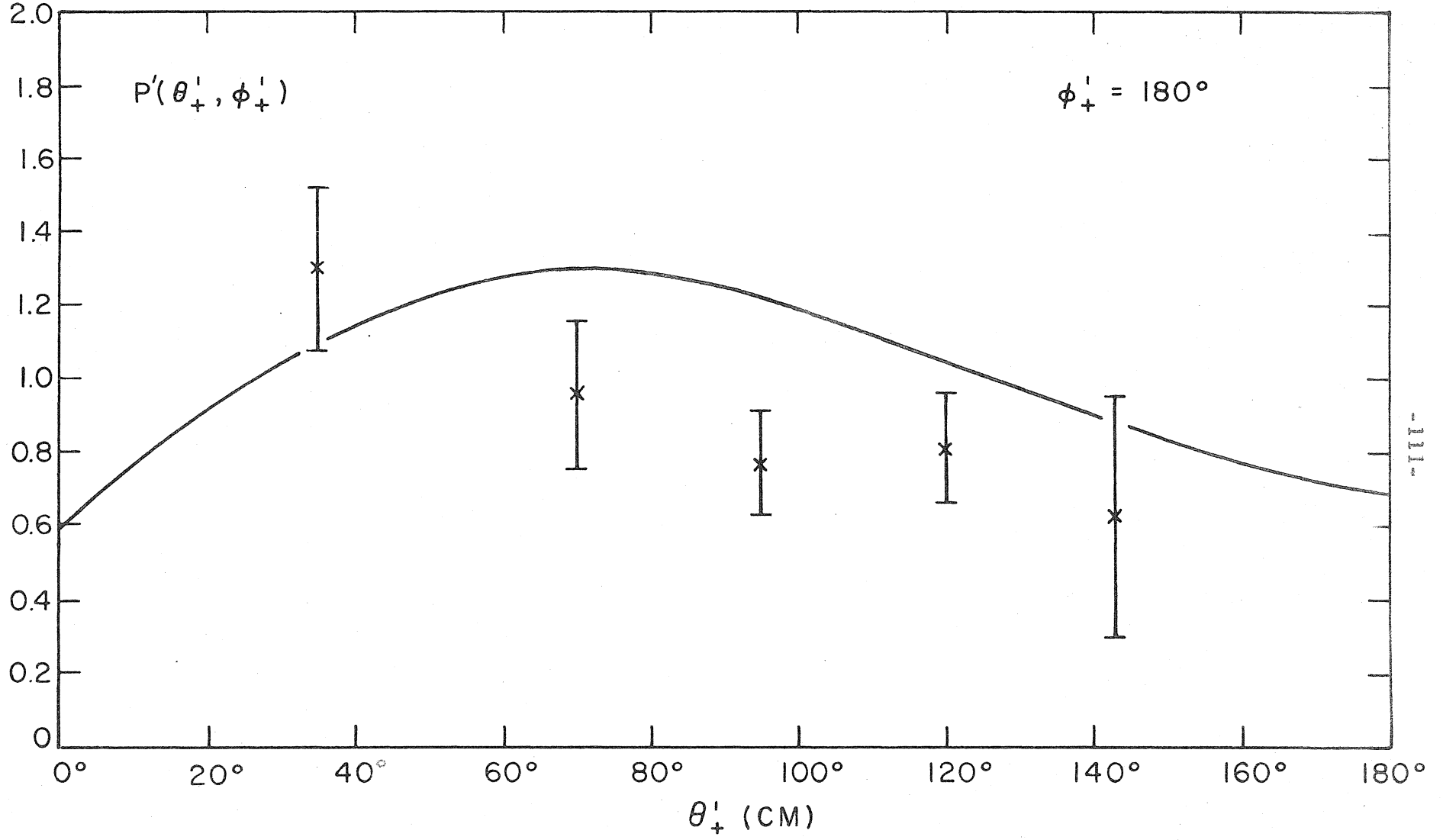
2.0
1.8
1.6
1.4
1.2
1.0
0.8
0.6
0.4
0.2
0
P'(θ'+, φ'+)
φ'+ = 180°
0°
20°
40°
60°
80°
100°
120°
140°
160°
180°
θ'+ (CM)

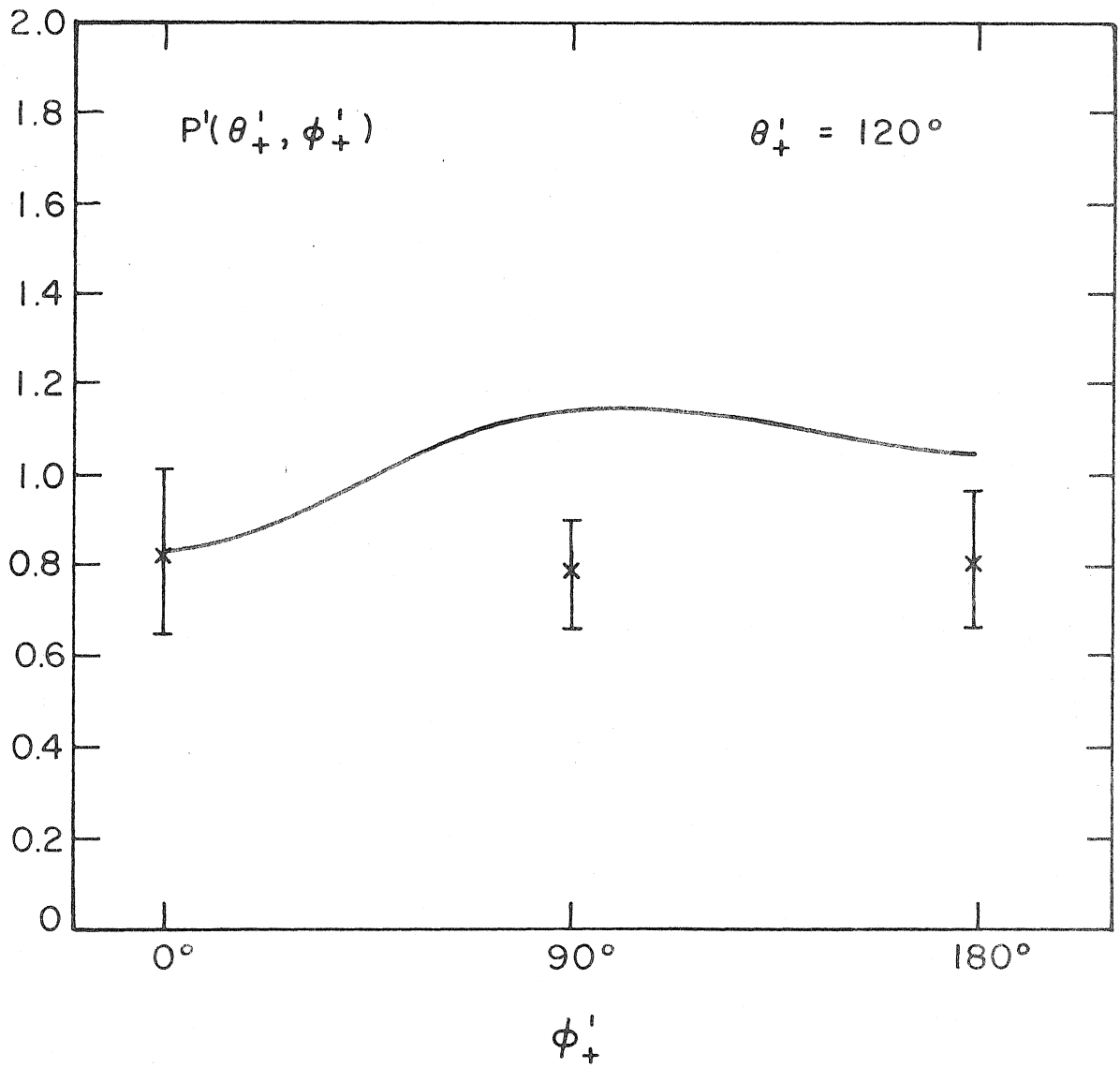
2.0
1.8
1.6
1.4
1.2
1.0
0.8
0.6
0.4
0.2
0
$P'(\theta'_+, \phi'_+)$
$\theta'_+ = 120°$
0°
90°
180°
ϕ'_+

system in which equation 32 was derived is not quite the C. M. system of the reaction. The system used by C - Z contained an infinitely heavy nucleon, however, the difference between the two systems has been neglected.

B. Density of States

A simple model is obtained from the assumption that the matrix element for the interaction is independent of the π^+ angle and energy. The angular correlation function is then simply proportional to the three body density of final states:

$$P(\theta_{+-}) = (\text{const.}) \frac{(E_o - E_+ - E_-) E_+ p_+^2 p_- E_-}{p_+ (E_o - E_-) + E_+ p_- \cos \theta_{+-}} \qquad (34)$$

where E_o is the total energy available for the reaction, and θ_{+-} is the angle between the two mesons. All quantities are in the C. M. system. In order to determine the constant of proportionality in equation 34, the distribution was plotted and numerically integrated over all π^+ directions. The value of the constant was chosen so that the integral was equal to 4π. The correlation function in equation 34 depends only on one angular coordinate, θ_{+-}, and so both the predictions of this model and the data were plotted on one graph as a function of θ_{+-} (see figure 32). The angles next to each experimental point in figure 32 are the values of ϕ_+ at which the point was measured. The agreement between the data and the correlation function predicted by the density of states is not satisfactory.

Figure 32. Comparison of the Density of States and the Data as a Function of θ'_{+-}. $\overline{k}$ = 740 Mev.

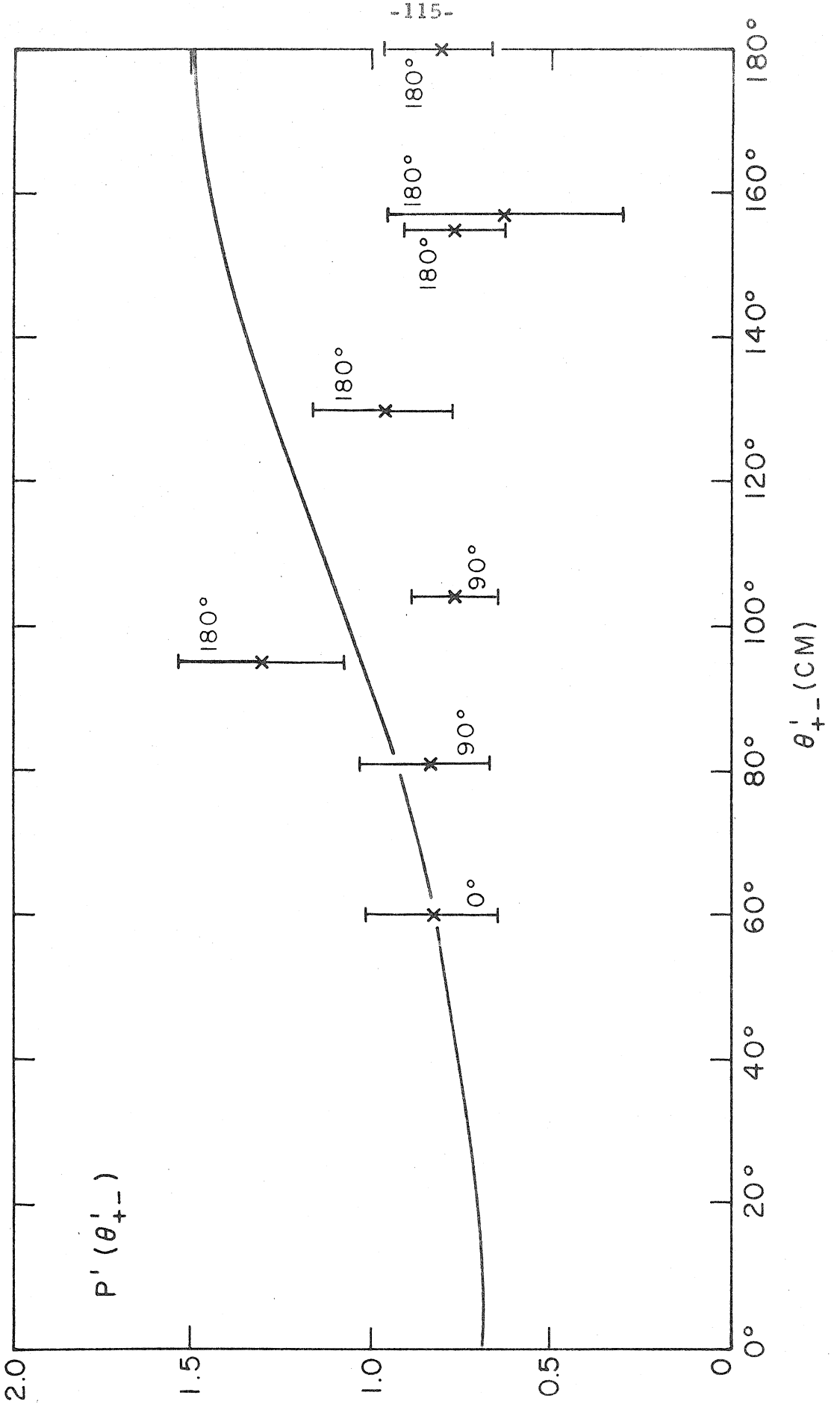
2.0
1.5
1.0
0.5
0
0°
20°
40°
60°
80°
100°
120°
140°
160°
180°
$P'(\theta'_{+-})$
θ'_{+-} (CM)
180°
90°
0°
180°
90°
180°
180°
180°

If indeed the experimental correlation function depends only on θ_{+-}, then it is seen from figure 32 that the function is consistent with isotropy. There is some indication, however, that such a simple angular dependence is not correct because of the disagreement between the two points at $\theta_{+-} = 95^{\circ}$ and $\theta_{+-} = 104^{\circ}$.

C. Isobar Model

There has been some success in interpreting some high energy pion experiments in terms of an "isobar model" which attempts to take into account the strong interaction between the pion and nucleon in the $T = \frac{3}{2}$, $J = \frac{3}{2}$ state by considering this state to be sufficiently narrow that it plays the role of a "particle" in the basic interaction. Such a model was first applied by Yuan and Lindenbaum (22) in interpreting the results of pion production in nucleon - nucleon collisions. In later work (24, 25) the model was applied to the problem of inelastic pion - nucleon scattering. Bloch and Sands (21) have investigated the properties of the isobar model applied to the photoproduction of pion pairs.

In the case of pion pair production, one considers that one pion (called the recoil pion) and an isobar with excitation energy Q (in its coordinate frame) are produced in the initial reaction. A short time later ($\sim 10^{-23}$ sec) the isobar decays into a proton and a pion (called the decay pion). If the decay pion is a π^+ the isobar is doubly charged, and if the decay pion is a π^- the isobar is neutral. In order to compute the angular correlation function of the π^+ from this model the following

assumptions are made. (a) The probability of producing an isobar is proportional to two factors. One factor is the two body density of final states ($\rho(E_o, Q)$) of the isobar and the recoil meson. The other factor is a function ($F(Q)$) which represents the relative probability of forming an isobar with excitation energy Q, and is gotten from pion-nucleon scattering data. (b) The isobar is emitted isotropically in the C. M. system. (c) The decay meson is emitted isotropically in the isobar rest system. From these assumptions the correlation function can be computed.

$$P(\theta_+, \phi_+) = (\text{const.})\, F(Q)\, \rho(E_o, Q)\, \frac{dQ}{dE_-}\, \frac{d\Omega_d'}{d\Omega_d} \tag{35}$$

The subscript d refers to the decay pion and the subscript r refers to the recoil pion, the primes indicate quantities in the isobar rest system, and the unprimed quantities are in the C. M. system of the initial reaction ($\gamma + P$). The values of E_o, Q, and ρ are computed from the equations:

$$E_o = \sqrt{M^2 + 2kM} \quad (k \text{ in LAB.}) \tag{36}$$

$$Q = \sqrt{E_o^2 + \mu^2 - 2E_o E_r} - M - \mu \tag{37}$$

$$\rho = \frac{(E_o - E_r)\, E_r p_r}{E_o} \tag{38}$$

Other workers (22, 23, 24, 25) have taken $F(Q)$ to be equal to the

observed total scattering cross-section for pions on protons. Sands (43) has shown that one should instead take $F(Q)$ equal to the total scattering cross-section divided by $\frac{\Gamma}{p^2}$, where p is the C. M. momentum of the incoming pion and Γ is the 3, 3 scattering resonance width. This modification corresponds to considering the scattering as the product of a non-resonant part and an enhancement factor which introduces the effect of the resonance. Only this enhancement factor contributes to the probability of isobar formation, and hence it alone should be used for $F(Q)$. Sands has shown that dividing the total cross-section by Γ/p^2 has the effect of removing the non-resonant part of the scattering. Figure 33 shows $F(Q)$ as a function of Q and the value of Γ was computed from the Chew - Low theory.

$$\Gamma = \frac{8}{3} f^2 p^3 \frac{\omega_o}{\omega^*} \tag{39}$$

where:

$$\omega^* = \sqrt{\mu^2 + p^2} + \frac{p^2}{2M} \tag{40}$$

p = C. M. momentum of incoming pion

μ = pion mass

M = proton mass

ω_o = 290 Mev

f^2 = 0.08

Figure 33. Relative Probability Distribution for the Formation of an Isobar with Excitation Energy Q as a Function of Q.

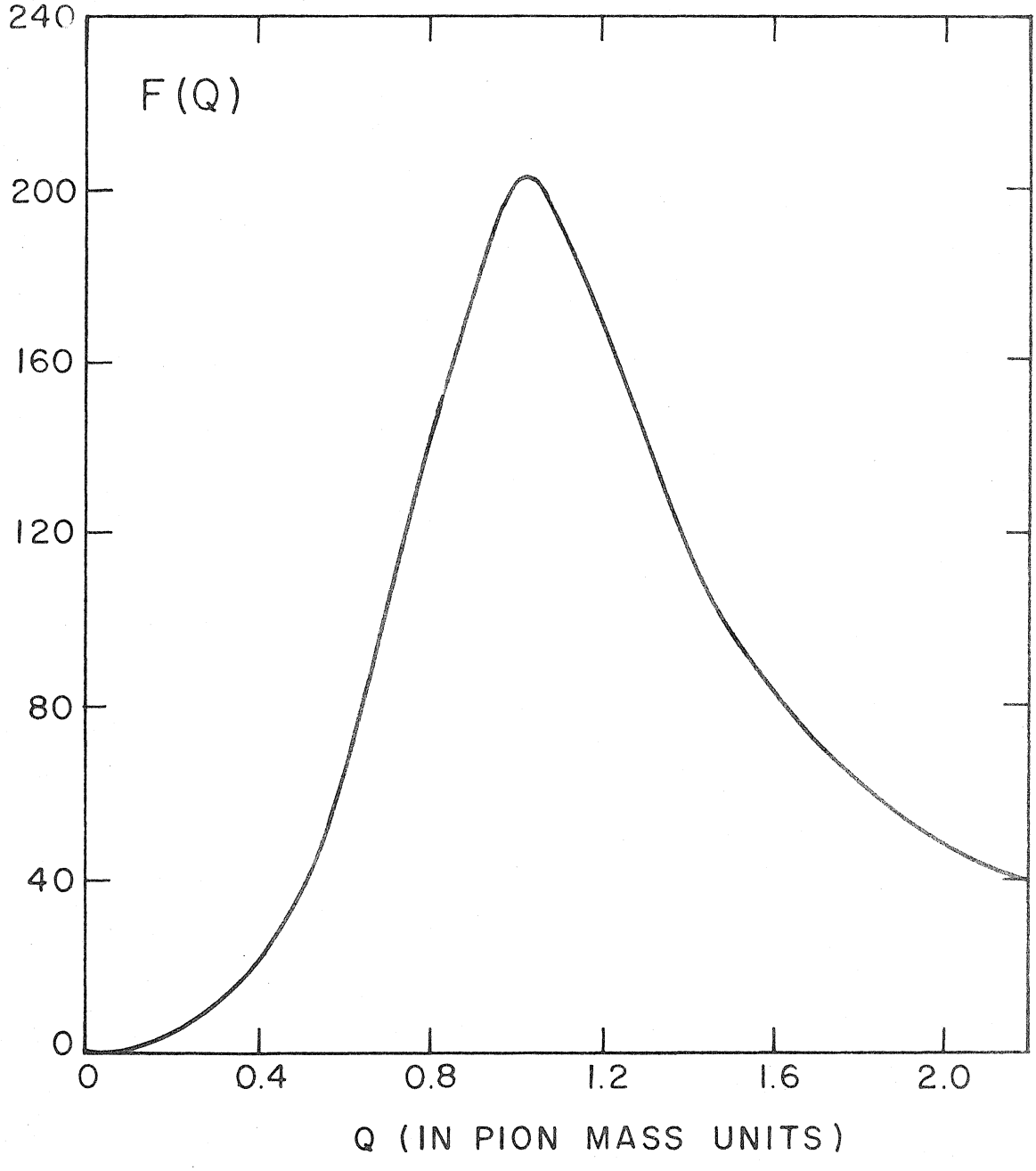
240
F(Q)
200
160
120
80
40
0
0
0.4
0.8
1.2
1.6
2.0
Q (IN PION MASS UNITS)

The two isobars (doubly charged and neutral) must now be considered separately.

1. Doubly Charged Isobar

In the case of our experiment where the angle and energy of the π^- were fixed, the correlation function predicted by the doubly charged isobar is simply proportional to $\frac{d\Omega'_+}{d\Omega_+}$, the other quantities in equation 35 being constant. (In this case, therefore, no assumption need be made about the form of $F(Q)$ or the angular dependence of the isobar production.)

$$P(Q_{+-}) = 4\pi \frac{p_+}{p'_+} \frac{M + \mu + Q}{E_o - E_- + \frac{p_-}{\beta_+} \cos \theta_{+-}} \tag{41}$$

The correlation function predicted from this model is shown in figure 34 and seems to be in fair agreement with the points lying between 60^o and 130^o. At the backward angles of 160^o and 180^o, however, the predicted value of the distribution is almost twice the value of the experimental points.

2. Neutral Isobar

The computation of the correlation function in the case of the neutral isobar is more complicated, and all the assumptions made in the general description of the model are necessary.

$$P(\theta_{+-}) = (\text{const.})\, F(Q)\, \rho(E_o, Q) \frac{dQ}{dE'_-} \frac{dE'_-}{dE_-} \frac{d\Omega'_-}{d\Omega_-} \tag{42}$$

Figure 34. Comparison of the Isobar Model and the Data as a Function of θ'_{+-}.

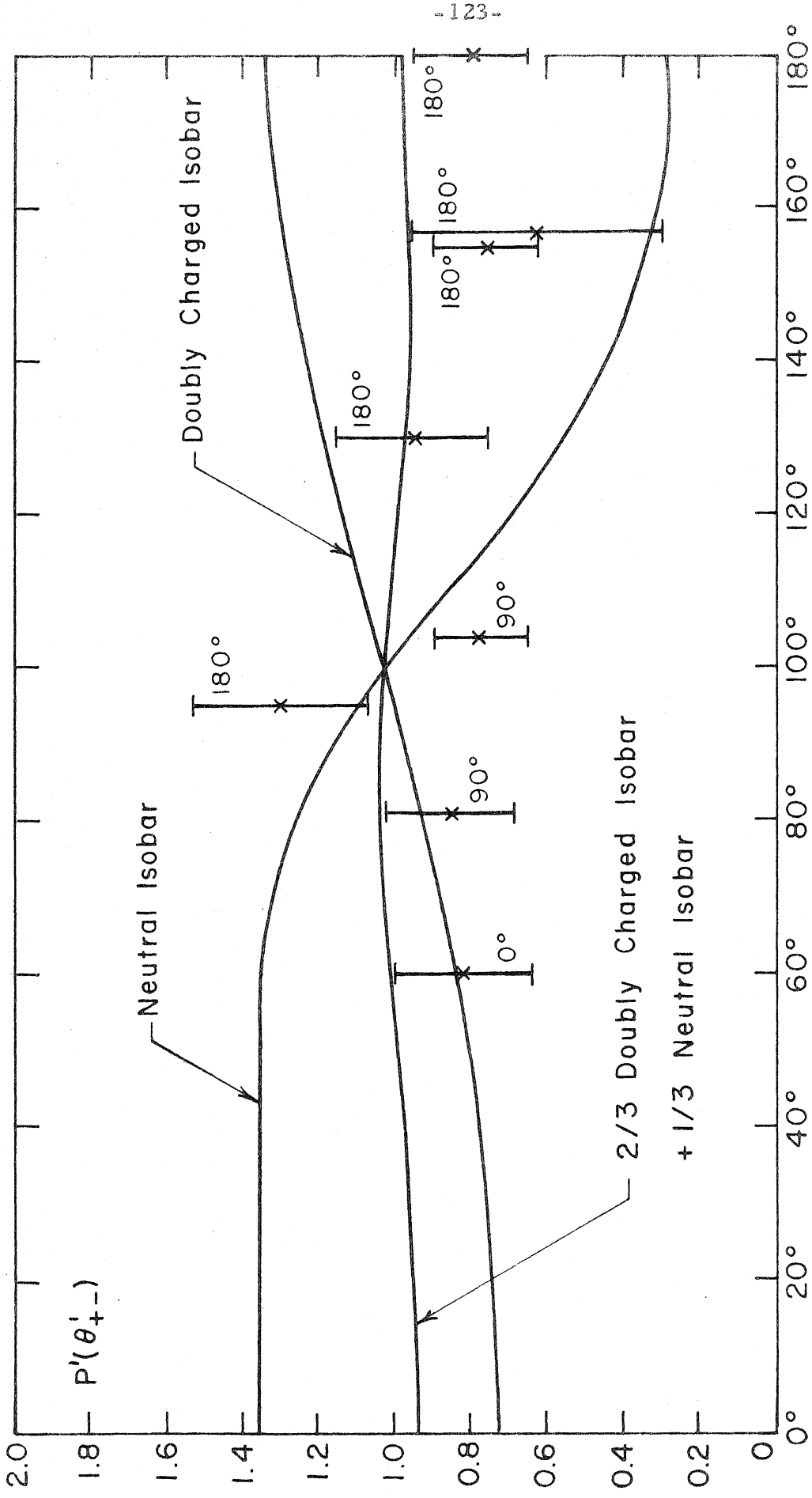
Doubly Charged Isobar
Neutral Isobar
2/3 Doubly Charged Isobar
+ 1/3 Neutral Isobar
180°
90°
0°
$P'(\theta'_{+-})$
θ'_{+-} (ANGLE BETWEEN TWO PIONS IN CM)
2.0
1.8
1.6
1.4
1.2
1.0
0.8
0.6
0.4
0.2
0
0°
20°
40°
60°
80°
100°
120°
140°
160°
180°

Where:

$$I = M + \mu + Q \quad \text{(mass of the isobar)} \tag{43}$$

$$E_-' = \frac{I^2 + \mu^2 - M^2}{2I} \tag{44}$$

$$\frac{dQ}{dE_-'} = \frac{I}{I - E_-'} \tag{45}$$

$$\frac{d\Omega_-'}{d\Omega_-} \times \frac{dE_-'}{dE_-} = \frac{p_-}{p_-'} \tag{46}$$

Figure 35 shows how each of the factors in equation 42 varies as a function of the total π^+ energy in the C. M. The arrows along the abscissas indicate the kinematical limits of the total energy for the pair reaction. The constant of proportionality in equation 42 was determined by numerically integrating the computed distribution over all π^+ directions, and choosing the constant so that the integral was equal to 4π. The correlation function predicted by this model is shown in figure 34 and the agreement with the data is again unsatisfactory.

Clegg (44) has suggested that one may be able to improve the agreement between the data and either of the two models by making a different choice for the angular dependence of the emission of the isobar in the initial reaction and for the angular dependence of the isobar decay. Considering only the first two lowest multipole photons, he has computed the angular dependence for the isobar emission (see Table XV). The angular dependence of the isobar emission has no

Figure 35. Curves of the Functions Involved in the Computation of the Correlation Function for the Neutral Isobar Model.

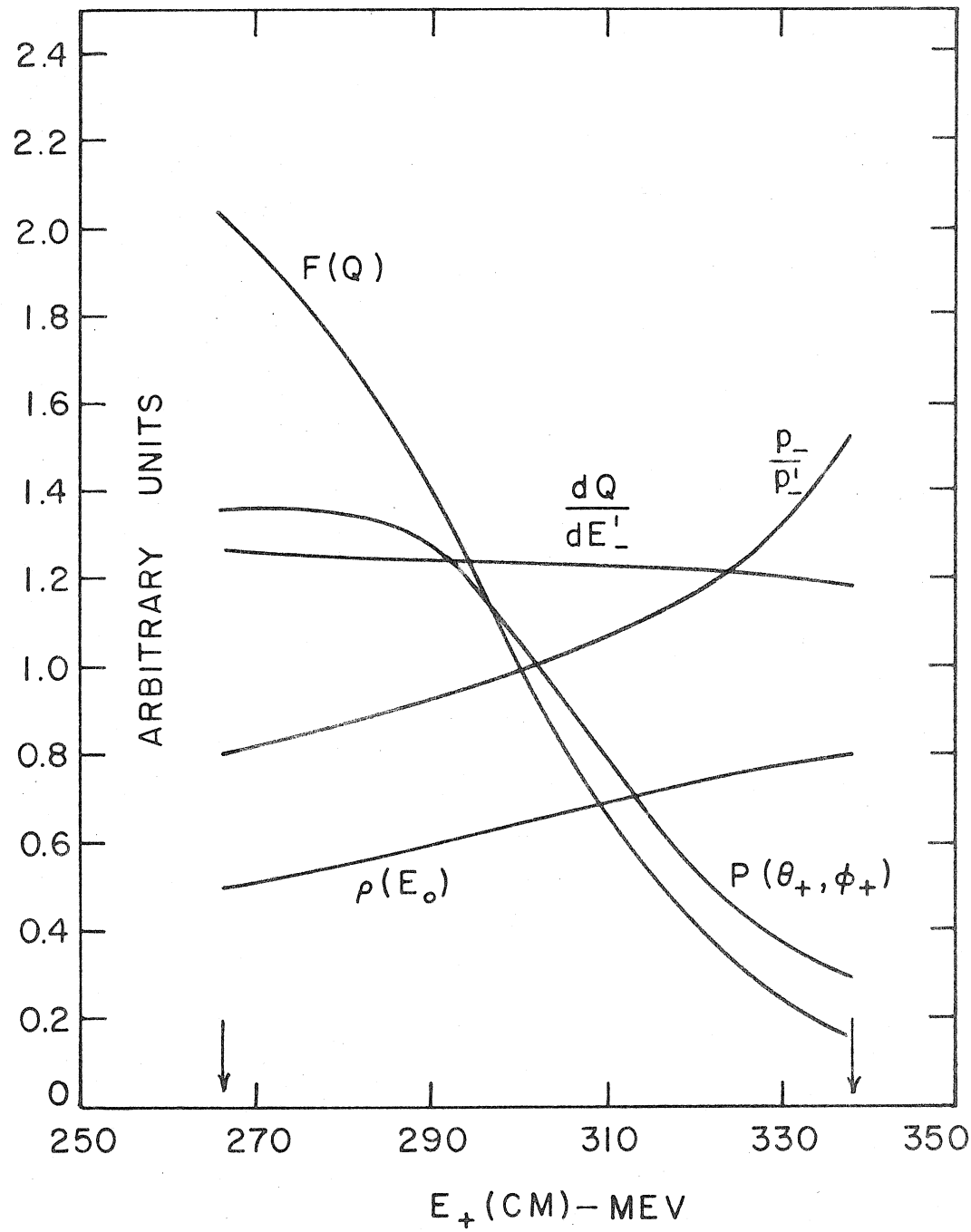
2.4
2.2
2.0
1.8
1.6
1.4
1.2
1.0
0.8
0.6
0.4
0.2
0
ARBITRARY UNITS
F(Q)
dQ/dE'_
p_/p'_
ρ(E_o)
P(θ+, φ+)
250
270
290
310
330
350
E+(CM)-MEV

TABLE XV.

Incoming Multipole	Spin and Parity of Compound State	Outgoing Orbital Angular Momentum	Angular Distribution of Isobar Emission
E 1	1/2 -	d-wave	isotropic
E 1	3/2 -	s-wave	isotropic
M 1	1/2 +	p-wave	isotropic
M 1	3/2 +	p-wave	$4 + 3 \cos^2\theta_{Iso.}$

effect on the doubly charged isobar because, as noted above, the angle of the recoil meson is fixed. In the case of the neutral isobar, however, the $4 + 3 \cos^2 \theta_{Iso.}$ changes the predicted correlation function and the effect is strongest in the forward direction. The modified distribution peaks at $\theta_{+-} = 60^\circ$ and falls to about 2/3 of the peak value at 0°. For θ_{+-} greater than 90° the change in the distribution is slight. The modified distribution is not plotted because it does not improve the agreement with the data at θ_{+-} greater than 90°, and worsens the agreement at $\theta_{+-} = 60^\circ$ and 80°.

Clegg has also pointed out that for each of the four entries in the Table XV one can compute an angular dependence for the decay of the isobar. The decay is not isotropic in general because the magnetic substates of the isobar are populated unequally. For one incoming multipole and one outgoing angular momentum the magnetic substates will be populated in the following way:

M_z =	+ 3/2	+ 1/2	- 1/2	- 3/2
Population =	a	b	b	a

where $\underline{a}$ and $\underline{b}$ are given in Table XVI. The angular distribution of the decay pion in the isobar rest system is given by:

$$1 + \frac{3(b-a)}{3a + b} \cos^2 \theta_d' \qquad (47)$$

where θ_d' is the angle of the decay pion with respect to the photon direction in the isobar rest system. In the case of the doubly charged

TABLE XVI.

Incoming Multipole	Spin and Parity of Compound State	Outgoing Orbital Angular Momentum	a	b
E 1	1/2 -	d-wave	$3(1-\cos^2\theta_{Iso.})$	$(1+3\cos^2\theta_{Iso.})$
E 1	3/2 -	s-wave	1	1/3
M 1	1/2 +	p-wave	$3(1-\cos^2\theta_{Iso.})$	$(1+3\cos^2\theta_{Iso.})$
M 1	3/2 +	p-wave	$3(1+8\cos^2\theta_{Iso.})$	$(13-12\cos^2\theta_{Iso.})$

isobar, only the distribution corresponding to the second case in Table XVI produces more than a slight effect, the main feature of which is the increasing of the correlation function at θ_{+-} greater than 120° by about 15 $^{o}/o$. This is a change in the wrong direction to improve the agreement with the data. In the case of the neutral isobar, the distribution corresponding to the third case in Table XVI produces only a slight effect; the fourth case produces an effect which would improve the agreement with the data somewhat, however, the angular dependence of the isobar emission (see Table XV) for this case produces an effect which essentially cancels the improvement; and the first and third cases put a large peak in the correlation function at $\theta_{+-} = 60^{\circ}$ and reduce the function to practically zero at θ_{+-} greater than 130°.

The comparison of the two isobars with the data seems to indicate that if the isobar model is meaningful, then at the photon energies near 740 Mev one isobar is not strongly preferred to the other even if the calculations are refined to include reasonable guesses for the angular distribution of the recoil and decay meson. In fact, only the case of a magnetic dipole photon interacting with the incoming proton, forming a compound state of $\frac{3}{2}$ +, and having an isobar-recoil meson p-state improves the agreement of either isobar with the data. The measurement of Bloch and Sands indicates that at a photon energy of 660 Mev the pair reaction proceeds through a pure doubly charged isobar, and at 1000 Mev the reaction prefers to go only through a neutral isobar. For lack of better knowledge one might assume that at intermediate energies the process can go through a mixture of the

two isobars of the form $\alpha I^{o} + \beta I^{++}$, where α and β are functions of the photon energy. (It is assumed that the two isobars are short-lived, real particles, consequently, there will be no interference between the two possible charge states.) The mixture which gives the best fit with the data at 740 Mev is roughly 1/3 neutral isobar plus 2/3 doubly charged isobar. This combination of the two isobars is shown in figure 34 and agrees much better with the data than either isobar separately. Since the absolute value of the experimental points is uncertain to within 20 °/o, the agreement could be quite good except for the point at 95°. This point might, of course, just be slightly more than one standard deviation above the true value.

The results of recent experiments show what may be a second resonance in π^{+} photoproduction at 700 Mev (9, 10). The evidence indicates that the state has T = 1/2, but the angular momentum is still uncertain and may be either 1/2 or 3/2. Since the resonance is in the range of photon energies involved in our experiment, one may try to extend the isobar model one step further and ask if the pair production goes through two intermediate states:

$$\gamma + P \longrightarrow I^{*} \longrightarrow \begin{array}{l} I + \pi \\ \quad \big\lfloor P + \pi \end{array}$$

where I^{*} corresponds to an isobar at the second resonance, and I to an isobar at the first resonance. If I^{*} has a definite isotopic spin, one can predict the branching ratio of the decay into I^{++} and I^{o}. For

$T = 1/2$, $I^{++}/I^{o} = 9/1$; and for $T = 3/2$, $I^{++}/I^{o} = 9/4$. The result of our experiment indicates that $I^{++}/I^{o} = 2/1$ which agrees with the $T = 3/2$ state. The evidence of the other workers is quite strong for $T = 1/2$, so one may conclude either that the pair reaction does not proceed through the second resonance isobar or that the isobar is no longer a meaningful model at these energies.

D. Peierls Analysis

Peierls (45) has derived a general expressions for the angular dependence of the cross-section for pion pair production in terms of the unknown spacial and spin parts of the wave functions involved. From this expression he has been able to show that if the azimuthal dependence of the angular distribution is Fourier analyzed into terms of $\cos 2n\phi_{+}$, then the Fourier coefficients will be zero for $n > \ell$ where ℓ is the maximum orbital angular momentum (of either meson) which contributes appreciably to the production process. (Both mesons must have similar energies.) Our results seem to indicate that all Fourier coefficients are zero except for the constant, and so one concludes that only s-wave pions are involved in the interaction. Of course, the experimental errors are so large that any term of the form $\cos 2n\phi_{+}$ could be present in the angular distribution, but it is predominately isotropic.

If one further assumes that the reaction proceeds through a compound state (corresponding to the 700 Mev resonance) with a definite angular momentum (J), assumes that both mesons are emitted in p-states, and assumes that both pions have energies relative to the

proton of about 150 Mev, then the coefficient of the cos $2\phi_+$ term in the angular distribution will be positive if $J = 1/2$ or $5/2$, and negative if $J = 3/2$. Our data shows no azimuthal dependence, and so it is not possible to identify the angular momentum of the proposed compound state.

VI. CONCLUSION

The angular correlation between the two pions produced from the reaction $\gamma + P \rightarrow P + \pi^+ + \pi^-$ has been studied as a function of the direction of emission of the π^+ for a fixed π^- energy (150 Mev) and angle (35°) and at two photon energies (740 Mev and 950 Mev). The data is presented as an angular correlation function in the C. M. system. At 950 Mev the experimental points have such large errors that the shape of the correlation function is undetermined. At 740 Mev the correlation function does not show any azimuthal dependence, and as a function of zenith angle the correlation is nearly constant but may be peaked somewhat in the forward direction. The predictions of the "isobar model" were compared with the experimental results at 740 Mev and there is satisfactory agreement in the case where the reaction proceeds through an intermediate state which contains a combination of the two different charge states of the isobar (2/3 doubly - charged isobar and 1/3 neutral isobar). The fact that neither of the two isobars dominates the production process at 740 Mev is consistent with the findings of Bloch and Sands.

The cross-section for the photoproduction of π^- from hydrogen has been studied at 35° in conjunction with the angular correlation measurement. When the cross-section is expressed in the C. M. system and compared with the results of Bloch and Sands (20, 21), it seems to indicate that the π^- is emitted preferentially in the forward direction. This result and the nearly isotropic distribution of the π^+ agrees with

the preliminary results of work done on pion pair production by Sellen et al. (28, 29).

The experimental arrangement used in this experiment seems to be quite satisfactory for studying the correlation between the two pions from the pair process. For the extension of the measurements to higher photon energies, however, a high energy spectrometer must be used. A measurement with good statistics of the correlation at 1000 Mev would be useful in checking the validity of the isobar model.

It is hoped that this study will spur further experimental interest in the photoproduction of pion pairs, and with the refinement of the measurements perhaps the attempts to interpret and understand the process will achieve success.

APPENDIX I.

π^- Backgrounds at 650 and 825 Mev.

No empty target runs were made when the π^- production rate was measured at the bremsstrahlung cut-off energies of 650 and 825 Mev. An empty target run was, however, made immediately afterwards at E_o = 1080 Mev, and the backgrounds at 650 and 825 Mev can be inferred from this data. At the time the spectrometer was first placed at 35° a number of empty target runs were made at several bremsstrahlung cut-off energies, and these results are given in the top half of Table AI (see Section IV. A. 1 for the definition of n_3 and n_4). Although the errors are large the general behavior seems to indicate a constant background independent of E_o. Bloch's background measurements (20) as a function of E_o were also constant within the errors at 60° and at 120°. Such a constant background can be explained if the source of the background is π^- and π^o photoproduction and electron pair production in the steel ends of the target. The π^- could be scattered by the target walls or the lead bridges into the solid angle of acceptance of the spectrometer. Most of the π^- would be produced by photons which have energies near the resonance at 300 Mev, and so the only dependence on the bremsstrahlung cut-off energy of the π^- background would be due to the E_o dependence of the bremsstrahlung energy spectrum near 300 Mev. The spectrum is described in Section II. B. and is a slowly varying function of E_o. For k = 300 Mev the spectrum decreases by 20 °/o from E_o = 700 Mev to E_o = 1100 Mev. The electron component of the background could come from electrons produced in pairs in the target ends

and then scattered by the target walls or the lead bridges into the counting solid angle, or it could come from the conversion of the γ-rays from π^o decay. The electron background arising from the π^o decay should have the same E_o dependence as the π^- background. The E_o dependence of the electron background arising from the electron pairs could be calculated exactly from the Bethe - Heitler formula, however, for the purpose of this estimate the background was assumed to depend only on the total number of photons in the beam with energies greater than 250 Mev (the energy of an electron accepted by the spectrometer). This number also varies slowly with E_o, increasing by 30 ^{o}/o from E_o = 700 Mev to E_o = 1100 Mev.

The 650 and 825 Mev backgrounds have, therefore, been assumed to be the same as the background measured at 1080 Mev. The errors assigned to these two backgrounds are the statistical error in the 1080 Mev background plus an additional 20 ^{o}/o uncertainty to take account of possible slow variations in the background as a function of E_o due to the sources of background described above. The backgrounds are given in the bottom half of Table A I.

TABLE A I.

Background Counting Rates Per 10^{15} Mev in X-Ray Beam

E_o(Mev)	T(Mev)	n_3	n_4
1084	100	0.17 ± 0.07	0.02 ± 0.07
1084	150	0.17 ± 0.03	0.10 ± 0.03
972	100	0.04 ± 0.07	0.10 ± 0.06
972	150	0.09 ± 0.06	0.10 ± 0.05
896	100	0.10 ± 0.09	0.03 ± 0.09
896	150	0.23 ± 0.08	0.14 ± 0.06
708	100	0.15 ± 0.11	0.18 ± 0.14
708	150	0.05 ± 0.13	0.05 ± 0.12

Background Counting Rates Inferred from 1080 Mev Data

E_o(Mev)	T(Mev)	n_3	n_4
825	100	0.50 ± 0.12	0.07 ± 0.05
825	150	0.55 ± 0.15	0 ± 0.04
650	100	0.50 ± 0.12	0.07 ± 0.05
650	150	0.55 ± 0.15	0 ± 0.04

APPENDIX II.

Nuclear Absorption of Positive Pions in Lead

A number of workers (46, 47, 48, 49) have studied the absorption of negative pions in lead for pion energies from 85 to 140 Mev, and their results agree with a geometric absorption cross-section within the errors of the measurements which are typically $\pm$ 10 $^{o}/_{o}$. The absorption cross-section for positive pions can be deduced from the absorption cross-section for negative pions if the following assumptions are made.

(i) In the case of a large nucleus such as lead the absorption cross-section for pions of either charge has an upper limit which is essentially the geometric cross-section (for large enough pion energies to allow Coulomb effects to be neglected). This assumption would seem to be reasonable if the radius of the lead nucleus was much larger than the characteristic pion-nucleon interaction distance which is roughly the pion Compton wave-length. The radius of the lead nucleus is six times the pion Compton wave-length.

(ii) The absorption cross-section for positive pions is larger than for negative pions in lead because of the neutron excess.

The positive pion absorption cross-section is, therefore, bounded both above and below by the geometric cross-section for energies in the interval from 85 to 140 Mev. There is one experiment which has been reported on the absorption of π^{+} in lead at 700 and 1100 Mev (50) and the results agree with a geometric absorption cross-section to within the errors of $\pm$ 15 $^{o}/_{o}$. For negative pions in the energy interval from

30 to 80 Mev the absorption has been studied in nuclear emulsions (51) and in Al and Cu (52). The results are consistent with the geometric absorption cross-section for each of these materials. The summary of the above results indicated that the absorption cross-section for π^+ in lead is geometric for energies from 30 to 1100 Mev. The correction for nuclear absorption in the telescope for the experiment reported in this thesis is made assuming an absorption cross-section in lead which is independent of the pion energy and equal to

$$\sigma_{Abs.} = 2170 + 15\ ^{o}/o \text{ mb.}$$

This cross-section was computed for $r_o = 1.4 \times 10^{-13}$ cm. and gives a mean free path in lead of $15.0 + 15\ ^{o}/o$ cm.

In the experiments described above the attenuation of a pion beam passing through an absorber was measured in poor geometry. Some pions would be inelastically scattered in the absorber, but no discrimination was made between these and any other pions which were transmitted through the absorber. The effect of these inelastically scattered pions would be to lower the energy spectrum of the pions traversing the telescope. Kessler and Lederman (49) have studied the inelastic scattering of 125 Mev π^- in lead and found that the cross-section for those forward scattered pions ($\geq 80^{o}$) which loose more than 25 $^{o}/o$ of their energy is about 5 $^{o}/o$ of the geometric cross-section. In the largest case in our experiment ($\theta_+ = 22^{o}$) this inelastic scattering would cause a loss in the (1·2·3·5·6) rate of about 1 $^{o}/o$, and so the effect is negligible compared to the statistical error.

APPENDIX III.

LAB. to C. M. Cross-Section Transformation

The volume element in four-space is invariant under a Lorentz transformation because the transformation corresponds to just a rotation of the coordinate system. The differential four-momenta of a particle in two different inertial systems are, therefore, equal.

$$d^4p = p^2 dp d\Omega dE = p'^2 dp' d\Omega' dE' \tag{1}$$

The primed and unprimed systems can be taken to be the C. M. and LAB. systems, respectively. The condition

$$E^2 - p^2 = m^2 \tag{2}$$

is Lorentz invariant and can be imposed on momenta in equation 1.

$$p^2 dp d\Omega dE\ \delta(E^2-p^2-m^2) = p'^2 dp' d\Omega' dE'\ \delta(E'^2-p'^2-m^2) \tag{3}$$

Integrating both sides of equation 3 over all values of the momenta gives the result:

$$\frac{d\Omega}{d\Omega'}\ \frac{dE}{dE'} = \frac{p'}{p} \tag{4}$$

In order to go one step further and derive an expression for the ratio of the differential solid angles, the actual process being observed must be specified. We have taken the case of a three body final state.

$$E_o = E_1 + E_2 + E_3 \tag{5}$$

$$\vec{p}_o = \vec{p}_1 + \vec{p}_2 + \vec{p}_3 \tag{6}$$

The conservations of momentum and energy are Lorentz invariant and can be imposed on equation 4.

$$p_1 d\Omega_1 dE_1 \, \delta\left[(E_o - E_1 - E_2)^2 - m_3^2 - (\vec{p}_o - \vec{p}_1 - \vec{p}_2)^2\right] = p_1' d\Omega_1' dE_1' \, \delta\left[(E_o' - E_1' - E_2')^2 - m_3^2 - (\vec{p}_o' - \vec{p}_1' - \vec{p}_2')^2\right] \tag{7}$$

m_3 is the rest mass of the particle labeled number 3. Notice that we have arbitrarily chosen to solve for the ratio $\frac{d\Omega}{d\Omega'}$ for particle 1, and have eliminated all the kinematical variables of particle 3. This choice in no way restricts the identification of any of the three final state particles. Expanding the argument of the delta - functions in equation 7 and integrating over all values of the total energies give the result:

$$\frac{d\Omega_1}{d\Omega_1'} = \frac{p_1'}{p_1} \frac{(E_o - E_2) - (p_o \cos\theta_1 - p_2 \cos\theta_{12})\, 1/\beta_1}{(E_o' - E_\pi') - (p_o' \cos\theta_1' - p_2' \cos\theta_{12}')\, 1/\beta_1'} \tag{8}$$

where θ_1 is the angle between $\vec{p}_o$ and $\vec{p}_1$, θ_1' is the angle between $\vec{p}_o'$ and $\vec{p}_1'$, θ_{12} is the angle between $\vec{p}_1$ and $\vec{p}_2$, and θ_{12}' is the angle between $\vec{p}_1'$ and $\vec{p}_2'$. In the case that the primed system is the C. M.

system $p_o' = 0$. The LAB. to C. M. transformation for a three-body final state cross-section is given by:

$$\frac{d\Omega_1}{d\Omega_1'}\,\frac{d\Omega_2}{d\Omega_2'}\,\frac{dE_2}{dE_2'} = \frac{p_1'}{p_1}\,\frac{p_2'}{p_2} \times \frac{(E_o - E_2) - (p_o \cos\theta_1 - p_2 \cos\theta_{12})\, 1/\beta_1}{(E_o' - E_2') + p_2' \cos\theta_{12}'\ \ 1/\beta_1'} \tag{9}$$

REFERENCES

1. Bernardini, G., Nuovo Cimento Suppl. 2, Ser. 10, No. 1, 104 (1955).

2. Watson, K., Keck, J., Tollestrup, A., and Walker, R., Phys. Rev. 101, 1159 (1956).

3. De Wire, J. W., Jackson, H. E., and Littauer, R., Phys. Rev. 110, 1208 (1958).

4. Stein, P. C. and Rogers, K. C., Phys. Rev. 110, 2109 (L) (1958).

5. Vette, J. I., Phys. Rev. 111, 622 (1958).

6. Worlock, R. M., Ph. D. Thesis, California Institute of Technology (1958).

7. Heinberg, M., Mc Clelland, W. M., Turkot, F., Woodward, W. M, Wilson, R. R., and Zipoy, D. M., Phys. Rev. 110, 1211 (L) (1958).

8. Dixon, F. P. and Walker, R. L., Phys. Rev. Letters 1, 142 (1958).

9. Wilson, R. R., Phys. Rev. 110, 1212 (L) (1958).

10. Clegg, A. B., preprint.

11. Peterson, V. Z. and Henry, I. G., Phys. Rev. 96, 850 (1954).

12. Sands, M., Bloch, M., Teasdale, J. G., and Walker, R. L., Phys. Rev. 99, 652 (1955).

13. Peterson, V. Z., unpublished report.

14. Peterson, V. Z., Bull. Am. Phys. Soc. 1, 172 (1956).

15. Friedman, R. M. and Crowe, K. M., Phys. Rev. 100, 1799 (A) (1955).

16. Friedman, R. M. and Crowe, K. M., Phys. Rev. 105, 1369 (1957).

17. Woodward, W. M., Wilson, R. R., and Luckey, P. D., Bull. Am. Phys. Soc. 2, 195 (1957).

18. Bloch, M. and Sands, M., Bull. Am. Phys. Soc. 2, 321 (1957).

19. Bloch, M. and Sands, M., Phys. Rev. 108, 1101 (1957).

20. Bloch, M., Ph. D. Thesis, California Institute of Technology (1958).

21. Bloch, M. and Sands, M., preprint.

22. Yuan, L. C. L. and Lindenbaum, S. J., Phys. Rev. 103, 404 (1956).

23. Lindenbaum, S. J., and Sternheimer, R. M., Phys. Rev. 105, 1874 (1957).

24. Sternheimer, R. M. and Lindenbaum, S. J., Phys. Rev. 109, 1723 (1958).

25. Crew, J. E., Hill, R. D., and Lavatelli, L. S., Phys. Rev. 106, 1051 (1957).

26. Cutkosky, R. E. and Zashariasen, F., Phys. Rev. 103, 1108 (1958).

27. Chew, G. F. and Low, F. E., Phys. Rev. 101, 1570 (1956).

28. Sellen, J. M., Cocconi, G., Cocconi, V. T., and Hart, E. L., Phys. Rev. 110, 779 (1958).

29. Sellen, J. M., Cocconi, G., Cocconi, V. T., and Hart, E. L., preprint.

30. Gomez, R., unpublished report.

31. Wilson, R. R., Nuclear Instr. 1, 101 (1957).

32. Donoho, P., Emery, E., and Walker, R., private communication.

33. Heitler, W., The Quantum Theory of Radiation (Oxford University Press, London, 1936), p. 161.

34. Johnston, H. L., Bezman, I. I., Rubin, T., Swanson, C. A., Corak, W., and Rifkin, E. B., "Low Temperature, High Pressure Data of State for Hydrogen and Deuterium Between 64° and 300°K," A. E. C. MDDC-850.

35. Bloch, M., unpublished report.

36. Worlock, R. M., unpublished report.

37. Richman, C. and Wilcox, H., Phys. Rev. 78, 85 (1950).

38. Weissbluth, M., Phys. Rev. 78, 86 (1950).

39. Bethe, H. A. and de Hoffman, F., Mesons and Fields (Row, Peterson and Co., Evanston, Illinois, 1955) vol. 2, p. 341.

40. Wilson, R. R., Phys. Rev. 86, 261 (1952).

41. Walker, R. L., Teasdale, J. G., Peterson, and Vette, J. I., Phys. Rev. 99, 201 (1955).

42. Rossi, B., High-Energy Particles (Prentice - Hall, Inc., New York, 1952), p. 69.

43. Sands, M., unpublished report.

44. Clegg, A. B., unpublished report.

45. Peierls, R. F., Phys. Rev. 111, 1373 (1958).

46. Martin, R. L., Anderson, H. L., and Yodh, G., Phys. Rev. 85, 486 (1952).

47. Martin, R. L., Phys. Rev. 87, 1052 (1952).

48. Chedester, C., Isaacs, P., Sachs, A., and Steinberger, J., Phys. Rev. 82, 958 (1951).

49. Kessler, J. O. and Lederman, L. M., Phys. Rev. 94, 689 (1954).

50. Abashian, A., Cool, R., and Cronin, J. W., Phys. Rev. 104, 855 (1956).

51. Bernardini, G., Booth, E. T., Lederman, L., and Tinlot, J., Phys. Rev. 80, 924 (1950).

52. Camac, M., Corson, D., Littauer, R., Shapiro, A., Silverman, A., Wilson, R., and Woodward, W., Phys. Rev. 82, 335 (1951).